Hydrological Consequences of Land Use / Land Cover and Climatic Changes in Mesoscale Catchments

Von der Fakultät Bau- und Umweltingenieurwissenschaften der Universität Stuttgart zur Erlangung der Würde eines Doktor-Ingenieurs (Dr.-Ing.) genehmigte Abhandlung

von

Luis Eduardo Samaniego Eguiguren

aus Loja, Ecuador

Hauptberichter: Prof. Dr. rer. nat. Dr.-Ing. András Bárdossy

Mitberichter: Prof. Dr. sc. pol. Peter Treuner

Tag der mündlichen Prüfung: 13. Februar 2003

Die Deutsche Bibliothek – CIP-Einheitsaufnahme

Samaniego Eguiguren, Luis Eduardo:
Hydrological Consequences of Land Use / Land Cover and Climatic Changes
in Mesoscale Catchments / von Luis Samaniego.
Institut für Wasserbau der Universität Stuttgart .
- Stuttgart: Inst. für Wasserbau, 2003
(Mitteilungen / Institut für Wasserbau, Universität Stuttgart; H. 118)
Zugl.: Stuttgart, Univ. Diss., 2003
ISBN 3-9337 61-21-2
NE: Institut für Wasserbau <Stuttgart >: Mitteilungen

Herausgegeben: 2003 vom Eigenverlag des Instituts für Wasserbau

Druck: Sprint Druck, Stuttgart

Heft 118

Hydrological Consequences of Land Use / Land Cover and Climatic Changes in Mesoscale Catchments

von

Dr.-Ing.

Luis E. Samaniego Eguiguren

Eigenverlag des Instituts für Wasserbau an der Universität Stuttgart

Preface

This volume contains the thesis of Luis Samaniego. It is the result of an informal cooperation between the Institute of Regional Development Planning and the Institute of Hydraulic Engineering of the University of Stuttgart. The topic of the work – the quantification of the effects of land use and land cover changes on the hydrological cycle for regional planning made an interdisciplinary treatment indispensable. A pure hydrological treatment of the problem often remains a scientific exercise. On the other hand, decision-making without knowing their quantitative effects can lead to unnecessary risks and sub-optimal solutions. Therefore, a decision oriented hydrological treatment of the problem is required.

The purpose of this work is to develop a general methodology to assess the water balance related consequences of land use and land cover changes using regional characteristics. The model should enable the user to quantify the effect of any planned land use change on selected characteristics of the discharge series, such as mean values or extremes.

The scientific method of this work is to build models which quantify the effects of past and ongoing land use changes from observations and to use these for future extrapolation. There are sufficient cases for such studies as the landscape has already been strongly influenced by human activities in large parts of the world. Settlements and highways have been built and large areas are occupied by agriculture. Even forests are often cultivated and not left in a natural state. These non-natural conditions have already substantially influenced the local water cycle. For example, the increase of settlement areas leads to an increase of sealed surfaces and often causes more surface runoff. Agricultural plants are often seasonal, and have a strong influence on evapotranspiration. The sum of all possible effects is a changed water balance. The consequences can be more frequent floods and/or water shortages too. In several parts of the world, land use is changing rapidly and negative consequences were only recognized after irreversible changes occurred. The Neckar catchment was used to develop and to test the methodology. The results are very encouraging, and the methodology seems to be transferable to other regions as well.

Stuttgart, April 20, 2003 András Bárdossy

Table of Contents

List of Figures

List of Tables

List of Symbols

Symbol	Description
α	Level of significance
α_k	Exceedance probability
A	Set of abstract states (i.e. which occur in both space and time) of a natural system
β_j	Model parameter associated with the variable j
$\hat{\beta}_k(q,q')$	Estimated coefficient for the transition probability from q to q' corresponding to the k predictor
$\boldsymbol{\beta} = [\beta_l]$	Vector composed of all model parameters to be estimated
$\hat{\boldsymbol{\beta}}$, $\widehat{\boldsymbol{\beta}}$, $\hat{\boldsymbol{\beta}}_r^*$, $\hat{\boldsymbol{\beta}}_a$	Vectors composed of the estimated values of $\boldsymbol{\beta}$
$\hat{\gamma}^t(h)$	Sample variogram for daily (or annual) precipitation in time t
$\Gamma()$	Gamma function
δ	Threshold value employed for the definition of the floodplains
Δx	Change of the variable x
Δ_0, Δ_1	Constants denoting the duration of a peak event
ε	Tolerance value in [m]
ε_i^t	Independent additive error of the spatial unit i during the period t
$\overline{\varepsilon}$	Mean of ε_i^t
ζ	Temperature weighting multiplier for the previous day period
η_{il}^t	Predictor in a generalized model
ϑ, ϑ_r^*	Test statistic based on a given sample (The * denotes that the test statistic was obtained from a simulated data set)
$\theta, \theta_y, \theta_i^t$	Jackknife statistic
Θ	Test statistic
ι	Number of observations less than a given percentile value
κ	Recession constant [-]
$\kappa, \hat{\kappa}$	Dispersion parameters
$\Lambda_i^{t(k)}$	Duration of the low flow spell k occurring in basin i during the year t
λ_l^t	Interpolation weight for the raingauge station l in time t
μ	Mean value of the universe of a given variable. In the Poisson distribution it denotes the average occurrence rate
$\hat{\mu}, \hat{\mu}_{il}^t$	Maximum likelihood estimators
$\mu()$	Membership function
μ_1, μ_2	Lagrange multipliers
ν	Threshold parameter employed for assessing the dimensionality of a system

N	Natural system
$\xi_i^{t(k)}$	Low flow spell k occurring in the basin i during the year t
$\Xi_i^{t(k)}$	Intensity of the drought k occurring in the basin i during the year t [mm/day]
π	Constant Pi
ϖ	Random number drawn from the uniform distribution [0.1)
$\pi_{qq'}$	Transition probability from land use/cover q to q'
$\mathbf{\Pi}$	Transition probability matrix
ρ	Integer equal to the rounded value of the product σN_i
P	Range of potentially observed values of a natural system
σ	Proportion of observations excluded from each tail of a PDF
ς	Threshold value equal to $0.75N_i$
τ	Threshold value used for the definition of the permanent stream network
T	Number of days either in summer or in winter season during the period from 1.11.1960 to 31.10.1993
$\hat{\upsilon}_k^{t(d)}$	Linear estimator of the daily temperature of the cell k in time $t(d)$
$\overline{\upsilon}_i^{t(d)}$	Mean temperature of the basin i in time $t(d)$
$\mathbf{\Upsilon}$	Lattice containing the flow accumulation surface of a given catchment
φ	Parameter denoting the influence of the outliers in the estimation of $\hat{\boldsymbol{\beta}}$
φ_w	Parameter used for removing the heteroscedasticity of the error term in a model
$\Phi, \Phi_j, \widehat{\Phi}, \Phi_r^*, \Phi_a$	Estimators or objective functions
χ^2	Chi square distribution
$\boldsymbol{\Psi}$	Lattice containing the aspect of a topographic surface
ψ_k	Aspect of the cell k
ψ_k^*	Reclassified aspect of the cell k
ω_j	j^{th} eigenvalue
Ω	Basin or spatial unit
Ω_i	Spatial unit i
a	Shape parameter of the Weibull distribution
a_k	Area of the cell k
AIC	Akaike Information Criterion
A_i	Area of the spatial unit i
$\#(\mathcal{A})$	Number of permutations in which the clause $\mathcal{A}$ is true
$\lvert\mathcal{A}\rvert$	Cardinality of the set $\mathcal{A}$
$\langle\mathcal{A}\rangle$	Operator denoting the integral of the variable $\mathcal{A}$ over both the spatial and the temporal domains
b	Scale parameter of the Weibull distribution
$\mathcal{B}_i$	Floodplains and riparian zones of the basin i
c	Time index denoting the precipitation occurred c days before the event $t(d)$
c_{ij}^t	Absolute sensitivity coefficient
c_1, c_2	Constants for the EDK
C	Total number of days considered for the calculation of the API

C_{p^*}, C_{J^*}	Mallows' statistic
C_t	Lattice representing land cover in time t
c_k	Size of the cell k
C_k	Observed field capacity of the cell k [mm]
Cf	Climatic category according to Köppen's notation (1918)
$\mathrm{CP}(d)$	Circulation Pattern of the day d
CO_2	Carbon dioxide
CH_4	Methane
$d, (d)$	Indices for days
d_e	Number of days in a given year
d_w	Number of days in winter in a given year
d_0, d_1	Indices denoting the beginning and the end of a season in a water year
d_P	Day of occurrence of the peak event
$\mathcal{D}, \mathcal{D}_a$	Original set of observations
$\mathcal{D}^*, \mathcal{D}_r^*$	Simulated data set
$\widehat{\mathcal{D}}$	Set composed of all observations in $\mathcal{D}$ with the exception of those of the basin i in time t
D	Deviance of a generalized model
$D_i^{t(d)}$	Water deficit occurring in the basin i during the day d in the water year t [m^3s^{-1}]
$\mathbf{e}_j$	j^{th} eigenvector
e	Base of the natural logarithms
e_{ij}^t	Relative sensitivity of the model output with respect to $\hat{\beta}_j$
$\mathcal{E}_i^t$	Set composed of observations for the basin i in time t
$E[x]$	Expectation of the random variable x
$E_i^{t(k)}$	Total specific deficit of a drought k occurring at the basin i during the year t [mm]
E_1	Bias (BIAS)
E_2	Mean square error (MSE)
E_3	Square root of mean square error (RMSE)
E_4	Root mean square error (RRMSE)
E_5	Mean absolute error (MAE)
E_6	Relative mean absolute error (RMAE)
E_7	Pearson product-moment coefficient of linear correlation (r)
$\exp()$	Exponential function
$f(\bullet)$	Non-linear function
$\mathrm{F}()$	Distribution function
$\mathrm{F}^{-1}()$	Inverse of the distribution function $\mathrm{F}()$
$\hat{\mathrm{F}}()$	Empirical distribution function
$\mathrm{F}_{(0.95)}$	Value equal to the 95$^{\text{th}}$ percentile of a given random variable
$\mathcal{F}$	Neighborhood system
$\mathcal{F}_{ij}$	Neighbors of the cell (i, j)

g	Total number of input variables denoting morphological characteristics of a basin
$g(\bullet)$	Convex and continuously differentiable function. Link function in a generalized model
$\mathbf{G}_i^t$	Vector composed of variables that describe the morphological characteristics of the spatial unit i in time t
h	Distance between two raingauge stations [m]
$\vec{h}$	Vector denoting the separation between two raingauge stations [m]
H_0, H_0^j	Null hypothesis
H_A, H_A^j	Alternative hypothesis
$\mathcal{H}_i^t$	Total number of high flow events in the spatial unit i during the period t
H_2O	Water
I_k	Topographic index of the cell k
i	Index for a spatial unit (i.e. a basin or a subcatchment) or a cell of a lattice.
(i, j)	Pair denoting the location of a cell in a lattice
j, j', k	Indices for a variable or a land use/cover category
j	Index for a CP-type or a cell of a lattice.
j_G, j_U	Indices for variables in a model
J	Total number of input variables in a model or total number of land use/cover categories
J^*	Total number of model parameters
k	Index for a cell in a lattice. Lag between observations in a time series. Index for the low flow spells. Index for the eigenvectors
k	Number of occurrences of an event
$\vec{k}_l, \vec{k}_{l'}$	Position vectors of raingauge stations l and l' in [m] respectively
K	Constant for the logistic model. Number of exogenous variables regarded as driving forces behind a LUCC
K_i^t	Number of low flow spells occurring in basin i during the year t
l	Index for a model parameter or an explanatory variable, or a land cover category. Index for a raingauge station
$\mathcal{L}$	Total number of raingauge stations
$\ln()$	Natural logarithm function
$\ell(\cdot)$	Log-likelihood function
ℓ_{oj}^{i}	Length of the stream segment j belonging to the order o of the stream network i
L	Number of variables in a simpler model, at least equal to 3
L_1, L_2	Estimator types
L_i	Length of the basin i
$\mathcal{L}_i$	Adequate portion of the basin i
m	Total number of input variables denoting meteorological or climatic characteristics
M	Formal system (could be a model)
$M_{j,j}$	Maintenance of the land use/cover category j during a period of time

$\mathbf{M}_i^t$	Vector composed of variables that describe the climatic conditions for the spatial unit i during the period t
$\max()$	Maximum function
$\min()$	Minimum function
n	Total number of spatial units within the Study Area
$\mathrm{n}, nobs, n_0, n_{0a}$	Number of observations in a random sample
n_c	Number of neighbours of a given cell in a lattice
N	Number of cells in a side of a lattice
$\mathrm{N}(0, s^2)$	Normal distribution with zero mean and variance s^2
N_i	Number of cells within the spatial unit i
N_h	Number of raingauge stations separated by the distance $h + \varepsilon$ [m]
$\mathcal{N}_i$	The stream network of the spatial unit i
$N_{\mathcal{N}_i}$	The number of cells contained within the spatial unit i that belong to the stream network $\mathcal{N}_i$
$\mathrm{NO_x}$	Nitrogen oxides
o	Index for the order of a stream network
$p*$	Number of parameters in a given model
p-value	Significance probability
$\mathrm{Poisson}()$	Poisson distribution
p_{mc}	Monte Carlo p-value
$\hat{p}_k^t, \hat{p}_k^{t(d)}$	Linear estimator of the daily precipitation of the cell k in time t or $t(d)$
$\overline{p}_i^{t(d)}, \overline{p}_\Omega^d$	Mean daily precipitation of the basin i or Ω in water year t and day d
$p_{\Omega_j}^d$	Precipitation occurred in the Study Area Ω in day d under circulation pattern conditions of the type j [mm]
$p_{k_l}^t$	Observed daily precipitation at the raingauge station l in time t in [mm]
$p(x_{(i)})$	Empirical cumulative probability estimate for the i^{th} smallest data value
$p_{ij}^t(q, q')$	Transition probability from land use/cover q to q' in cell (i, j) in time t
P_i^t	Precipitation in the catchment i at the end of the water year t
P_k	Random function occurring at the cell k
$\Pr()$	Probability
P_{75}	75$^{\text{th}}$ percentile
P	Total summer or winter precipitation in [mm] occurred at the Study Area during the period from 1.11.1960 to 31.10.1993
q, q'	Indices for the land use/cover states
$q_i^{t(d)}$	Mean daily discharge recorded at the outlet of the basin i in day d of the water year t
Q_{obs}	Observed value of the variable Q
Q_{cal}	Calculated value of the variable Q
$\overline{Q}$	Mean of the observed values
$\hat{\overline{Q}}$	Mean of the estimated values
Q_i^t	Output variable measured in the spatial unit i during the period t

$\hat{Q}_i^t, \widehat{Q}_i^t$	Estimated value of Q_i^t
Q_3	Upper quartile
Q_1	Annual specific discharge [mm]
Q_2	Total discharge in winter [mm]
Q_3	Total discharge in summer [mm]
Q_4	Specific peak in winter [mm]
Q_5	Specific peak in summer [mm]
Q_6	Specific volume of the annual peak [mm]
Q_7	Specific volume of high flows in winter [mm]
Q_8	Specific volume of high flows in summer [mm]
Q_9	Total duration of high flows in winter [day]
Q_{10}	Total duration of high flows in summer [day]
Q_{11}	Frequency of high flows in winter [year^{-1}]
Q_{12}	Frequency of high flows in summer [year^{-1}]
Q_{13}	Maximum drought duration [day] (evaluated in summer)
Q_{14}	Total drought duration [day] (evaluated in summer)
Q_{15}	Maximum drought intensity [mm/year] (evaluated in summer)
Q_{16}	Cumulative specific deficit [mm] (evaluated in summer)
r	Index for a simulation or a realization
r	Pearson correlation coefficient
$\mathbf{r}_k$	Position vector of the cell k in geographic coordinates
r_p	Constant denoting the range of the theoretical variogram for daily precipitation [m]
r_v	Constant denoting the range of the theoretical variogram for daily temperature [m]
$r(k)$	Value of the autocorrelation function with the lag k
R	Number of permutations, simulations, or realizations
$[\mathbf{R}]$	Correlation matrix
$\mathbb{R}^n$	n dimensional euclidean space
$R^2_{p*}, R^2_J, \overline{R}^2$	Coefficient of determination
s_ε	Estimated sample standard deviation of random errors
s_k	Slope in the cell k [°]
s_q	Land use/cover state q
$\vec{\mathbf{S}}_k$	Vector parallel to the topographic surface at the cell k
$\mathbf{S}$	Finite set composed of mutually exclusive land use/cover types
ΔS	Change of the underground storage
$t,\ t(),\ t(d)$	Time indices [e.g. year, day, or year (day)]
$\tan^{-1}()$	Arctangent function
$t0, t1$	Indices for years if the validation phase of the LUCC model
T	Total number of observations in a time series
$T_{j,k}$	Transformation of land use/cover category j to k
u	Total number of input variables denoting land use/cover states
U	Land use/cover category

$\mathbf{U}^t$	Lattice denoting the land use/cover in time t
$\mathbf{U}_i^t$	Vector composed of variables that describe the land use/cover states in the spatial unit i in time t
$\mathrm{v}(k)$	Proportion of the total variance retained by the first k eigenvectors
$\mathrm{var}()$	Variance of a random variable
$V(\bullet)$	Variance function
$\mathbf{V}^t$	Lattice denoting the land use/cover in time t
V_k^t	Land use/cover of the cell k in time t
$\mathcal{V}$	Evapotranspiration
x	Observable or derived information from a natural system. A random variable in a model
$\mathbf{x}$	Vector of input variables
X	Generic random variable
x^*	Random permutation of x
$\overline{x}$	Mean of the variable x
x_{ij}^t	State of the variable j in the spatial unit Ω_i in time t
x_1	Area of the basin [km²]
x_2	Mean slope [°]
x_3	Median of the slope [°]
x_4	Trimmed mean of the slope $\mathrm{F}_{(15)} - \mathrm{F}_{(85)}$ [°]
x_5	Trimmed mean of the slope $\mathrm{F}_{(30)} - \mathrm{F}_{(70)}$ [°]
x_6	Mean stream slope [°]
x_7	Mean slope in floodplains [°]
x_8	Drainage density [km^{-1}]
x_9	Shape factor [-]
x_{10}	Fraction of north-facing slopes [-]
x_{11}	Fraction of south-facing slopes [-]
x_{12}	Mean basin elevation [m]
x_{13}	Difference between the maximum and the minimum elevations in a basin [m]
x_{14}	Fraction of saturated areas [-]
x_{15}	Mean field capacity [mm]
x_{16}	Fraction of karstic formations [-]
x_{17}	Fraction of forest cover [-]
x_{18}	Fraction of impervious cover [-]
x_{19}	Fraction of permeable cover [-]
x_{20}	Annual precipitation [mm]
x_{21}	Cumulative winter precipitation [mm]
x_{22}	Cumulative summer precipitation [mm]
x_{23}	Mean annual precipitation [mm]
x_{24}	Mean winter precipitation [mm]
x_{25}	Mean summer precipitation [mm]

x_{26}	Antecedent precipitation index [mm]
x_{27}	Maximum annual API [mm]
x_{28}	Maximum API in winter [mm]
x_{29}	Maximum API in summer [mm]
x_{30}	Mean temperature in January [°C]
x_{31}	Mean temperature in July [°C]
x_{32}	Maximum temperature in January [°C]
x_{33}	Maximum temperature in July [°C]
x_{34}	Antecedent temperature index [K]
x_{35}	Maximum annual ATI [K]
x_{36}	Maximum ATI in winter [K]
x_{37}	Maximum ATI in summer [K]
x_{38}	Total number of "dry periods" with decreasing API in summer [day]
x_{39}	Total number of "dry periods" in summer [day]
x_{40}	Total number of "wet periods" in summer [day]
x_{41}	Total number of "wet periods" occurring simultaneously with an API greater than a given threshold in winter [day]
$x_k(i,j)$	Potential predictor k of LUCC
$\{x_i\}$	Set of observables or derivative information
x, y	Cartesian directions of the reference system of a DEM [m]
$y_{qq'}$	Binary indicator variable for a LUCC transition
y	Number of groups of observations with equal number of elements
$\{x_{(1)}, x_{(2)}, \ldots, x_{(n)}\}$	Set composed of n observations of the variable x sorted in ascending order
w_i^t	Weighting factor for the observation of the basin i in time t
w_0, w_P, w_{ij}^t	Calibration, scaling, and control parameters for LUCC model
W_j	Seasonal wetness index corresponding to the CP type j
$\mathrm{Weibull}()$	Weibull distribution
z_k, Z_k	Topographic elevation of the cell k [m]
Z_c	Threshold value used for removing outliers
$\mathbf{Z}$	Lattice containing the elevation of a spatial unit (i.e. DEM) [m.a.s.l.]

Acronyms and Abbreviations

AIC	Akaike Information Criterion
API	Antecedent Precipitation Index
ATI	Antecedent Temperature Index
BBR	Bundesamt für Bauwesen und Raumordnung
BE	Backward Elimination
BOD	Biochemical Oxygen Demand
CDF	Cumulative Distribution Function
CI	Confidence Interval
CP	Circulation Patterns
DEM	Digital Elevation Model
DWD	Deutscher Wetterdienst
EDF	Empirical Distribution Function
EDK	External Drift Kriging
EIA	Environmental Impact Assessment
FS	Forward Selection
GCM	General Circulation Model
GDP	Gross Domestic Product
GLM	Generalized Linear Model
GRG	Generalized Reduced Gradient
HBV	Hydrologiska Byråns Vattenbalansavdelning (water balance section of the hydrological bureau of the Swedish Meteorological and Hydrological Institute)
HILLFLOW-3D	Name of a rainfall-runoff model
IER	Institut für Energiewirtschaft und Rationelle Energieanwendung, Universität Stuttgart
ILPÖ	Institut für Landschaftsplanung und Ökologie, Universität Stuttgart
IMSL	Mathematics and Statistics Libraries
IPCC	Intergovernmental Panel on Climate Change
IPF	Institut für Photogrammetrie und Fernerkundung, Universität Karlsruhe
IREUS	Institut für Raumordnung und Entwicklungsplanung, Universität Stuttgart
INS	Institut für Navigation, Universität Stuttgart
IWS	Institut für Wasserbau, Universität Stuttgart
LUC	Land Use/Cover
LUCC	Land Use/Cover Change
LVA	Landesvermessungsamt Baden-Württemberg

LfU	Landesanstalt für Umweltschutz Baden-Württemberg
m.a.s.l.	Meters above sea level
MAE	Mean Absolute Error
MDS	Model Development and Simulation
MLE	Maximum Likelihood Estimate
MLP	Multi-Linear Potential model
MSE	Mean Square Error
MRF	Markov Random Field
PDF	Probability Density Function
PET	Potential Evapotranspiration
POT	Potential model
Pr	Probability
PRMS	Precipitation-Runoff Modeling System
RMAE	Relative Mean Absolute Error
RMSE	(Square) Root of Mean Square Error
RRMSE	Relative Root Mean Square Error
Q-Q	Quantile-quantile
SCS	U.S. Soil Conservation Service, Agency of the USDA
SHE	Systeme Hydrologique European
SLA	Statistisches Landesamt Baden-Württemberg
TOPMODEL	Name of a rainfall-runoff model
TOPOG	Name of a rainfall-runoff model
UN	United Nations
USDA	U.S. Department of Agriculture
USGS	U.S. Geological Survey
USLE	Universal Soil Loss Equation
UTM	Universal Transverse Mercator
WCED	World Commission on Environment and Development

Acknowledgement

It is a great pleasure for me to express my sincere gratitude to all those who contributed to the preparation of this dissertation. To begin with, I would like to thank both Professor Dr. András Bárdossy and Prof. Dr. Peter Treuner for their continuous encouragement, time, and advice during all phases of this study. Indeed, without their generous support it would have been impossible to reach this stage.

In particular, I would like to thank Professor Bárdossy for his outstanding guidance during those moments when technical difficulties arose and the path was lost. Thanks to his profound understanding of the subject and his programming skills, his suggestions and comments always led me to find a proper solution. I would like to also thank Professor Treuner for giving me the challenging opportunity to work in his Institute as a teaching and research assistant and for letting me work on integrating two disparate scientific disciplines. This opportunity, and Professor Treuner's broad vision of the planning field, allowed me to embrace the subject of this dissertation with confidence.

I am grateful to all members of the Institute of Regional Development Planning who have always provided assistance and critical remarks, which, in turn, have helped me to improve several parts of this dissertation.

I am also deeply indebted to Mr. Pablo Beltran for all the time he generously devoted to the proofreading of my manuscript and for all his useful comments. Any remaining mistakes are the sole responsibility of the author.

Finally, let me express my very special thanks to my family, who have provided unconditional moral support and comprehension since I started this dissertation. This work is dedicated to them: My wife María Eugenia and my children Eduardo and Sofía.

Zusammenfassung

Einleitung

Die vorliegende Arbeit beschäftigt sich sowohl mit den hydrologischen Wirkungen der Veränderung der Landnutzung und Bodenbedeckung und den klimatischen Änderungen in Wassereinzugsgebieten mittlerer Größe als auch mit der Berücksichtigung dieser Wirkungen in einer Flächennutzungsplanung, die der Nachhaltigkeit verpflichtet ist.

Die Untersuchungen stützen sich auf folgende allgemein anerkannte Thesen:

1. Die Bodenbedeckung und die Flächennutzung in einem Raum ändert sich im Lauf der Zeit entweder auf Grund von anthropogenen Einflüssen oder auf Grund von natürlichen Phänomenen wie beispielsweise dem Klima. (McNeil et al, 1994).
2. Die Umwandlungsgeschwindigkeit von einem Flächennutzungstyp in einen anderen hängt von einer Reihe von raumspezifischen Einflussfaktoren ab, die sich in folgende vier Hauptkategorien einteilen lassen: Politische Faktoren, wirtschaftliche Faktoren, demografische Faktoren und Umweltfaktoren (Turner und Mayer, 1994).
3. Eine Veränderung der Flächennutzung kann kurz- oder langfristig eine Änderung des Wasserkreislaufs nach sich ziehen. Diese Änderung beeinflusst die Aufteilung des Niederschlags in Oberflächenabfluss, Infiltration, Interzeption und Verdunstung der Bodenfeuchte (Savenije 1995).
4. Das Ausmaß der Wirkungen hängt von der Lage im Raum und seine Abbildung von dem räumlichen Maßstab ab, in dem eine Untersuchung durchgeführt wird (Calder, 1993).
5. Es besteht ein dringender Bedarf an anwendungsorientierter Forschung, die den Planern hilft, die Komplexität des Wasserhaushalts zu verstehen und zu berücksichtigen (BBR 2000).

Unter Berücksichtigung der tatsächlichen Komplexität des Wasserhaushalts, der oben genannten Thesen und des Stands der Forschung im Bereich der hydrologischen Modellierung und benachbarter Disziplinen versucht die vorliegende Arbeit eine Frage zu beantworten, die hohe Bedeutung für die Ansätze der räumlichen Planung hat. Diese Frage lautet:

> *Wie und in welchem Ausmaß beeinflusst eine Veränderung der Bodenbedeckung und der Flächennutzung unter bestimmten geografischen Gegebenheiten die spezifischen Merkmale des Wasserkreislaufs?*

Die Beantwortung dieser Frage kann in zwei unterschiedlichen Vorgehensweisen versucht werden.

Zum einen kann ein vorhandenes Niederschlags-Abfluss-Modell, wie beispielsweise HBV (Bergstrom und Forsmann 1973), PRMS (Leavesley et al, 1983), SHE (Abbot et al, 1986) oder HILLFLOW-3D

(Bronstert, 1995), mit Hilfe von Beobachtungen der Vergangenheit kalibriert und validiert werden, um dann für eine Abschätzung der Wirkungen zukünftiger Szenarien der Veränderungen der Flächennutzung herangezogen zu werden.

Dieser Ansatz, der auf den ersten Blick sehr differenziert und angepasst zu sein scheint, kann die Aufgabe aber aus mehreren Gründen nicht in befriedigender Weise erfüllen.

- Erstens besteht häufig ein Mangel an hinreichend verlässlichen Daten über die räumliche Verteilung aller Variablen auf einer mittleren räumlichen Maßstabsebene, die mehr als ein paar Hektar, aber weniger als 5000 km^2 umfasst (Vertessy et al, 1993).
- Zweitens liegt eine unbekannte Heterogenität der Parameter auf der mittleren Maßstabsebene (Abbott et al, 1986 Reefsgard 1997; Nandakumar und Mein, 1997) vor.
- Drittens ist diesem Ansatz ein Risiko der Überparametrisierung während der Kalibrierung des Modells inhärent (Bergström, 1995).
- Viertens umfasst die Komplexität des Systems auch eine Abhängigkeit von der Zeit und von Zufälligkeiten der betrachteten Prozesse, die von den aufgeführten Modellen nicht erfasst werden.

In dieser Arbeit wird deshalb ein zweiter Ansatz verfolgt.

Er besteht darin, dass auf der Grundlage von Daten aus der Vergangenheit empirische Ursachen-Wirkungs-Zusammenhänge abgeleitet werden, die mit Hilfe von nicht-linearen Optimierungs-Algorithmen angepasst werden. Anschließend wird die Robustheit dieser Modelle mit Hilfe von Kreuz-Validierungs-Techniken bewertet, und abschließend wird die Unabhängigkeit zwischen jeder erklärten Variablen und gegebenen erklärenden Variablen mit Hilfe von nicht-parametrischen Tests überprüft.

Um den beschriebenen Ansatz umsetzen zu können, wurde folgende Konzeption des Wasserhaushalts zu Grunde gelegt:

Bestimmte Abflussmerkmale eines Einzugsgebietes und eines Zeitraums werden durch eine Menge von erklärenden Variablen bestimmt. Diese erklärenden Variablen gehören zu den drei Kategorien physiografische Faktoren, Flächenbedeckungstypen und klimatische oder meteorologische Faktoren.

Folgende Arbeitsschritte der Untersuchung lassen sich zusammenfassen:

1. Die Entwicklung einer allgemeinen Methodik, die darauf ausgerichtet ist, die Wirkungen auf den Wasserabfluss, die auf exogene makroklimatische Veränderungen zurückzuführen sind, von jenen Wirkungen zu trennen, die von menschlichen Aktivitäten verursacht werden.
2. Die Auswahl und Validierung von Modellen, die diese Wirkungen auf der Grundlage von Merkmalen des hydrologischen Kreislaufs auf einer mittleren räumlichen Maßstabsebene quantifizieren.

3. Die Überprüfung der gefundenen Modelle im Hinblick auf deren Eignung, die Wirkungen von klimatischen Veränderungen und von Änderungen der Flächenbedeckung bzw. –nutzung auf den Wasserkreislauf auf einer mittleren räumlichen Ebene zu bewerten.

Methodik

Mit der in dieser Arbeit verwendeten Methode soll festgestellt werden, welcher Satz von Variablen auf einem statistisch signifikanten Niveau den höchsten Beitrag für die Erklärung der Veränderungen des beobachteten Systems liefert. Dabei sollte einerseits in Abhängigkeit von der Dimensionalität des Systems die Zahl der verwendeten Variablen möglichst klein sein und andererseits jede Kategorie der erklärenden Faktoren mindestens mit einer Variablen vertreten sein. Die Anpassungsgüte jedes der geprüften (a priori plausiblen) Modelle wurde mit Hilfe von Mallows Cp Statistik, des Akaikes-Informationskriteriums und einer Jackknife–Statistik geschätzt.

Mit dieser Vorgehensweise war es möglich, die im Laufe der Zeit auftretenden Schwankungen eines Merkmals des Abflusses eines Wassereinzugsgebietes in zwei unabhängige Komponenten zu zerlegen. Die eine Komponente wird nur durch klimatische Schwankungen erklärt, während die zweite Komponente ausschließlich durch Veränderungen der Bodenbedeckung erklärt wird. Es muss auch betont werden, dass die Modelle innerhalb des Untersuchungsraumes für verschiedene Wassereinzugsgebiete mit unterschiedlichen physiografischen Merkmalen angepasst wurden. Die beschriebene Vorgehensweise erlaubt es, in einer effizienten Weise das erstgenannte Ziel zu erreichen.

Diese Vorgehensweise hat zwei Vorteile. Das Risiko der Überparametrisierung und des möglichen Auftretens von Multikollinearitäten bei den erklärenden Variablen konnte deutlich verringert werden; eine unmittelbare Folge dessen ist eine signifikante Verringerung der Konfidenzintervalle aller Modellparameter.

Die Einführung von statistisch signifikanten Variablen in ein Modell ist von entscheidender Bedeutung für die Auswahl von "guten" und "einfachen" Modellen aus der Vielzahl von Möglichkeiten, die sich aus dem gegebenen Satz von erklärenden Variablen ableiten lassen. Der Hauptgrund dafür ist, dass eine nicht-signifikante Variable die Gesamtvarianz zwar erhöht, sie aber überhaupt nicht erklärt. Mit anderen Worten, die nicht-signifikanten Variablen erhöhen das „Rauschen“ im System und vermindern den Erklärungsgehalt anderer signifikanter Variablen. In dieser Hinsicht zeigte sich, dass der verwendete Permutations-Test im Vergleich mit konventionellen parametrischen statistischen Tests ein unerlässliches analytisches Werkzeug ist.

In den Fällen, in denen die gemeinsame multivariate Verteilungsfunktion der erklärenden Variablen unbekannt ist, hätten die herkömmlichen parametrischen Tests zu irreführenden Ergebnissen hinsichtlich der Auswahl von signifikanten Variablen für die Modelle geführt. Solche Ergebnisse wären entstanden, weil alle parametrischen Tests sich auf Annahmen bezüglich der Verteilungsfunktion der Variablen und der Teststatistiken gründen.

In der vorliegenden Arbeit wird die Verteilung der Teststatistik, die zur Prüfung der Nullhypothese (Unabhängigkeit der erklärten und erklärenden Variablen) verwendet wird, durch Simulation erstellt, indem aus dem ursprünglichen Datensatz ein künstlicher Datensatz durch Permutation generiert wird.

Die Verwendung des Jackknife-Verfahrens für die Kreuz-Validierung des besten Modells erleichtert die Aufgabe der Auswahl des "besten" Modells für ein gegebenes Abflussmerkmal erheblich. Zusätzlich war es für diese Arbeit von besonderer Bedeutung, weil es eine gleichzeitige Schätzung des Niveaus der Vorhersagbarkeit ermöglicht. Weiterhin sind dadurch die Modelle gegenüber eventuellen Ausreißern robust. Ein weiterer Vorteil dieses Verfahrens ist, dass es unabhängig vom Schätzer eingesetzt werden kann.

Die vorgestellte Methode wurde im Einzugsgebiet des Neckars oberhalb des Pegels Plochingen angewendet (Abb. 1). Das Einzugsgebiet umfasst eine Fläche von rund 4000 km^2. Die Daten für das Untersuchungsgebiet stammen aus mehreren Quellen.

- Die physiografischen Variablen wurden aus einem digitalen Höhenmodell mit einer Auflösung von 30×30 m, aus einer digitalisierten Bodenkarte im Maßstab 1 : 200 000 und aus einer digitalisierten Geologischen Karte im Maßstab 1 : 600 000 abgeleitet.
- Die Bodenbedeckung wurde hauptsächlich aus zwei Quellen ermittelt. Zum einen wurden Topographische Karten im Maßstab 1 : 25 000 aus dem Jahr 1961 verwendet. Zum anderen lagen drei LANDSAT-Aufnahmen für die Jahre 1975, 1984 und 1993 vor. Die Auflösung dieser Aufnahmen beträgt 30×30 m und erlaubt die Ableitung von drei Flächenbedeckungs-Klassen: Wald, versiegelte Flächen und durchlässige Bodenbedeckung.
- Die beiden klimatologischen Variablen "täglicher Niederschlag" und "Temperatur" lagen für 288 Wetterstationen in Baden-Württemberg für den Zeitraum 1.11.1961 bis 31.10.1993 vor. Diese Informationen wurden mit Hilfe einer geostatistischen Methode (External Drift Kriging) für ein Raster mit einer Maschenweite von 300×300 m interpoliert.
- Die Zeitreihen des täglichen Abflusses standen für den oben genannten Zeitraum für 46 Pegel im Untersuchungsraum zur Verfügung.

Auf der Grundlage der aufgeführten Informationen wurden für jedes der 46 Wassereinzugsgebiete im Untersuchungsraum und jedes Halbjahr des Zeitraumes 1961 bis 1993 eine Anzahl von Indikatoren abgeleitet. Beispielsweise wurden für die Beschreibung der physiografischen Merkmale die folgenden Indikatoren verwendet: Gesamtfläche, durchschnittliche Hangneigung, Median der Hangneigung, getrimmter Median der Hangneigung, durchschnittliches Gefälle der Fließgewässer, durchschnittliche Hangneigung der Überschwemmungsgebiete, Gewässerdichte, Form des Wassereinzugsgebietes, Anteil der nach Norden und Süden exponierten Hänge, durchschnittliche Höhe des Wassereinzugsgebietes, Reliefenergie, Anteil der Flächen mit gesättigten Böden, durchschnittliche Feldkapazität und Anteil der Karstflächen.

Die Veränderung der Bodenbedeckung wurde mit Hilfe von Zeitreihen abgebildet, die die jeweiligen Anteile der Waldflächen, der versiegelten Flächen und der nicht-versiegelten Flächen an der Gesamtfläche der Wassereinzugsgebiete und der Überschwemmungsgebiete abbilden.

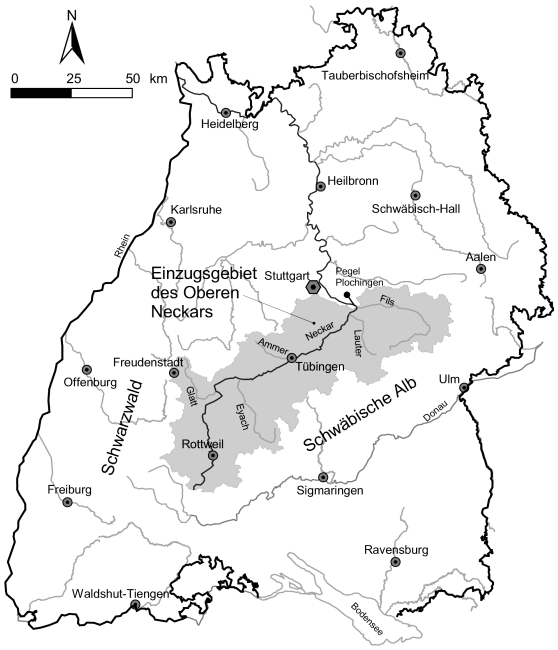

Abbildung 1 Lage des Einzugsgebietes des Oberen Neckars in Baden-Württemberg

Das Klima wurde mit Hilfe von Zeitreihen folgender Indikatoren jeweils für das hydrologische Sommer- und Winterhalbjahr beschrieben: Kumulierte Niederschlagshöhe, durchschnittliche Niederschlagshöhe, Vor-Regen-Index, mittlere Temperatur im Januar und im Juli, mittlere Halbjahrestemperatur, Maximum und Minimum der Temperatur im Januar und im Juli, Vor-Temperatur-Index sowie ein auf Großwetterlagen basierter Feuchtigkeitsindex.

Die erklärten Variablen beruhen auf Zeitreihen für Abflussmerkmale im Sommer und im Winter, nämlich: Gesamter Abfluss, spezifischer Scheitelabfluss, Abflussmenge der Hochwässer, Gesamtdauer der Hochwässer, Häufigkeit der Hochwässer, Gesamtdauer der Trockenheit, Intensität der Trockenheit, kumulatives Defizit.

Der Umfang der untersuchten Stichproben umfasst ungefähr 1000 Beobachtungen. Die Größe der Wassereinzugsgebiete reicht von $4\,km^2$ bis $4000\,km^2$. Die kalibrierten Modelle für einige Abflussmerkmale im Winter und im Sommer zeigten, dass die Variablen zur Bodenbedeckung statistisch signifikante Erklärungskomponenten des Wasserkreislaufs in mittelgroßen Einzugsgebieten sind. Ihr Erklärungsbeitrag ist für das Winterhalbjahr jedoch höher als für das Sommerhalbjahr.

Integrierte Bewertung der hydrologischen Wirkungen der Veränderung der Bodenbedeckung und des Klimas in einem mittelgroßen Wassereinzugsgebiet

Die Integration zweier Bereiche des Wassersystems, nämlich des Abflussverhaltens eines Einzugsgebietes und der Bodennutzung zu einem entsprechenden Zeitpunkt, konnte in dieser Arbeit auf Grund der Einfachheit der verwendeten hydrologischen Modelle und der Eigenschaften des Land Use/Cover Change Modells (LUCC) weitgehend erreicht werden. Außerdem wurde eine Abschätzung der Größenordnung der Wirkungen der Änderung der Bodenbedeckung auf den Wasserkreislauf in einem mittelgroßen Wassereinzugsbereich mit Hilfe einer sequentiellen Monte-Carlo-Simulation, die im besonderen Testgebiet (Einzugsbereich der Körsch) vier relevante Entwicklungsszenarien (C1S1,

C1S2, C2S1, und C2S2) zur wahrscheinlichen Entwicklung von makro-klimatischen und sozio-ökonomischen Zuständen lieferte, durchgeführt.

Die verwendeten Szenarien lassen sich wie folgt skizzieren:

Das **Szenario S1** trägt den Titel "Status-quo-Szenario". Die zukünftige Entwicklung im besonderen Testgebiet wird als Fortsetzung der in der Vergangenheit beobachteten Trends betrachtet. Das Szenario geht von der Annahme aus, dass aufgrund eines stetigen Wachstums des Pro-Kopf-Einkommens im Zusammenspiel mit einem gut ausgebauten Straßennetz und einer moderaten Besteuerung von fossilen Brennstoffen die enge Korrelation zwischen dem Besitz eines PKWs und der Nachfrage nach Wohnbauland erhalten bleibt.

Die Wohnungsmieten werden im Raum Stuttgart aufgrund seiner hohen Zentralität steigen.

Die Folgen dieser Annahme sind, dass trotz einer weitgehenden Konstanz der Einwohnerzahl die Nachfrage nach größeren Wohnungen und freistehenden Häusern in Siedlungen mit einer guten Straßenverbindung stark zunehmen wird. Neue Wohngebiete und großflächige Einzelhandelseinrichtungen mit großen Parkplätzen werden am Rande von Stuttgart entstehen, während in der Stadtmitte Dienstleistungseinrichtungen zunehmend Flächen in Anspruch nehmen werden. Das Szenario beschreibt eine starke Zersiedlung der Landschaft im besonderen Testgebiet.

Unter diesen Annahmen wurden mit Hilfe einer Markov-Kette, deren Übergangswahrscheinlichkeiten mit Hilfe von Informationen aus der Vergangenheit kalibriert wurden, die Flächen der drei Kategorien für das Jahr 2025 geschätzt; demnach hätte Wald eine Fläche von 1280 ha, die undurchlässige Fläche würden 5950 ha und die durchlässigen 5390 ha umfassen.

Das **Szenario S2** trägt den Titel "lokale Nachhaltigkeit". Es unterscheidet sich in einigen Punkten vom ersten Szenario. Erstens werden aus der Einsicht heraus, dass eine ungebremste Zersiedelung der Landschaft zu einer Zunahme von Umweltrisiken führen kann, Regelungen der Flächennutzung verschärft und Grundsteuern erhöht. Die Nachfrage nach Wohnflächen je Einwohner wird dadurch deutlich vermindert.

Zweitens wird die Mineralölsteuer erhöht. Die Steuererhöhung verteuert das Pendeln. Gleichzeitig wird das Angebot der öffentlichen Verkehrsmittel erhöht. Folglich wird die Nachfrage nach zusätzlichen Verkehrsflächen stark abnehmen.

Als Folge der genannten Einschränkungen wird die jährliche Wachstumsrate der undurchlässigen Flächen von 1,3% im Status-quo-Szenario auf 0,4% im S2-Szenario sinken.

Drittens wird die im Zeitraum 1975 bis 1993 im besonderen Testgebiet beobachtete Abnahme der Waldflächen durch Ausgleichsmaßnahmen gebremst.

Am Ende des Simulationszeitraumes wird der Wald im Durchschnitt eine Fläche von 2160 ha bedecken. Undurchlässige Flächen bedecken im Durchschnitt 4390 ha und 6075 ha sind durchlässige Flächen.

Das **Szenario C1** ist ein pessimistisches Klimaszenario und beschreibt den ungünstigsten Fall. Es orientiert sich an Szenarien zur weltweiten Entwicklung der Umweltsituation und des Klimas und geht von einer Wirtschaftsweise aus, die die natürlichen Ressourcen wenig schont.

In Deutschland wird sich wahrscheinlich die Niederschlagsmenge im Winter erhöhen und im Sommer aufgrund einer verstärkten Evapotranspitation abnehmen. Zusätzlich werden die Häufigkeit und die Intensität von außergewöhnlichen Niederschlagsereignissen im Sommer zunehmen. Die Häufigkeit und die Intensität von Hochwasser wird sehr wahrscheinlich zunehmen. Gleichzeitig ist es sehr wahrscheinlich, dass die Perioden der Trockenheit aufgrund der verstärkten Verdunstung zunehmen werden. Die durchschnittliche Temperatur wird im Sommer und im Winter wahrscheinlich ansteigen. Die Häufigkeit des Auftretens von Extremwerten der Temperatur wird sich ebenfalls ändern: Die Zahl der Frosttage im Winter wird abnehmen und die Zahl der heißen und trockenen Tage im Sommer wird zunehmen. Insgesamt wird der Wetterverlauf in Zukunft sprunghafter und intensiver.

Das **Szenario C2** ist ein optimistisches Klimaszenario. Als Ergebnis einer weltweiten Substitution von nicht erneuerbaren Energiequellen durch erneuerbare Energiequellen wird die Konzentration von CO_2 und anderen Treibhausgasen langsamer zunehmen als im Szenario C1. In Deutschland werden die klimatischen Änderungen weniger stark ausgeprägt sein als im Szenario C1. Sowohl die Zehnjahresrate der Zunahme der Niederschläge als auch der Temperatur wird ungefähr ein Drittel der entsprechenden Raten des Szenarios C1 betragen. Beispielsweise wird die Zunahme der durchschnittlichen Temperatur bis zum Jahr 2020 im 95%-Konfidenzintervall der natürlichen Schwankungen liegen. Die Zunahme des durchschnittlichen Niederschlages im Winterhalbjahr wird aber sicherlich die natürlichen Schwankungen des letzten Jahrhunderts übersteigen.

Grundsätzlich geht das LUCC-Modell davon aus, dass die Übergangswahrscheinlichkeit von einem Bodennutzungstyp zu einem anderen von der geographischen Lage und externen Einflussfaktoren abhängt, die räumlich differenziert sind, aber sich im Untersuchungszeitraum nicht ändern. Diese Einschränkung wurde in der vorliegenden Untersuchung vor allem auf Grund der zeitlichen Restriktionen vorgenommen.

Als potentielle Bestimmungsgrößen der Veränderung der Bodennutzung werden in dieser Untersuchung aufgrund der vorgenommenen Überprüfungen die Entfernung zu Autobahnen, die Entfernung zu Siedlungen mit einem Haltepunkt des schienengebundenen Personenverkehrs, die Entfernung zu Fließgewässern, die Hangneigung und die Ausrichtung nach Süden betrachtet. Trotz der Einfachheit des Modells zeigte sich in der Validierungsphase, dass in dem gewählten besonderen Testgebiet in der Nähe von Stuttgart (Einzugsgebiet der Körsch) (Abb. 2) eine Vorhersagegenauigkeit von 85 % erreicht werden konnte.

Abschließend wurde eine stochastische Simulation angewendet, um zu bestimmen, wie stark eine Veränderung der Bodennutzung das hydrologische System in einem bestimmten Wassereinzugsgebiet beeinflusst. Die Wirkungen auf das hydrologische System wurden mit Hilfe von empirischen Modellen für einige Abflussmerkmale kalibriert. Die verwendeten Variablen zur Bodenbedeckung stammen für jeden gegebenen Zeitpunkt aus dem LUCC-Modell, die Variablen zur Morphologie sind im Simulationszeitraum konstant, und die klimatischen Variablen wurden als Stichprobe aus den

gemeinsamen multivariaten Verteilungen gezogen. Hierzu musste eine sequentielle Simulation durchgeführt werden, um die Abhängigkeiten der meteorologischen Größen zu berücksichtigen.

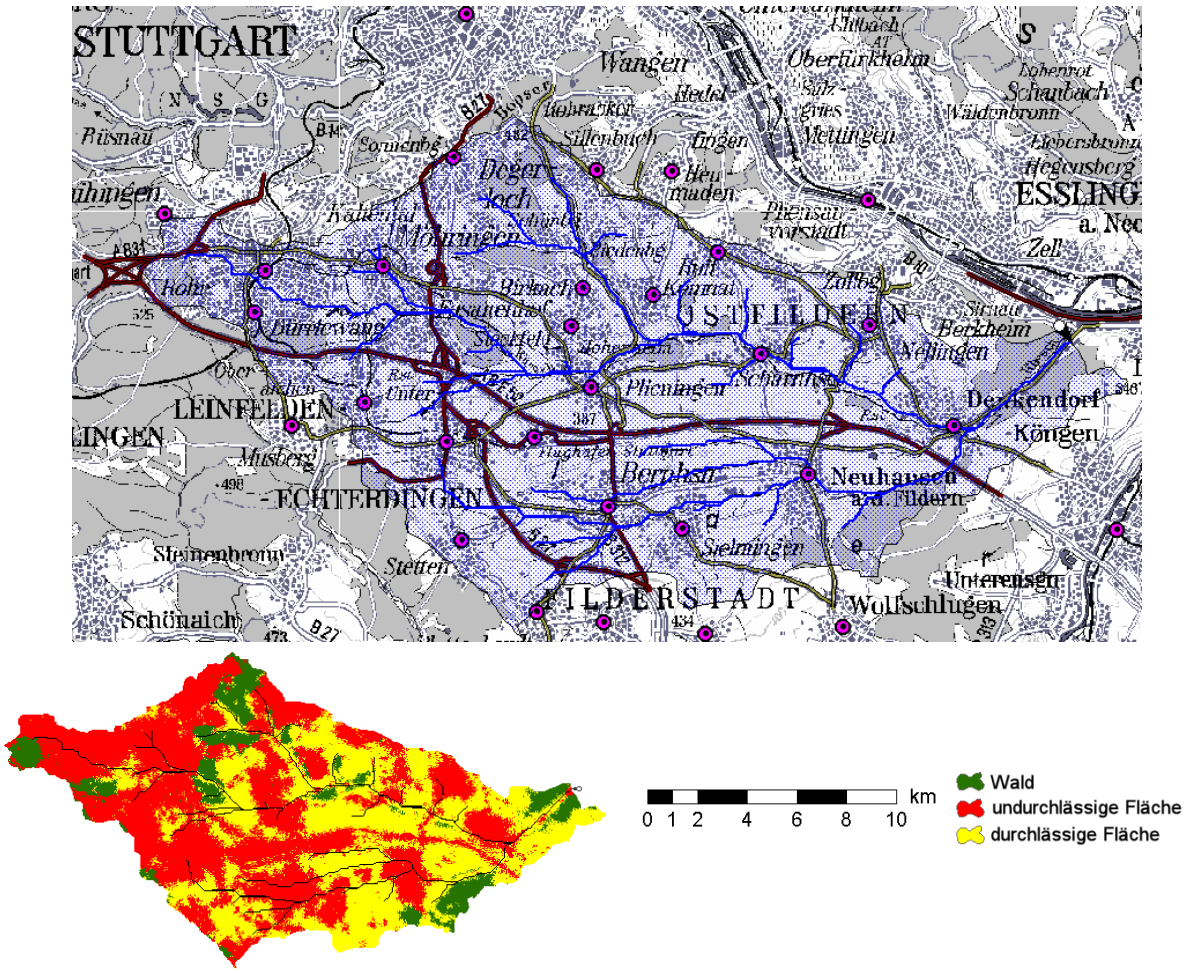

Abbildung 2 Oben: Besonderes Testgebiet (Einzugsgebiet der Körsch) in der Nähe von Stuttgart. Unten: Ergebnisse einer Simulation des LUCC-Modells für das Szenario S1 im Jahr 2025.

Ergebnisse

In Tabelle 1 ist deutlich erkennbar, dass das hydrologische System des betrachteten Einzugsgebietes die größten Störungen bei der Szenarienkombination C1S1 erleidet. Die geringsten Störungen treten bei der Szenarienkombination C2S2 auf.

Der Gesamtabfluss im Winterhalbjahr (Q_2) wird im ungünstigsten Fall um ungefähr 6,9% pro Dekade ansteigen. Dieser Fall (Szenario C1S1) geht von einer starken Zersiedlung der Landschaft und einer stetigen Zunahme der durchschnittlichen Lufttemperatur durch die globale Erwärmung aus.

Der Gesamtabfluss im Sommerhalbjahr (Q_3) wird im allgemeinen aufgrund der höheren Temperaturen und der zunehmenden Evapotranspiration abnehmen. Lediglich im Szenario C2S1 kann es zu einer Zunahme des Abflusses im Sommerhalbjahr kommen.

Die spezifischen Scheitelabflüsse im Winterhalbjahr (Q_4) neigen in allen Szenarien zu einer Zunahme. Die größte Abweichung von dem in der Vergangenheit beobachteten Mittelwert tritt im Szenario S1C1 auf. Änderungen der Bodenbedeckung spielen für die spezifischen Scheitelabflüsse eine

entscheidende Rolle. Die relative Differenz dieser Variablen zwischen den sozio-ökonomischen Szenarien S1 und S2 beträgt ohne Berücksichtigung der klimatischen Einflüsse ungefähr 3% pro Dekade.

Die spezifischen Scheitelabflüsse im Sommerhalbjahr (Q_5) nehmen mit Ausnahme von Szenario C2S1 in allen Szenarien ab. Im Szenario C2S1 werden die Sommer nicht wesentlich wärmer sein als in der Referenzperiode. Die Zunahme der versiegelten Flächen wird aber eine Zunahme der Scheitelabflüsse pro Dekade bewirken.

Die Abflussmenge der Hochwässer (Q_6) ist das Merkmal, das am stärksten durch die simulierten Änderungen der Bodenbedeckung im besonderen Testgebiet beeinflusst wird. Unter gleichen klimatischen Verhältnissen schwankt diese Variable zwischen den beiden sozio-ökonomischen Szenarien um 5,8% pro Dekade bei mäßigen Niederschlägen und um 6,7% bei hohen Niederschlägen.

Die Gesamtdauer der Hochwässer im Winterhalbjahr (Q_9) ist bei gleichen klimatischen Bedingungen im Szenario S2 im Durchschnitt höher als im Szenario S1.

Tabelle **1** Durchschnittliche relative Veränderung jeder simulierten Variablen pro Dekade (in %) (Bezugsjahr 1994)

Variable	**Symbol**	**Entwicklungsszenario**				**Entwicklungsszenario**			
		C1S1	**C1S2**	**C2S1**	**C2S2**	**C1S1**	**C1S2**	**C2S1**	**C2S2**
Gesamtabfluss im Winter	Q_2	6.9	5.4	3.7	2.4				
Gesamtabfluss im Sommer	Q_3	-2.6	-6.8	0.4	-4.1				
Spezifischer Scheitelabfluss im Winter	Q_4	8.8	5.4	5.4	2.5				
Spezifisches Scheitelabfluss im Sommer	Q_5	-3.7	-1.6	0.1	-0.6				
Abflussmenge der Hochwässer	Q_6	9.9	3.2	8.0	2.2				
Gesamtdauer der Hochwässer im Winter	Q_9	5.6	6.2	2.3	2.7				
Gesamtdauer der Hochwässer im Sommer	Q_{10}	-1.9	-4.5	1.8	-1.1				
Häufigkeit der Hochwässer im Winter	Q_{11}	7.1	3.5	4.4	1.3				
Häufigkeit der Hochwässer im Sommer	Q_{12}	-2.8	-2.6	-1.2	-1.8				
Gesamtdauer der Trockenheit im Sommer	Q_{14}	8.4	8.0	3.7	3.8				

Legende der Farbskala

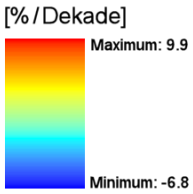

Die Gesamtdauer der Hochwässer im Sommerhalbjahr (Q_{10}) neigt im allgemeinen dazu, abzunehmen. Der wesentliche Grund dafür ist die Zunahme der durchschnittlichen Lufttemperatur. Die Wachstumsrate ist im Szenario C2 niedriger, weil in diesem Szenario die Waldflächen größer sind als im Szenario C1 und dadurch die Evapotranspiration zunimmt. Der Oberflächenabfluss verringert sich entsprechend. Eine Ausnahme bildet das Szenario C2S1, bei dem der Oberflächenabfluss um 0,1% pro Dekade zunimmt.

Die Häufigkeit von Hochwässern nimmt im Winterhalbjahr (Q_{11}) zu und im Sommerhalbjahr (Q_{12}) ab. Das Szenario S1 weist unter gleichen klimatischen Bedingungen höhere Wachstumsraten der Hochwasserhäufigkeit auf.

Die Dauer der Trockenheit (Q_{14}) neigt dazu, im Klimaszenario C1 stärker zu wachsen als im Szenario C2. Veränderungen der Landnutzung haben zwar einen Einfluss auf diese Variable, er ist aber geringer als der Einfluss der klimatischen Veränderungen.

Folgerungen

In der vorliegenden Studie wurde versucht, die Auswirkungen von klimatischen Veränderungen und Veränderungen der Bodenbedeckung und der Landnutzung auf den Wasserkreislauf in einem Wassereinzugsgebiet mittlerer Größe zu erfassen. Im Hinblick auf diese Zielsetzung können aus den Ergebnissen einige Folgerungen gezogen werden.

1. Ein Hauptelement im analytischen Teil dieser Arbeit bestand in der Verwendung von zeitlich und räumlich differenzierten Daten aus dem Zeitraum 1961 bis 1993 für 46 Pegel im Einzugsgebiet des Oberen Neckars. Auf der Grundlage der Vielzahl von Einzelinformationen und mit Hilfe von fortschrittlichen Optimierungsmethoden und nichtparametrischen statistischen Verfahren war es möglich, Modelle zu entwickeln und zu validieren, die den Zustand des Systems zu jedem Zeitpunkt und für jede räumliche Einheit beschreiben können. Die gefundenen numerischen Zusammenhänge haben es auf einer mittleren räumlichen Maßstabsebene erlaubt, Wirkungen, die von klimatischen Veränderungen bestimmt werden, von Wirkungen, die auf Änderungen der Bodenbedeckung zurückzuführen sind, zu trennen. Die Quantifizierung der Größenordnung der Wirkungen einer gegebenen Änderung der Bodenbedeckung ist dann relativ einfach.

2. Die kalibrierten Modelle für einige Abflussmerkmale im Sommer und im Winter haben gezeigt, dass die Variablen zur Bodenbedeckung statistisch signifikante Komponenten des Wasserkreislaufs auf der gewählten räumlichen Ebene darstellen. Die Anpassung der Modelle ist für die Winterhalbjahre besser als für die Sommerhalbjahre.

3. Eine Verknüpfung dieser hydrologischen Modelle mit einem einfachen stochastischen Bodenbedeckungs- bzw. Landnutzungsmodell war durchführbar und lieferte aufschlussreiche Erkenntnisse. Obwohl das verwendete Bodenbedeckungs- bzw. Landnutzungsmodell ziemlich einfach gestaltet ist, zeigten die Ergebnisse, dass es sich dabei um ein viel versprechendes Planungswerkzeug handelt, welches eine Überprüfung der Wirkungen einiger Szenarien zur Änderung der Landnutzung und des Klimas auf den Wasserkreislauf erlaubt.

4. Weitere Forschungen sind notwendig, um die Bodenbedeckungs- bzw. Landnutzungsmodelle zu verbessern, insbesondere in Hinblick auf die Berücksichtigung anderer zeitabhängiger Einflussfaktoren.

5. Weitere Schritte sollten unternommen werden, um die Entwicklung und den Einsatz von integrierten Planungswerkzeugen als logische und systematische Hilfsmittel für Planungen, die die Komplexität natürlicher Systeme und deren Beziehungen zu menschlichen Aktivitäten betreffen, zu fördern. Wenn dies umgesetzt wird, wird damit ein Schritt in Richtung einer nachhaltigen Entwicklung getan.

Chapter 1

Introduction

"Our land, compared with what it was, is like a skeleton of a body wasted by disease."

***Plato** (4th century B.C.)*

"O earth, what changes hast thou seen!"

***Alfred Tennyson** (1809–1892)*

"Russian forests crash down under the axe, billions of trees are dying, the habitations of animals and birds are layed waste, rivers grow shallow and dry up, marvellous landscapes are disappearing forever.... Man is endowed with creativity in order to multiply that which has been given him; he has not created, but destroyed. There are fewer and fewer forests, rivers are drying up, wildlife has become extinct, the climate is ruined, and the earth is becoming ever poorer and uglier."

***Anton Pavlovich Chekhov** (1860–1904)*

1.1 Description of the Problem

The adaptations of the landscape by the action of man either to create better living conditions or to cope with the demand of resources required to fulfil man's subsistence have taken place since the dawn of mankind. The impacts associated with them, though insignificant at the beginning, have transformed the face of earth for good or bad as no other living species has ever done. Since the Industrial Revolution, the availability of new machinery powered by more efficient energy sources has multiplied the human power by thousands, making, as a result, this transformation process even faster.

Many writers and philosophers in the past have clearly documented these misdoings; unfortunately such alterations were often associated with progress and prosperity. Consequently, a coordinated action against them was rarely implemented. Nowadays, many regions on earth remain deeply transformed, with all their beauty and wealth lost forever. In those cases, the natural system was forced to a new state with higher entropy (i.e. disorder) and where the point of no-return has been largely surpassed. Fortunately, many sectors in the political and scientific spheres have become aware of these issues, but still much is to be done in this respect.

The present study deals with the hydrological consequences of land use, land cover, and climatic changes and their integration in a holistic land use planning framework that pursues sustainability[1].

This research is based on the following facts:

1. The land use and land cover of a region is changing over time due to either anthropogenic reasons or natural phenomena (i.e. climate). Well known, and devastating examples can be found in both the Amazon and the Aral Sea basins (McNeill et al. 1994),
2. The transition rates from one land use type to another depend on several place-specific driving forces that can be categorised into four major classes: political, economic, demographic, and environmental (Turner and Mayer 1994),
3. A change in land cover will originate sooner or later a change in the water cycle based on the actual knowledge of the physio-chemical laws that govern it. This change will influence the proportion of surface runoff, infiltration, interception, and transpiration from soil moisture (Savenije 1995),
4. The magnitude of the impacts may vary according to the geographic location and the scale at which the analysis is carried out (Calder 1993), and
5. The acknowledged urgent need for more practical research that helps planners to understand the complexity of the water system (BBR 2000).

In this study, the term *land use* is used in the sense of human employment of the land, whereas the term *land cover* is used to denote the physical state of the land (Turner and Meyer 1994). The former is related with the anthropogenic system whereas the latter is related with the natural system. These two concepts are connected in principle, but it is not necessarily true that one land use category has to correspond to a unique land cover class. The level of agreement depends upon how such categories have been defined.

Land use change may "involve either a *shift* to other land use type or an *intensification* of an existing one"; while *land cover change* implies a *conversion* and/or a *modification* of the land surface. C*onversion* is understood to mean "the change from one land cover class to another" (e.g. from forest to grassland, or from grassland to cropland), while *modification* is "the change of condition within a land cover class" (e.g. thinning of a forest or cropland intensification) (Turner and Mayer 1994, Skole 1994).

Firstly, an attempt to systematize the complex interactions between anthropogenic activities and the natural system is to be presented, whose schematic representation is depicted in Figure 1.1. As a direct consequence of anthropogenic activities, large amounts of toxic substances, either in solid, liquid or gaseous phase, are yearly returned to Nature as a result of the chemical and physical processes associated with such activities. These outflows are called emissions, and in general they disrupt the natural system (e.g. climate or the ecosystems' equilibrium) in various intensities. For instance, there

---

[1] **Sustainability**: Term coined by the famous Brundtland Commission (UN) in 1987. This term defines the utmost principle of a development plan that enforces to "meet present needs without compromising the ability of future generations to meet their needs" (WCED, 1987).

is strong evidence, and it is widely accepted within the scientific community, that the increasing concentrations of greenhouse gases (e.g. CO_2,NO_x,CH_4,H_2O, and chlorofluorocarbons) are responsible for a steadily increasing global average surface temperature at the rate of about (0.3°C/decade) (Houghton et al. 1990, 1992, 2001, Wigley and Raper 1992, Rowland 2000), a phenomenon commonly known as global warming. Although this problem, along with many others such as non-point source pollution, water bodies pollution by untreated sewage, groundwater contamination due to over fertilizing, are serious threats to mankind at the moment, they will not be thoroughly considered in this study.

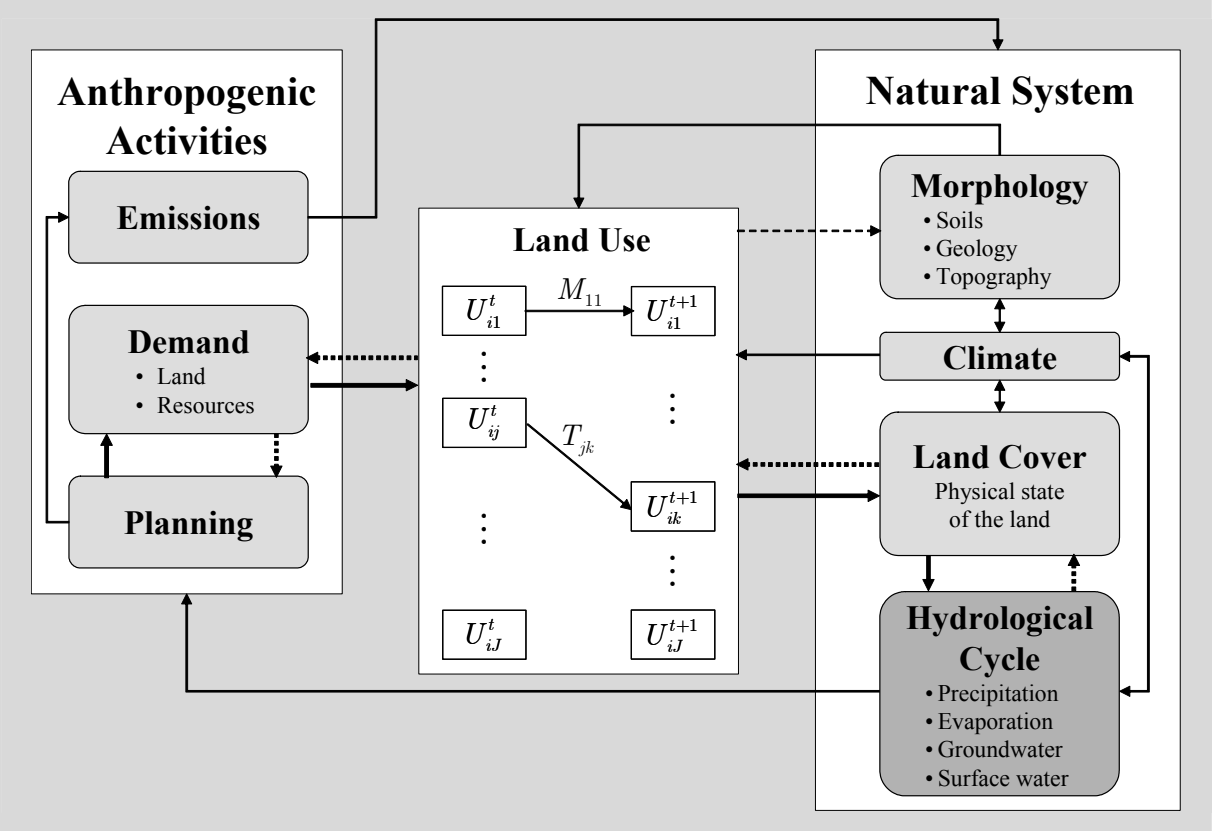

Figure 1.1 Interactions between anthropogenic activities and the natural system.

Land is one of the essential production factors for almost all human activities, such as: agriculture, mining, forestry, manufacturing, energy generation, water catchment and storage, transportation, settlement and recreation. However, it is a finite resource whose use is constrained by either Nature (i.e. vegetation -land cover-, soils, topography -slopes-, and climate) or human regulations (e.g. planning laws, property rights), or both (Turner et al. 1993).

Since the onset of the Industrial Revolution human actions rather than natural forces are the main source of change in the states and flows of the biosphere (Turner and Meyer 1994). As said before, most human activities demand land to be accomplished satisfactorily, hence, they constitute the proximate driving forces that maintain ($U_{ij}^t \rightarrow U_{ij}^{t+1}$) or transform ($U_{ij}^t \rightarrow U_{ik}^{t+1}$) a land use ($U$) category j to a category k in a given spatial unit i from time point t to time point $t+1$ (see Figure 1.1). According to Turner and Meyer (1991) and Stern et al. (1992) possible human driving forces can be grouped into six categories, namely: demographic factors, technology, level of affluence, political

structure, economic factors, and attitudes and values. These driving forces also change over time due to many reasons (e.g. economic cycles or population attitudes), hence, the transition rates from one type of land use to another may be influenced as well (see Figure 1.2).

In general, it is possible to state that the resulting land use in a given spatial unit i is the outcome of competing potential uses - seldom complementary to each other - under certain constraints imposed by land use planning laws, administrative systems, political institutions, property rights laws, market and culture (Rayner et al. 1994).

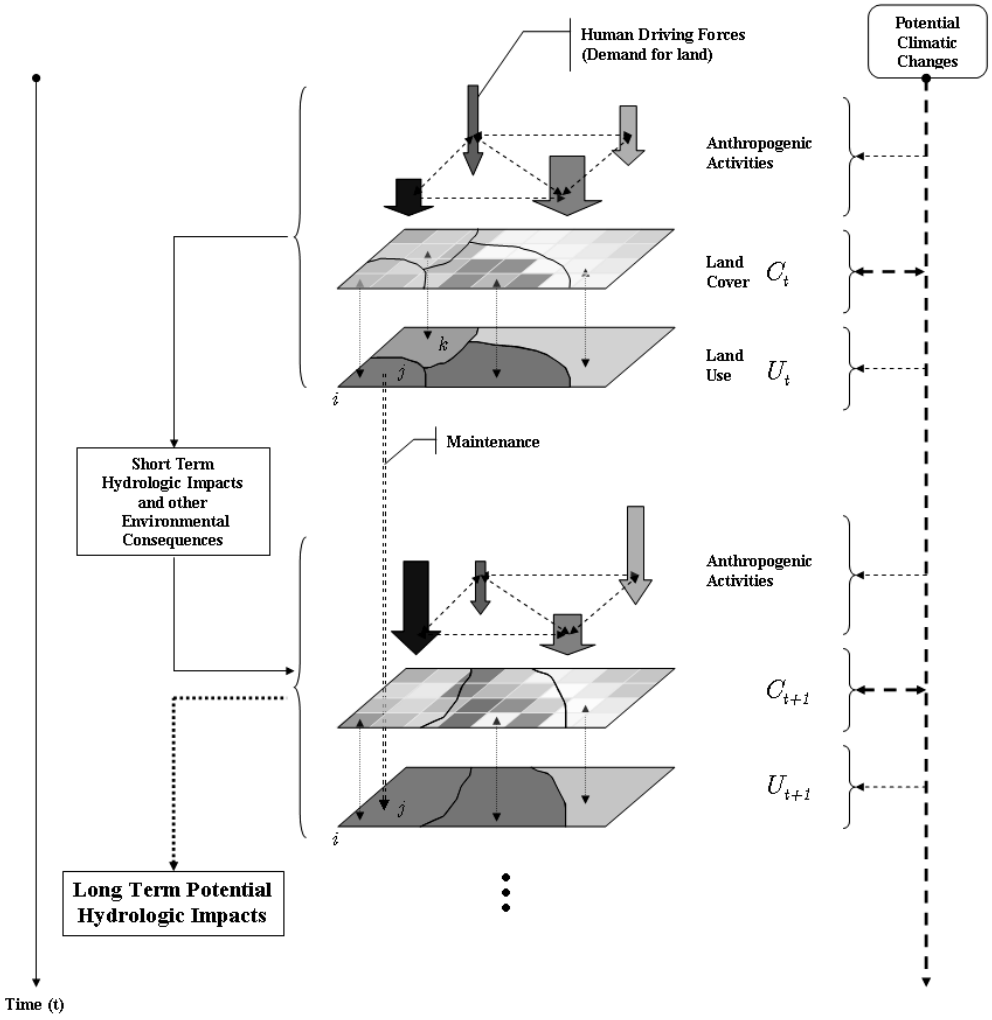

Figure 1.2 Mechanism of land use/cover changes induced by underlying human driving forces along the time axis.

Moreover, if the land use k in a spatial unit i and time t changes due to anthropogenic reasons to land use j in time $t+1$, then this change of land use will likely cause sooner or later a land cover change in the affected area of the spatial unit i, and conversely, a land cover category in this spatial unit may change to a different one even if the land use j remains unaltered during the same period as it is depicted in Figure 1.2.

The interactions between the atmosphere and the lithosphere involve exchanges of mass, momentum, and energy that are closely dependent upon the nature and structure of the earth's surface (Avisar and Verstraete 1990). At the global scale, atmospheric circulation is also affected by land cover changes as

has been shown by recent applications of the state-of-the-art global circulation models (Henderson-Sellers 1990, 1992, 1993 and Foley et al. 1998). A feedback effect of such distorted circulation patterns is the alteration of the global precipitation distribution, which, in turn, may alter the actual vegetation coverage and the existent land uses (Salati et al. 1979).

As shown in Figure 1.2 land cover changes may have a large scope of influence in space (at micro, meso, or at macroscale) and time (short term or long term). Changes of land cover often occur at microscale (e.g. at parcel level) with no apparent impacts in the climatic and/or the hydrologic regime of the basin (i.e. mesoscale) in the short term (Sartor 1998). Conversely, their *long-term-cumulative* hydrologic consequences will be only perceived at mesoscale (Reimold 1998). Consequently, land cover changes will occur in the future because it seems that nothing has been affected. This characteristic of the problem is what makes it difficult to be assessed and to be perceived by the population. It simply takes time to undermine the fragile water balance of a mesoscale basin. Those infinitesimal but cumulative impacts will be aggregated by the stream network (Cada and Hunsaker 1990) until someone realizes that they have been caused by anthropogenic activities, and eventually takes serious actions to stop them. Even if the rate of a land cover change is reduced to zero and some measures are taken to recover the original land cover, there is no guarantee that the original state will be reached again. By the time the measures are taken, there may be a number of irreparable damages on the basin, for instance a river bed will be deepened by erosion, hillslopes will have lost large quantities of valuable fertile soil, and the micro climatic regime of the basin may have changed, among others.

It is known that "*streams and rivers serve as integrators of terrestrial landscape characteristics and as recipients of pollutants from both the atmosphere and the land*", hence, rivers are good indicators of cumulative impacts (Cada and Hunsaker, 1990). Cumulative impacts, according to Dickert and Tuttle (1985) are "*those that result from the interactions of many incremental activities, each of which may have an insignificant effect when viewed alone, but which become cumulatively significant when seen in the aggregate. Cumulative effects may interact in an additive or a synergistic* (sic!) *way, may occur onsite or offsite, may have short-term or long-term effects, and may appear soon after disturbance or be delayed.*" Land cover change is a good example of cumulative impacts.

Finally, the long-term impacts of the hydrological cycle will eventually have feedback effects on the demand for land and the land use. The correctives of the misdoings can only be addressed by applied research and integrated planning.

1.2 The Complexity of Modelling the Water System at the Mesoscale Level

In the hydrologic cycle, water passes through the hydrosphere, the lithosphere and the atmosphere driven by two external energy sources: the thermal radiation emitted by the sun and the gravity force. The former is responsible for evaporation and condensation, and the latter for precipitation, infiltration, and runoff. It is a process with no beginning or end, and it has been present since the beginning of the earth's atmosphere and will be present until this ceases to exist. This does not mean

that this process has been stationary; the weather and climate of the earth have fluctuated dramatically over time, mainly due to very long periods of cyclical deviations of the Earth's orbit that are collectively termed the *Milankovitsch cycle* or due to extraordinary natural events. However, the basic functioning of the system has remained the same.

The hydrologic cycle within a drainage basin has been defined as a sequential, dynamic system in which water is the major throughput (Chow, 1964). Due to the great complexity of the relationships among the components of the system it is very sensitive to alterations of its actual state. This means that unpredictable consequences may be triggered by small changes that occurred inside or outside the basin. For this reason, the water cycle is also considered as a stochastic process.

Why is this system so complex? The intricacy of the water cycle is not only a consequence of the intertwined linkages of the sub-processes involved such as physical, biological, and geological ones, but also due to the large range of time and spatial scales at which the feedback mechanisms operate (Savenije 1995). On top of that, another continuous cause for disruption of the system has appeared - the anthropogenic activities - which, as was explained before, will convert and/or modify the land cover.

Since the present study deals with mesoscale catchments, the global scale atmospheric processes governing the circulation of large amounts of moist air from the sea to the continents will not be considered. Therefore, it is assumed that the influx of moist air that will eventually condensate and precipitate in a mesoscale basin are controlled by the macroclimate.

The functioning of the system within the basin can be summarized as follows. The moist air originated outside the boundaries of a given basin, plus that originated due to evapotranspiration within such basin, will precipitate to the basin's surface in the form of ice, snow or rain. Part of this precipitation will evaporate before even reaching the surface due to the activity of the sun. Effects of land cover changes will operate at this stage since land cover determines surface roughness, albedo[2], and latent and sensible heat flux, variables which, in turn, are related to wind speed, air temperature at the surface, and hence, with the evaporation process (Savenije 1995). When the rest, called net precipitation, reaches the earth's surface, it may face four alternatives in general. Either it hits bare soil, a surface covered by vegetation, impervious materials or a water body.

The paths for a drop of water which reaches a part of the earth's surface covered by vegetation are twofold; either it is intercepted by the canopy, or it passes trough the gaps in the canopy without being intercepted and finally reaches the earth's surface. If a drop of water is in contact with the foliage it can be either evaporated or rundown the tree trunk and become stemflow, and then eventually reach the earth's surface.

Once a drop of water reaches the earth's surface composed of either soil or a semi-permeable material the long process of infiltration and percolation to the underground will begin only if the upper soil

---

[2] A measure of the reflecting power of a nonluminous body, such as the surface of a planet, expressed as the ratio of energy reflected in all directions to total incident energy (Chambers Dictionary of Science and Technology).

horizon has not reached the soil's water holding capacity, in other words, if it has not reached its saturation level. If the opposite takes place the remaining net precipitation will be converted into surface runoff.

The fraction of water that reaches the upper soil horizon can be evaporated by the vapour pressure gradient between the earth's surface and atmosphere, and the wind profile, or it can be evaporated by the action of the plant physiology (evapotranspiration). Vegetation plays also in this stage of the water cycle a very important role because it is a key factor for determining the soil moisture in the root zone, which, in turn, governs the subsurface flow or interflow. Due to this reason bare soil is less permeable than vegetated soil (Savenije 1995).

Within the soil matrix and the underlying rock, very slow and complex processes will occur, namely: macro- and micropore infiltration and then deep percolation. Macropore infiltration is mainly governed by gravity, whereas micropore infiltration and deep percolation are governed by capillary forces (Bronstert 1995), which will lead water to percolate the rock stratum and hence to form groundwater reservoirs, or to the formation of subsurface flows which are responsible for maintaining the baseflow of streams and rivers.

If a drop of water reaches the earth's surface covered by impervious materials, mostly all net precipitation will be rapidly transformed into surface runoff, the rest will be evaporated. In such a case, a significant increment of the flooding hazard may be expected downstream from such locations. The effects of this land cover are twofold: the concentration time and the infiltration potential will be drastically decreased. As a result, groundwater recharge will be significantly diminished, too.

Eventually, the sum of all contributions of surface runoff and subsurface flows will become streamflow of a drainage system, and then, either be transported to the sea and then returned to the atmosphere due to evaporation, or be evaporated along the way to the sea. The same fate will befall the share of precipitation that has reached a water body. In this way the water cycle will continue forever.

Based on this short description of the water cycle, the following question can be stated: How can this complex system be analysed? In principle, there may be two different approaches, namely:

1. The first alternative consists in calibrating and validating a known rainfall-runoff model with past observations. Later, such a model can be used, for instance, to assess the impacts of land cover change based on future land use scenarios. The application of PRMS[3] in a municipal watershed in Ecuador by Samaniego (1997) is an example of this method. This technique, however, has many shortcomings that will be conveyed next.

   The state-of-the-art in hydrological modelling, either the conceptual type models such as HBV (Bergström and Forsman 1973), PRMS (Leavesley et al. 1983) or the physically-based and distributed-parameter models, for instance TOPMODEL (Beben, 1986), SHE (Abbott et al. 1986),

---

[3] PRMS "*is a modular-design, deterministic, distributed-parameter modelling system developed to evaluate the impacts of various combinations of precipitation, climate, and land use on streamflow, sediment yields, and general basin hydrology*" (USGS, 2002).

TOPOG (O'Loughlin et al. 1989), HILLFLOW-3D (Bronstert 1995), require temporal and spatially distributed data with high resolution in both domains. The main difference between these two modelling approaches lies in the fact that the conceptual models consider analogies to the perceived system's behaviour whereas the physically-based and distributed-parameter ones are based on the differential equations describing the phenomena.

Nevertheless, the existing generation of distributed models are really *lumped-conceptual models,* according to Beven (1989), because their governing equations are based on small scale physics, which then are applied at the mesoscale. Regarding data availability, only in ideal cases, after costly surveys, model parameters have been measured (Vertessy et al. 1993); generally, most of the existing models just determine these parameters during the calibration phase of the model because of the uncertainty and unknown heterogeneity associated with their spatial distribution (Abbott 1986, Refsgaard 1997).

It can be said in general that these models work satisfactorily for small and well-documented catchments, but would provide poor results at mesoscale basins due to the following reasons:

- Lack of data describing the spatial distribution of all variables employed in a model with a reasonable small uncertainty (Vertessy et al. 1993);
- The unknown spatial heterogeneity of parameter values at mesoscale (Abbott et al. 1986, Refsgaard 1997, Nandakumar and Mein 1997);
- The high risk of overparameterization during the calibration phase of the model (Bergström 1995); and,
- The inherent complexity of the system as to temporal scales and the stochasticity of the processes concerned (Savenije 1995).

Considering these limitations, it would be very difficult, if not impossible, to use existing rainfall-runoff models to assess hydrological impacts of land cover change (Nandakumar and Mein 1997).

2. The second alternative consists of using past data to derive empiric cause-effect relationships and linkages among observed variables. In this case, statistical methods or fuzzy rule-based modelling can be applied. This study will deal with this approach only.

1.3 Empirical Quantifications

There are, at the moment, many empiric relationships that have been used by soils scientists, engineers, and planners to assess the effects of land cover changes; unfortunately, their applicability is constrained by several facts:

1. They can be applied only for micro-catchments ($\ll 5\,\mathrm{km}^2$);
2. They are meant only to assess peak flows or total soil loss, and
3. Normally, their use would involve a high uncertainty when applied to mesoscale catchments.

Examples of such methods are, for instance, the SCS curve number method (USDA-SCS, 1985), the rational method, which is often employed in urban hydrology [Kuichling (1889) in Chow (1964)], or

the USLE (Wischmeier and Smith, 1978) among others. Therefore, such methods are not suitable for assessing the effects of land cover change at mesoscale basins.

1.4 Research Question and Objectives

Hitherto, there are still many important open questions regarding the issues discussed above. One of those questions that has strong implications to the planning system can be stated as follows:

> *How will a land use/cover change under certain geographic conditions affect a specific characteristic of the hydrological cycle and in what intensity?*

For example, if the settlement area at a certain location is expected to grow by one percent per year, how much will the flooding and/or drought hazards of those areas located downstream change in the future? If the answers to similar questions were known in advance, a planning authority might take adequate measures and employ land use restrictions to mitigate the future impacts of the forecasted land use changes.

In order to provide convincing answers to the question stated above, the following objectives shall be considered:

1. To develop a general methodology aimed at differentiating between the impacts produced by an exogenous macroclimatic change and those originating from anthropogenic activities,
2. To select and validate numerical models that quantify such impacts on several characteristics of the hydrological cycle at mesoscale level, and
3. To test these numerical models within the context of an integrated approach aimed at the assessment of the impacts of climatic and land use/cover changes on the hydrological cycle at mesoscale level.

Chapter 2

Foundations of the Study

2.1 Introduction

The role and importance of mathematical models in the planning field has been addressed by many authors (e.g. Forrester, 1969, Steiss 1974, Karlqvist 1978, Allen 1997). By simulating a part of "reality" or a *system*[1] using a set of rules and algorithms that mimic the behaviour and relationships of the observed data, a modeller may gain expertise, get a deep understanding of the underlining processes and their mutual interactions, forecast future trends, and estimate likely outcomes of plausible scenarios.

However, data availability must be "carefully considered" (Wilby 1997) before any modelling attempt is carried out. This implies that a *model*[2] should have variables that can be obtained or derived either from existing data bases or by direct surveying. This remark is of great importance when a model is projected to become a planning tool; in other words, it must avoid variables that cannot be estimated because there is a lack of technical capabilities, or their acquisition is too costly or, even worse, it is too complex or even impossible to acquire them. If these guidelines are not observed, a model, perhaps interesting from a theoretical point of view, would be unpractical and most probably misleading in the realm of planning. Due to the reasons stated above, it is worthy at the present stage of this research to have an overview of the relevant information available for the chosen Study Area.

---

[1] In general a system is "an orderly complex of elements and patterns constituting a functioning whole" (McArthur, 1992). More formally (based on Casti, 1984), let A be a set of abstract states (i.e. which occur in both space and time) of a natural system N and P be some range of potentially observed values. Then an observable of N is a mapping $x : \mathrm{A} \rightarrow \mathrm{P}$. "An observation, by contrast, is the concrete realization of an observable". Usually the potentially observed values are a subset of a n dimensional euclidean space, i.e. $\mathrm{P} \subset \mathbb{R}^n$. Then, "a natural system N comprises the sets A and P, together with a collection of observables $\{x_i\}$. In other words, a system N is defined by what we see, and the usual labels for systems, such as a 'national economy', a 'vibrating string', a 'chemical plant', and so forth, are interpreted only as conventions or labels introduced to account for situations where most observers are equipped to 'see' with the same set of observables, using the same sets A and P. Thus, by changing the sets or the observables, the same system N may be seen quite differently by different observers."

[2] A formal system M (i.e. a man-made construct composed of axioms, symbols, equations, and rules of logical inference) is called a model of N only if 1) it establishes a faithful correspondence between its elements and the observables $\{x_i\}$ and linkages of N; and 2) it can be used for describing N to a prescribed degree of accuracy (Casti, 1984). Moreover, if a model includes a set of rules describing the transitions from one state in time to another then it can be used for making specific predictions of N.

2.2 General Description of the Study Area

The Study Area is located to the south and southeast of Stuttgart, Germany. It comprises the upper catchment of the Neckar River upstream of the Plochingen gauging station (N3 530 930 and E5 396 740 m in Gauss-Krueger coordinates) covering an area of about 4002 km^2. The Neckar is a right-bank tributary of the Rhine; it is 367 km long and flows 40% of its course in direction north and northeast within the Study Area. The Upper Neckar Catchment (see Figure 2.1) is bounded by the north-western edge of the Swabian Jura on the right bank side of the Neckar and by the Black Forest on its left bank. Its elevation ranges from 240 to 1014 m.a.s.l. (from DEM LFU) and has a mean elevation of 546 m.a.s.l.. Slopes are in general mild; 90% of its area has slopes varying from 0° to 15°, although some areas in the Swabian Jura or in the Black Forest may have values as high as 50°.

The main geological formations in the Upper Neckar Catchment are originated in the Triassic and Jurassic periods, both corresponding to the Mesozoic Era. The main formations are composed of altered *keuper*, claystone-jura, claystone-keuper, limestone-jura, loess, sandstone and shelly limestone (*Muschelkalk*). Conversely, the river bed of the Neckar and its tributaries are relatively young compared with the previous formations. They are mainly composed of Quaternary sediments originated mainly from the erosion of outcrops of aforementioned rock types (Geyer and Gwinner 1991).

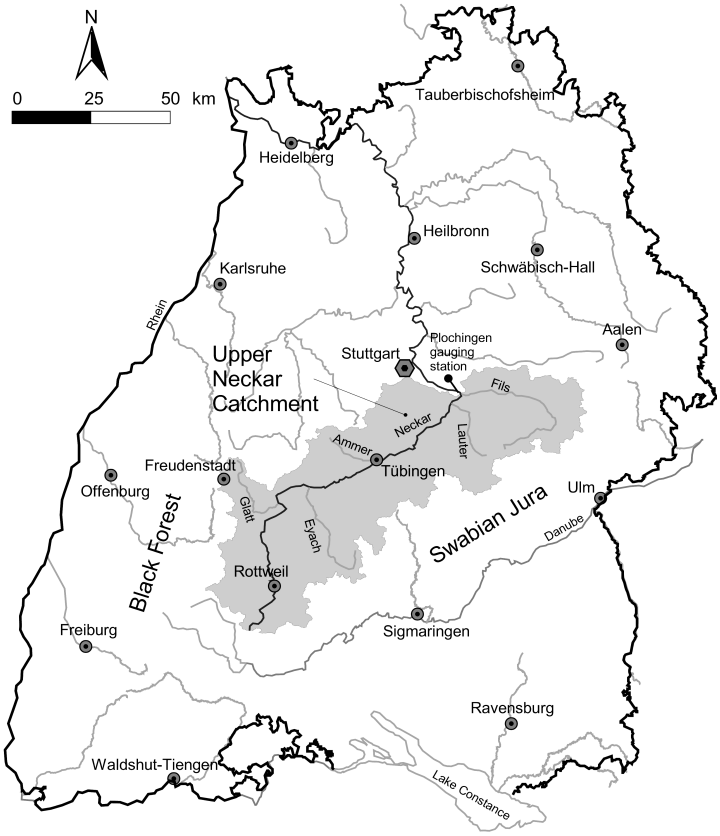

Figure 2.1 Map showing the location of the Upper Neckar Catchment within the State of Baden-Württemberg, Germany.

The climate of the Study Area can be classified as *Cf* according to Köppen's notation (1918), i.e. moist mid-latitude climates with mild winters. This climatic type is characterized by having warm-to-hot summers with generally mild winters, and it is wet all seasons. The coldest and hottest months in

the Study Area are January and July respectively. The daily mean air temperature in the former is about -0.8°C whereas in the latter is about 17°C according to the daily mean temperature readings available for the period 1961 to 1990 (DWD). Although the climate of the area is moderate, a maximum annual range of about 47.4°C has been observed in the past decades.

The annual variation of precipitation in the Study Area exhibits a multimodal distribution. Precipitation-events may arise the whole year round, the rainiest month being June and the driest one October, whose monthly means are 126 mm and 64 mm respectively (according to daily readings from 1961 to 1995, DWD). The mean annual precipitation observed during this period is 908 mm.

With regard to land use, the Study Area has endured rapid land use transitions from cropland or grassland to built-up area or industrial usages from 1960 to 1993. Among the principal driving forces behind these land use changes are the following:

1. The high level of affluence of the Stuttgart Region originated by the steady technological and industrial development during the last decades. According to recent information, the Greater Stuttgart Region is among the top ten richest regions of the European Union (GDP expressed in purchasing power standard, Eurostat 1996), and having a relatively low unemployment rate of 5.75% (SLA, 1996).

2. The excellent transportation infrastructure available in the region has contributed to improve the accessibility from anywhere in the countryside to all urban centres and vice versa. This fact together with the high income per capita of the region's inhabitants has modified the commuting behaviour of a large part of the population. This behavioural change is one of the reasons for the steady growth of car ownership in the region since 1974, at an average rate of 2.5% per year, whose absolute value rose up to 0.529 car/inh in 1997 (SLA) (see Figure 2.2).

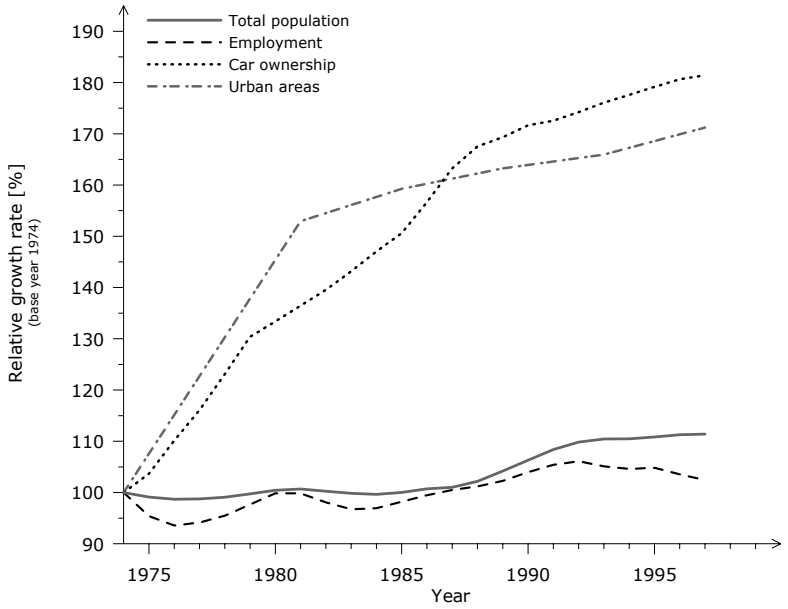

Figure 2.2 Relative growth ratio of population, car ownership, employment, and share of urban space (i.e. residential areas, commerce, manufacturing, and transportation) expressed in percentage. The base year for all indicators is 1974 (SLA).

As a direct consequence of that, a large part of the population would prefer to commute a long distance from home to work daily rather than a shorter one in order to have a dwelling with enough floor space located in a green, quiet, and peaceful environment where to live instead of a flat in a congested, noisy and crowded urban district. A further consequence of that is the rapid growth of floor space per capita in the past decades. This indicator increased in average from less than 15 m²/inh in 1950 to more than 38 m²/inh in 1997 (BBR 2000). In general, the demand for urban space, which includes transportation, commerce, and manufacturing, has grown 71% from its value in 1974, whilst the population has increased merely 11% in the same period.

3. Another driving force behind this phenomenon is in a lesser scale the population growth, especially its immigration component (from 1987 onwards, see Figure 2.2). As mentioned above, Stuttgart City as well as the counties located within the Study Area (i.e. Rems-Murr, Göppingen, Esslingen, Reutingen, Böblingen, Tüblingen, Zollernalbkreis, Freudenstadt, Rottweil, Schwarzwald-Baar-Kreis, and Tuttlingen) are ranked among those with the highest gross income per capita in Germany, namely, more than € 25 000/inh. in 1997 (Bundesanstalt für Arbeit in BBR 2000). This fact plus the very good living conditions in the region can be considered as proximate sources explaining the relatively high attractiveness of this region to immigrants.

The aforementioned land use changes of the Study Area have triggered a rapid land cover change as can be seen in Figure 2.3.

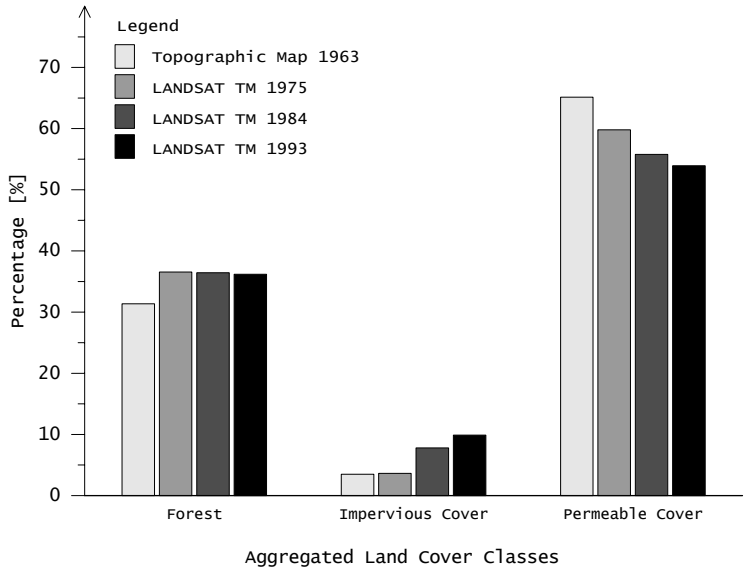

Figure 2.3 Land cover changes observed in the Upper Neckar Basin from 1960 to 1993. (Sources: for 1960: topographic maps of the area at scale 1 : 25 000 from LVA; for 1975, 1984 and 1993: LANDSAT TM scenes).

2.3 Conceptualisation of the Runoff Process at the Mesoscale Level

The hydrologic cycle within a drainage basin has been defined as a "*sequential, dynamic system in which water is the major throughput"* (Chow, 1964). This system is dynamic because it comprises several intertwined spatial phenomena, or processes, that are changing constantly over time. It is

sequential because there are inputs, an output, and a working fluid (i.e. water) called throughput passing through the system.

Based on the previous definition, and since one of the objectives of this study is to determine statistically significant variables representing the main processes involved in the system at mesoscale level, as well as their evolution over time; the available information has been divided, for analytical purposes, into two major categories, namely:

1. Inputs or explanatory variables, and
2. Output or explained variable.

In general, the complexity of the water cycle is due not only to the intertwined linkages of the physical, biological, and geological processes involved, but also due to the different temporal and spatial scales at which these processes interact. In addition to that, the water cycle can be disturbed from its normal behaviour by exogenous processes such as land cover changes, which are mainly caused by anthropogenic activities taking place within a basin. The spatial domain at which the water cycle spans varies from 10^{-8} m (at a molecular scale) to 10^{7} m (at a planetary scale). Nevertheless, the present study will only analyse the system at mesoscale catchments, i.e. those whose length ranges from 10^{2} to less than 10^{5} m, or whose area is greater than a few hectare but less than 5000 km^2 (Dooge, 1988).

Because of these reasons and others related with posterior analyses, the available input data has been further subdivided into three main subcategories, namely:

- **Physiographical factors**. This category comprises all those variables that can be regarded as constant or quasi-static since the period needed to appreciate a significant change has an order of magnitude greater than 10^{5} years. These factors comprise basin and channel characteristics mentioned by Chow, 1964. Among them are the following: 1) geological formations that constitute the basin's underground; 2) the basin's soil layers and their specific soils types; and 3) geometric factors of the drainage basin such as slope, aspect, shape, size, elevation, and drainage density. The symbol G symbolizes this subcategory.
- **Land cover types**. These variables have in general a slow changing rate over time (excluding some local exceptions, land use and land cover seldom change more than 5% per year, Robinson et al. in Meyer and Turner, 1998). The order of magnitude of a time interval necessary to perceive a significant change in their values varies from place to place, but in general, it would be ranging from 10^{0} to 10^{1} years. These variables stand for the observable consequences of anthropogenic activities happening within a basin. Land cover variables and their associated land uses are denoted by the symbol U.
- **Climatic or meteorological factors**. These variables are characterized by huge changes in their order of magnitude in very short periods of time. The period in which a significant change can be expected ranges from 10^{1} to even less than 10^{-4} years (Kleeberg and Cemus, 1992). In general, their behaviour exhibits some periodicity combined with partly chaotic and stochastic processes. This category comprises the following variables: precipitation, evaporation, solar radiation,

temperature, circulation patterns (closely related with relative humidity and wind velocity, among others). These variables are represented by the symbol M .

In the Figure 2.4, the main subcategories in which the input data has been subdivided as well as a simplified representation of the system's evolution along the time axis has been depicted. In this schematic diagram, the output of the system, or simply runoff, has been denoted by the symbol Q .

2.4 Spatial Units

Any integrated water management plan or related studies should be accomplished within a spatial unit called watershed (Singh, 1995). A watershed (originally from the German word *Wasserscheide*) is an "area with natural hydrological boundaries draining to a particular watercourse or water body". This spatial unit comprises the surface and ground waters, soils, fauna, and flora in the drainage basin, as well as humans and their anthropogenic activities (Reimond, 1998). In this study, 46 watersheds of various sizes are analysed, each one corresponds to the drainage basin at a geographic point i where a runoff gauging station is located (see Figures 2.4 and 2.5). These locations define the shape and size of a spatial unit. These points have been chosen because only there the outflow of a given watershed is measured continuously by State Agencies (e.g. LfU, DWD).

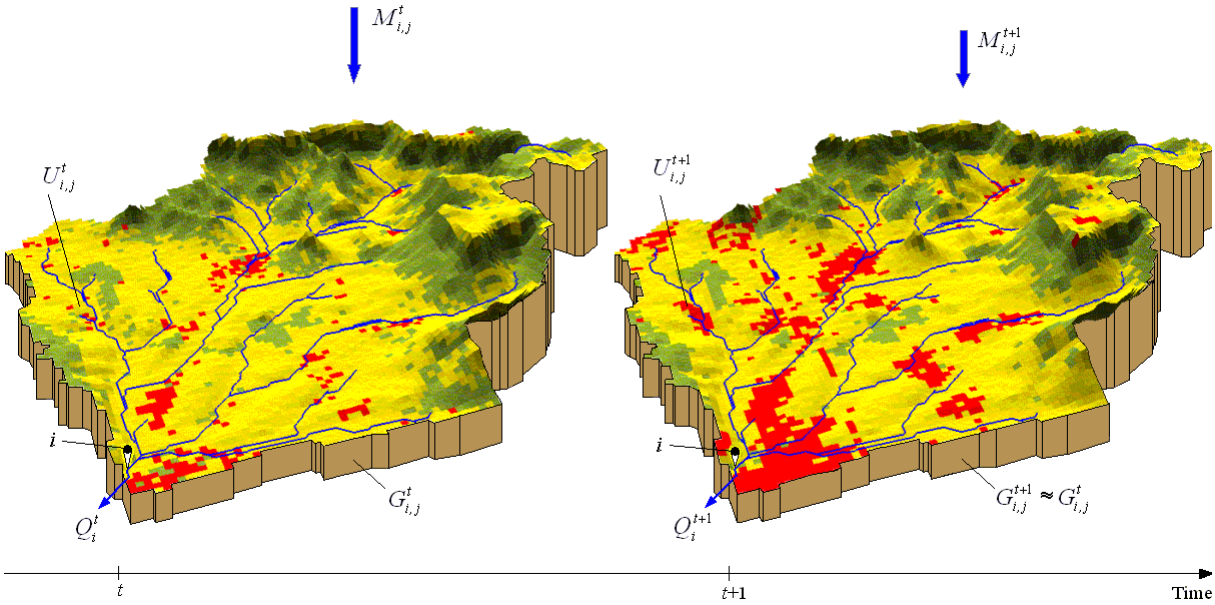

Figure 2.4 Schematic representation of the evolution of the system within a spatial unit i along the time axis t . The main inputs into the system are represented by the letters M (climatic factors), G (physiographical factors) and U (anthropogenic influences in the form of the land use/cover). The output is denoted by the letter Q (e.g. the total specific annual discharge in [mm]).

Figure 2.5 depicts the location of the stations within the Study Area and the delineation of corresponding subcatchments. Since the impacts of land cover change are cumulative (Dickert and Tuttle 1985), the delineation of the spatial units should be consistent with this phenomenon. Thus, a watershed draining to a point i should cover the watersheds of all those stations located upstream from it (e.g. the watershed Nº 4 comprises the sub-catchments Nº 4 and Nº 30, see Figure 2.5). In the

Appendix 1, a correspondence table shows how the sub-catchments depicted in Figure 2.5 have been aggregated to shape each spatial unit.

The delineation of a watershed is based on the algorithm proposed by Jenson and Domingue (1988). This algorithm requires as input data a DEM free of "sink holes". This means that the DEM has to be corrected in advance to ensure that a given drainage basin must have a single pour point, which normally corresponds to that one with the lowest elevation. Using this "corrected" DEM the delineation algorithm calculates the flow direction and the flow accumulation for each cell of the DEM. Based on this additional information, a watershed of any given point within the DEM can be obtained. The boundaries for the 46 watersheds were estimated by means of this procedure.

In order to validate the polygons that enclose the 46 watersheds, their areas were estimated and then compared with the official drainage area for the corresponding gauging station (hydrological yearbooks LfU). The results are very satisfactory as can be seen in Figure 2.6.

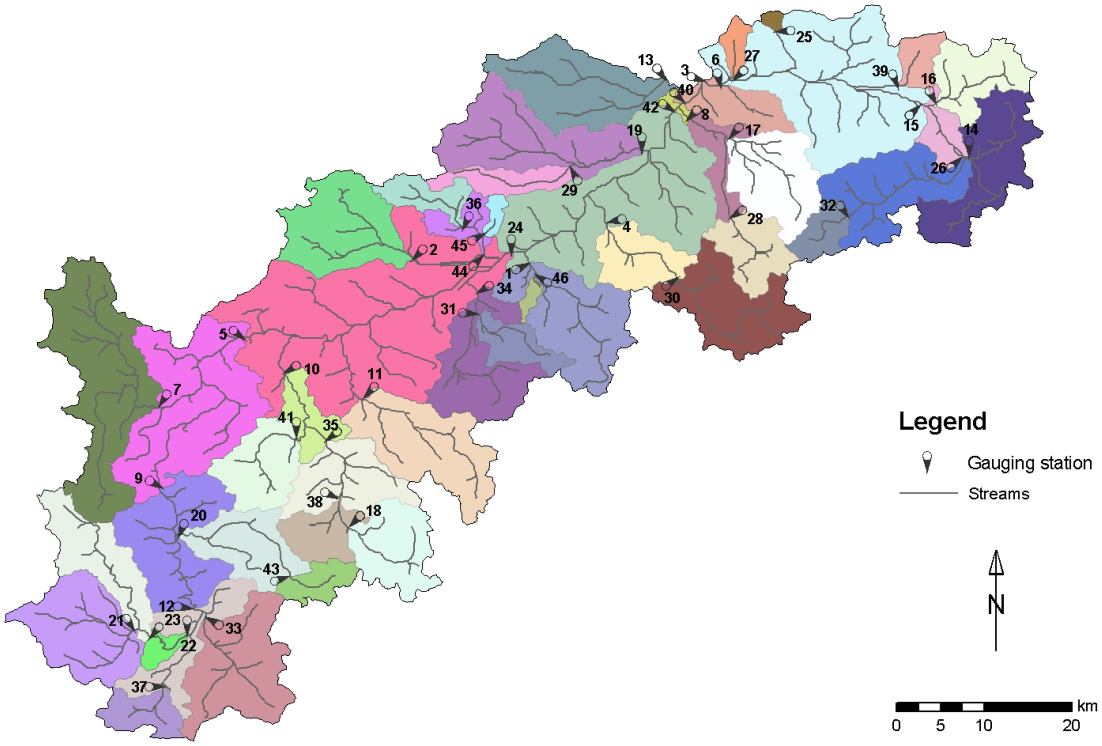

Figure 2.5 Subcatchments and stream network delineated from a corrected DEM (30×30 m, LfU).

2.5 Physiographical Factors

The physiographical factors considered in this study have been derived from different sources, mainly: 1) DEM available for the Study Area with a spatial resolution of 30×30 m (from LfU); 2) a digitized soil map of the State of Baden-Württemberg at the scale 1 : 200 000 (LfU-IER-ILPÖ); 3) a digitized geological map of the State of Baden-Württemberg at the scale 1 : 600 000 (LfU-IER-ILPÖ). A detailed explanation of the meaning, relevance, and calculation of these factors is given below.

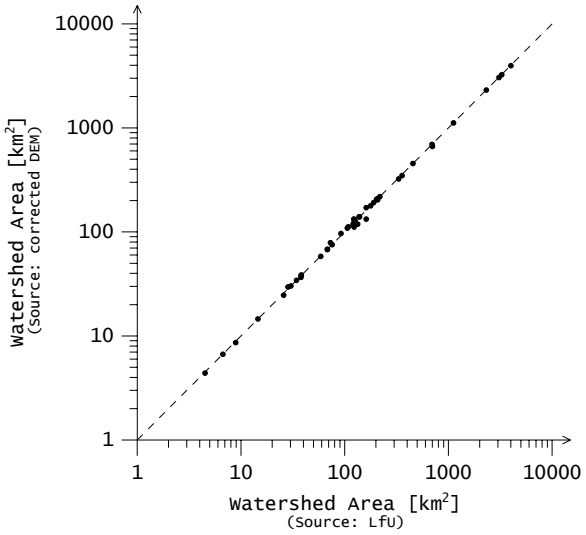

Figure 2.6 Comparison between the area of a given watershed estimated from a corrected DEM and its official drainage area (from LfU).

2.5.1 Basin's Area [km²]

According to the several studies conducted by Leopold and Miller (1956) and Hack (1957) among others, the area of a basin is positively correlated with its average discharge and inversely correlated with peak discharges (Dalrymple in Chow 1964). Because of this empiric evidence, the basin's area has been considered as a probable explanatory variable. Its estimation is as follows.

Let x_{i1} be the area of the spatial unit Ω_i in [km²]. A spatial unit Ω_i may be composed of one or several subcatchments as indicated in Appendix 1, hence its area is calculated as follows:

$$x_{i1} = A_i = \sum_{k \in \Omega_i} a_k \tag{2.1}$$

where

a_k is the area of a cell k (i.e. $30 \times 30\,\mathrm{m}^2 = 0.9 \times 10^{-3}\,\mathrm{km}^2$) that is fully contained within the spatial unit Ω_i.

2.5.2 Mean Slope [°]

Let x_{i2} be the arithmetic mean of the slope (i.e. gradient) in degrees of all cells k located within a spatial unit Ω_i. In general, the slope at a given point k is defined as the plane parallel to the topographic surface that is represented by an array of elevation points contained in the DEM ($\mathbf{Z}$). This plane can be mathematically represented as a vector $\vec{\mathbf{S}}_k$ that indicates the maximum rate of change in altitude. As a vector, it has two components, namely: 1) its magnitude called gradient or simply "slope", which is equal to the first derivative of the elevation z_k with respect to $\vec{\mathbf{S}}_k$; and, 2) its direction with respect to the North, or simply aspect ($\boldsymbol{\psi}$) (Burrough 1986).

In order to calculate the slope of a cell k, a plane is fitted by least squares to the elevation of its eight neighbours and itself. Then the gradient is estimated by the average maximum algorithm proposed by Burrough (1986). Finally, the mean slope within a spatial unit is

$$x_{i2} = \frac{1}{N_i} \sum_{k \in \Omega_i} \left\| \vec{\mathbf{S}}_k \right\|, \tag{2.2}$$

where

N_i is the number of cells within the spatial unit Ω_i

$$\left\| \vec{\mathbf{S}}_k \right\| = s_k = \tan^{-1}\left(\sqrt{\left(\frac{dz_k}{dx}\right)^2 + \left(\frac{dz_k}{dy}\right)^2} \right) \frac{180}{\pi} \ [°], \tag{2.3}$$

z_k is the elevation of cell k contained in the DEM [m], and

x, y the Cartesian directions of the reference system of the DEM [m].

The figure 2.7 shows the slope map s_k derived for the Study Area.

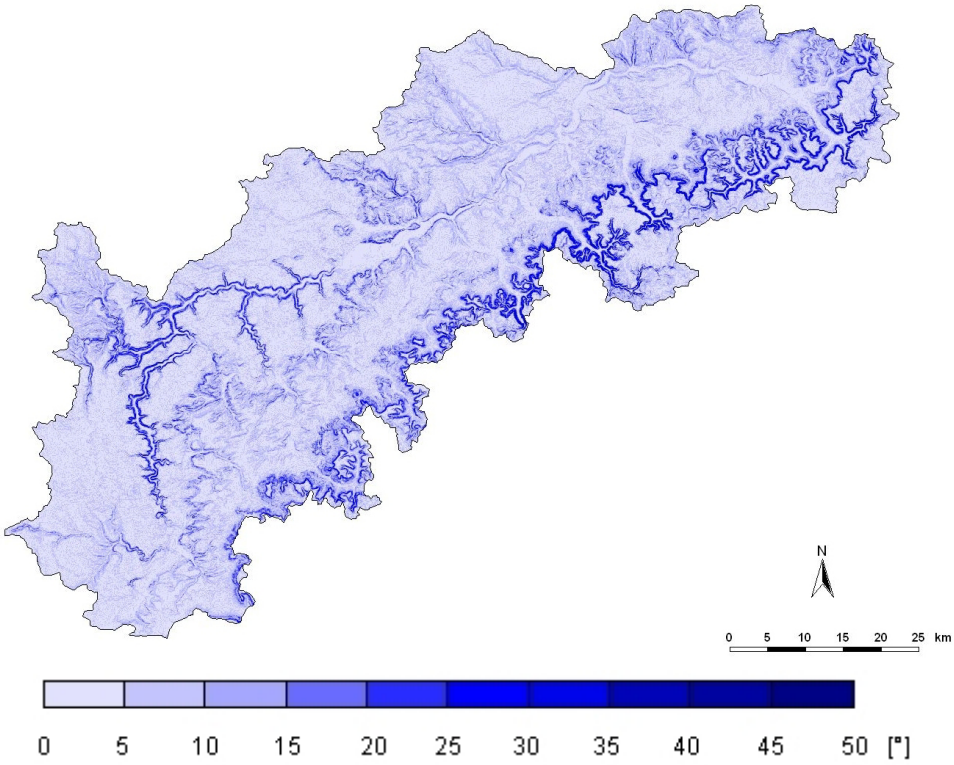

Figure 2.7 Slope map in [°] for the Study Area derived from a DEM (LfU).

2.5.3 Median of the Slope [°]

Non-linear problems generally have variables whose empiric probability density functions, or (PDFs), exhibit multimodal and skewed distributions. In such cases *the sample average is not a resistant*[3] *characterization of the centre of the data set* (Wilks, 1995). Instead of the arithmetic mean, other resistant measures of location such as the median or the trimmed means can be used. In order to estimate the median of the slope (s) in a spatial unit Ω_i the following definitions are needed. Let be $\{s_1, s_2, s_3, \ldots, s_k, \ldots, s_{N_i}\}_i$ the set of data containing the slope for each cell within a spatial unit Ω_i.

[3] A resistant method "*is not unduly influenced by small number of outliers or 'will data'* " (Wilks, 1995).

The same data set, but sorted in ascending order, can be denoted using parenthetical sub indices as $\{s_{(1)}, s_{(2)}, s_{(3)}, \ldots, s_{(k)}, \ldots, s_{(N_i)}\}_i$; where $s_{(1)}$ and $s_{(N_i)}$ represent the minimum and maximum slope values respectively. Based on this ranked set, the median can be defined as follows

$$x_{i3} = \begin{cases} s_{([N_i+1]/2)} & \text{if} \quad N_i \quad \text{is} \quad \text{odd} \\ \dfrac{s_{(N_i/2)} + s_{([N_i/2+1])}}{2} & \text{if} \quad N_i \quad \text{is} \quad \text{even} \end{cases} \tag{2.4}$$

2.5.4 Trimmed Mean of the Slope [°]

As mentioned before, another measure to obtain a robust and resistant measure of location with low sensitivity to outliers and extreme values is the trimmed mean. In the present study this indicator may play a significant role describing the water budget of a given basin because extreme slope values may come from both very steep slopes on mountainous regions and very flat areas such as water bodies. Both types of locations are not likely to have had a land cover change in the past, and hence their influence in the overall water budget of the given basin may be insignificant. In general, this variable can be calculated by

$$x_{i4} = \frac{1}{N_i - 2\rho} \sum_{k\,=\rho+1}^{N_i-\rho} s_{(k)} \qquad k \in \Omega_i, \tag{2.5}$$

where

ρ an integer equal to the rounded value of the product σN_i, and

σ the proportion of observations excluded from each tail of the data set $\{s_{(1)}, s_{(2)}, s_{(3)}, \ldots, s_{(k)}, \ldots, s_{(N_i)}\}_i$. In this case $\sigma = 0.15$, i.e. the 30 % extreme observations are excluded as a whole.

Another trimmed mean, i.e. x_{i5}, can be calculated using (2.5) but with $\sigma = 0.3$.

2.5.5 Mean Stream Slope [°]

Let x_{i6} be the arithmetic mean of the slope of all cells k belonging to the stream network $\mathcal{N}_i$ located within the spatial unit Ω_i, thus

$$x_{i6} = \frac{1}{N_{\mathcal{N}_i}} \sum_{k \,\in\, \mathcal{N}_i} s_k \qquad \mathcal{N}_i \subset \Omega_i, \tag{2.6}$$

where

$N_{\mathcal{N}_i}$ is the number of cells contained within the spatial unit Ω_i that belong to the stream network $\mathcal{N}_i$.

The stream network has been delineated based on the corrected DEM mentioned above. The delineation algorithm requires two additional grids, namely: the flow direction and the flow accumulation grid. The flow direction, which has also been derived from the DEM, defines for each cell k of the DEM the direction(s) in which the surface water may flow freely over the land surface. Using this additional information it is possible to calculate how many cells (or areas) are pouring into

a given cell k. This procedure is repeated for all cells within the Study Area and the result stored in the so-called flow accumulation grid Υ (Jenson and Domingue 1988). In order to have a stream with permanent flow of water over the year a minimum number of contributing cells is required. Such threshold is represented here with τ (Tarboton et al. 1993). Based on these definitions the stream network $\mathcal{N}_i$ can be defined as follows

$$\mathcal{N}_i = \left\{ \ (k) \ \middle| \ k \in \Omega_i \ \wedge \ \Upsilon_k \geq \tau \ \right\}. \tag{2.7}$$

The threshold $\tau = 300\,[\text{cells}]$ has been used in the present study following the recommendations of Tarboton et al. (1993), which corresponds to a drainage area of 27 ha. The stream network derived under these conditions is shown in Figure 2.8.

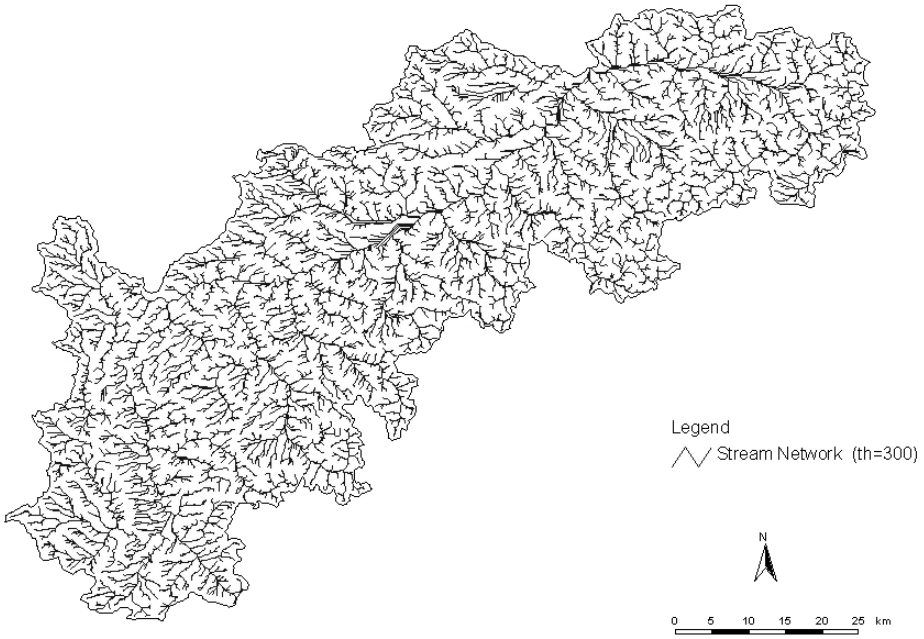

Figure 2.8 Drainage network of the Study Area derived from a DEM (30×30 m LfU) and a threshold value of 300 cells.

2.5.6 Mean Slope of the Areas Located at the Floodplains and Riparian Land of the Stream Network [°]

From previous research studies, it is known that floodplains and riparian land play a very important role in the hydrological cycle of a basin because they serve as potential reservoirs in case of extreme events; this is the reason why, apart from their high biodiversity, they are considered as very sensitive areas (Dalrymple in Chow 1964), and are often protected by law. Unfortunately, this is not always the case as the historical evidence points out (Meijerink and Mannaerts in Schultz 2000). In fact, many land cover and land use changes happened in these zones in the Study Area during the last 40 years as is depicted in Figure 2.9.

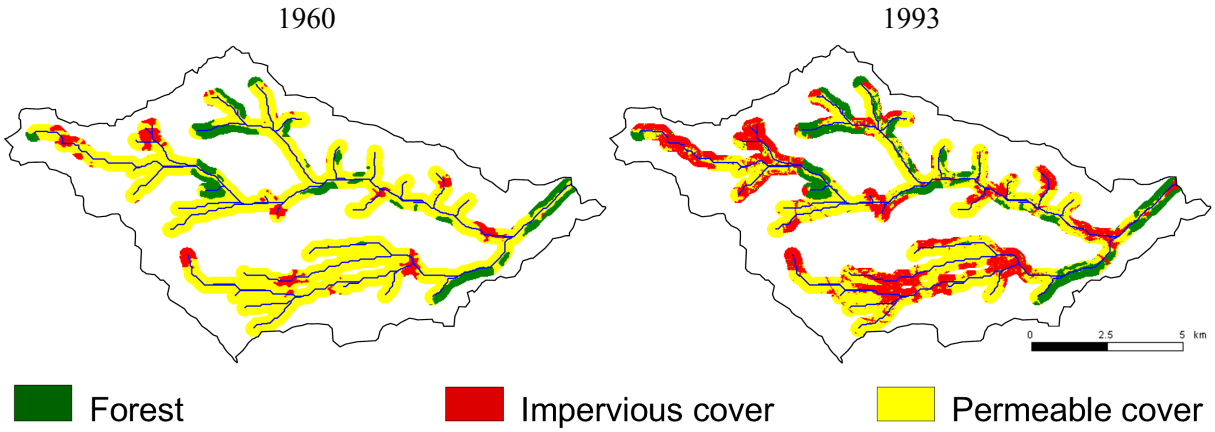

Figure 2.9 Sample of land cover and land use changes along floodplains and riparian zones along the main streams of river Körsch.

Based on these premises, it is reasonable to presuppose that if the land cover and the land use of those sensitive areas have changed in the past, the mean slope where these changes took place would have influenced the overall water budget of the basin; hence, they have been evaluated to estimate their expected influence.

Let x_{i7} be the arithmetic mean of the slope of all cells k located within the floodplains and riparian zones $\mathcal{B}_i$ belonging to the spatial unit Ω_i. Based on this definition this variable can be estimated as follows

$$x_{i7} = \frac{1}{N_{\mathcal{B}_i}} \sum_{k \in \mathcal{B}_i} s_k \qquad \mathcal{B}_i \subset \Omega_i \,, \tag{2.8}$$

where

$N_{\mathcal{B}_i}$ is the number of cells contained within the spatial unit Ω_i that belong to the riparian zones and floodplains $\mathcal{B}_i$ of the stream network $\mathcal{N}_i$.

The floodplains and riparian zones for each stream located within a spatial unit Ω_i have been defined using a simple concept, i.e. a cell k belongs to $\mathcal{B}_i$ only if its Euclidean distance from it to the closest cell belonging to the stream network $\mathcal{N}_i$ is less than or equal to the threshold δ [m], whose value in the present case is $\delta = 150$ m. The latter definition can be written formally as follows

$$\mathcal{B}_i = \left\{ (k) \,\middle|\, k \in \Omega_i \quad k^* \in \mathcal{N}_i \quad \wedge \quad \left\| \mathbf{r}_k - \mathbf{r}_{k^*} \right\| \leq \delta \right\}, \tag{2.9}$$

where

$\mathbf{r}_k$ denotes the position vector of the cell k in geographic coordinates, and

$\mathbf{r}_{k^*}$ represents the position vector of the cell k^* whose distance to cell k is smaller than or equal to δ.

2.5.7 Drainage Density [km^{-1}]

There is empiric evidence showing that the drainage density of a given basin x_{i8} correlates with many variables governing its water budget. This variable, originally introduced by Horton (1945) and complemented later by Melton (1958), is a function of climate, vegetation, rock and soil types, i.e. the

composition of the geological strata, rainfall intensity, infiltration capacity and relief are related with this variable. Strahler (in Chow 1964) also proposed that the drainage basin is a function of the runoff intensity (the volume rate of flow per unit of area of cross section), an erosion-proportionality factor, relief -which represents the potential energy of the system-, density of the fluid, and gravity. Carlston (1963, 1966) found that the drainage density has a negative correlation with the basin's base flow and a positive correlation with the mean annual flood.

The drainage density should consider all streams with permanent flow located within a given basin (Chow, 1964), as has been shown in Figure 2.8. This variable is estimated by

$$x_{i8} = \frac{\sum_{o}\sum_{j} \ell^{i}_{oj}}{A_i}, \tag{2.10}$$

where ℓ^{i}_{oj} is the length of the stream segment j belonging to order o of the stream network $\mathcal{N}_i$.

2.5.8 Shape Factor [-]

This morphological indicator may influence stream discharge characteristics. According to Chow (1964) "long narrow basins with high bifurcation ratios would be expected to have attenuated flood-discharge periods, whereas rotund basins of low bifurcation ratios would be expected to have sharply peaked flood discharges". Due to this reason it is considered as a potential explanatory variable.

The shape factor of a given basin i, x_{i9}, is defined as the ratio between the catchment length squared and its area. The length of a basin (L_i) is by definition the distance from the basin's pour point to the furthest point located on its perimeter (Chow, 1964). Hence it is calculated as follows

$$x_{i9} = \frac{L_i^2}{A_i}. \tag{2.11}$$

2.5.9 Fraction of North- and South-facing Slopes [-]

The proportion of south-facing slopes in the Northern Hemisphere is linked with the daily amount of received solar radiation, and this in turn is linked with the potential evapotranspiration (PET), and air temperature of those places (Hamon 1961, Frank and Lee 1966, Swift 1976, Leavesley 1983 and 1995). Due to these reasons, the fraction of both north- and south-facing slopes should be considered as a potential explanatory variable at mesoscale.

In order to estimate the percentage of north- and south-facing slopes, the direction of each vector $\vec{\mathbf{S}}_k$ with respect to the north axis has been stored in an array called the aspect grid $\boldsymbol{\psi}$, which is shown in Figure 2.10.

The aspect is given by

$$\psi_k = \tan^{-1}\left(-\frac{dz_k}{dy}\Big/\frac{dz_k}{dx}\right)\frac{180}{\pi}[^\circ]. \tag{2.12}$$

The reclassification of all cells ($\boldsymbol{\psi}^*$) into north- or south-facing slopes has been done as follows

$$\psi_k^* = \begin{cases} 1 & \text{if} \quad 0° \le \psi_k \le 45° \ \vee \ 315° \le \psi_k \le 360° \\ 2 & \text{if} \quad 135° \le \psi_k \le 225° \\ 0 & \text{otherwise} \end{cases} \tag{2.13}$$

where ψ_k^* takes the value of 1 for slopes mainly toward the north, 2 for slopes mainly toward the south, and 0 otherwise. Then, the proportion of north-facing slopes x_{i10} within a spatial unit Ω_i have been calculated by

$$x_{i10} = \frac{\left|\left\{(k) \middle| \ k \in \Omega_i \ \wedge \ \psi_k^* = 1\right\}\right|}{N_i}. \tag{2.14}$$

In (2.14) the symbol $||$ denotes the cardinality of a given set, i.e. its total number of elements. Furthermore, the proportion of south-facing slopes is

$$x_{i11} = \frac{\left|\left\{(k) \middle| \ k \in \Omega_i \ \wedge \ \psi_k^* = 2\right\}\right|}{N_i}. \tag{2.15}$$

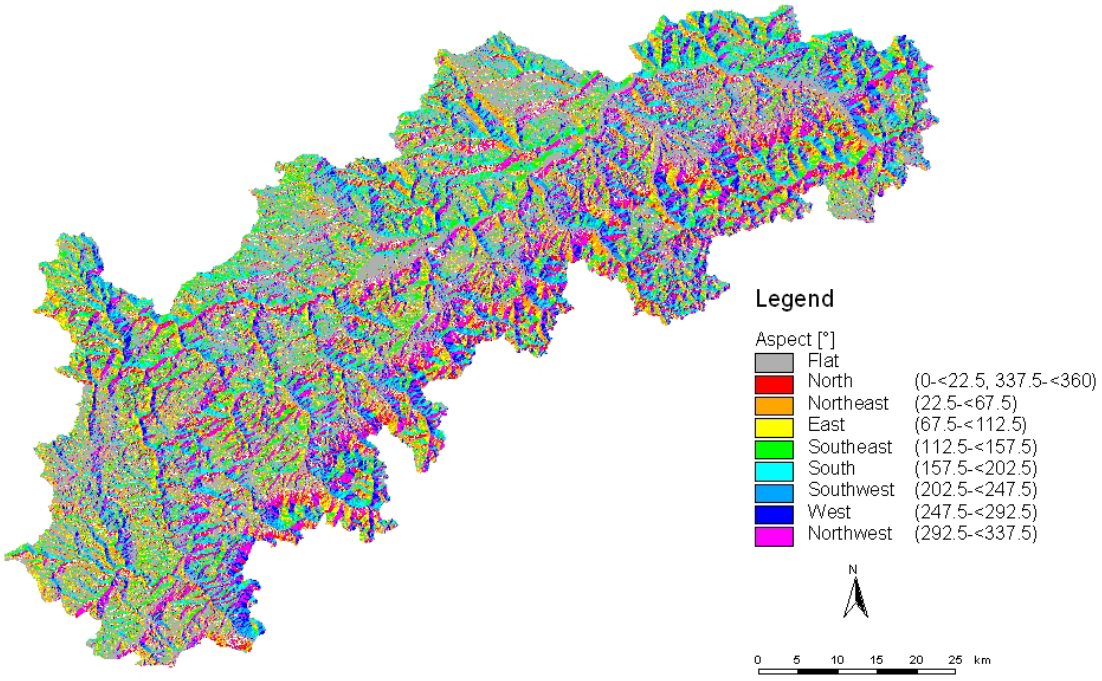

Figure 2.10 Aspects map in [°] for the Study Area derived from a DEM (30×30 m LfU).

2.5.10 Mean Basin Elevation and Difference between Maximum and Minimum Altitudes [m]

Both the mean elevation and the difference between maximum and minimum altitudes of a basin Ω_i are variables related with the potential energy of the system (Haggnett and Chorley 1969), as well as with the maximum air temperature and PET of the basin (Leavesley 1983). A number of validated models, for instance Hewlett and Hibbert (1967), Freeze (1974), Anderson and Burt (1978), and Beven and Kirkby (1979), have recognized the role of topography in determining areas of downslope movement of moisture, saturation-excess flow, and hence its influence in controlling throughflow

generation in a basin's hillslopes. Because of these reasons, the following indicators derived from a DEM shown in Figure 2.11 are considered potentially important explanatory variables.

Mean elevation has been estimated by

$$x_{i12} = \frac{1}{N_i} \sum_{k \in \Omega_i} z_k \,, \tag{2.16}$$

and the difference between maximum and minimum altitudes as

$$x_{i13} = \max(z_k) - \min(z_k) \quad k \in \Omega_i \,. \tag{2.17}$$

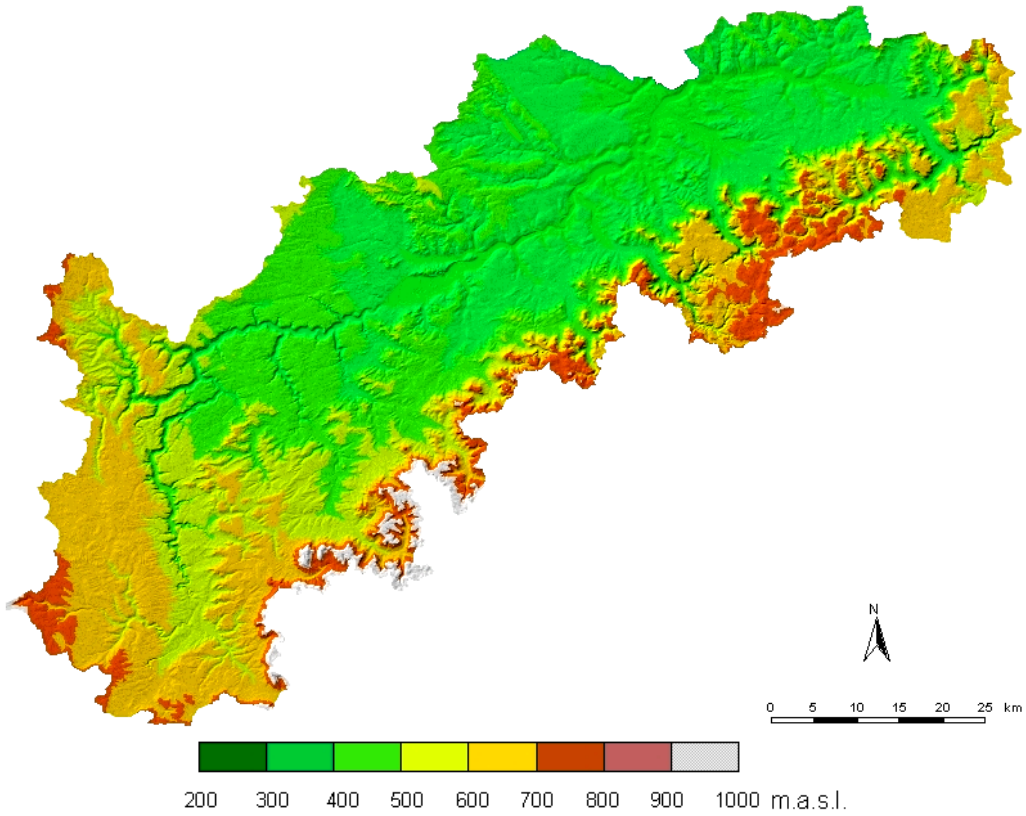

Figure 2.11 Topography of the Study Area represented by a DEM (LfU).

2.5.11 Fraction of Saturated Areas [-]

Many hydrological models (e.g. TOPMODEL or TOPLOG) assume that a wetness index based only on topography can be used to estimate the depth of the ground water table[4], which in turn, is a variable closely related with the runoff generation (Beven and Kirkby 1979, O'Loughlin 1981, Moore et al. 1991, Wolock 1993a). The most common and simple indicator, which is called the topographic index I_k, can be computed in the present case by

$$I_k = \ln\left(\Upsilon_k \frac{a_k}{c_k} \frac{1}{\tan s_k}\right). \tag{2.18}$$

[4] A water table by definition is the top of an unconfined aquifer, which correspond to a surface at atmospheric pressure defined by the level to which water will rise in a well (Chow, 1964).

Where a_k and c_k are the area and the size of the cell k (i.e. 30 m). In (2.18), the term $\Upsilon_k a_k / c_k$ represents the total upstream drainage area of the cell k per unit of contour, and $\tan s_k$, denotes the hydraulic gradient for saturated water flow (slope is expressed in radians). Υ_k is the flow accumulation grid as in Section 2.5.5. As a result of these calculations Figure 2.12, depicting a subcatchment of the Study Area, has been obtained.

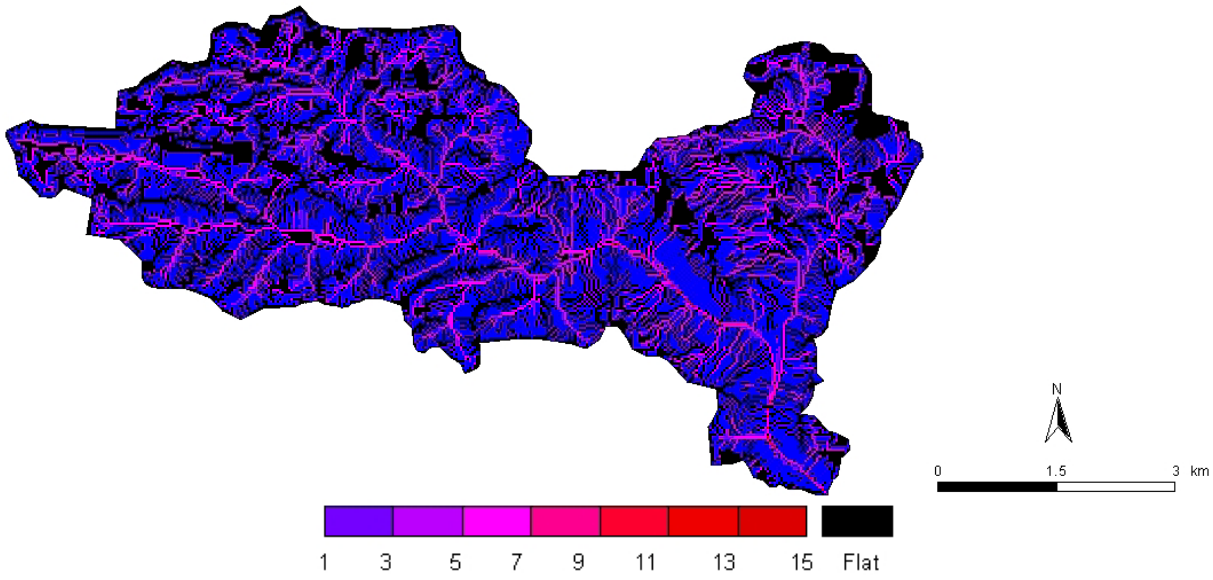

Figure 2.12 Topographic index derived according to the method proposed by Beven and Kirkby (1979) for the subcatchment No. 36 located in the Study Area.

Those areas of the catchment having higher values of the topographic index are prone to become saturated during a precipitation event, and hence, to contributing most to surface runoff generation (Beven and Kirkby 1979). Even though the topographic index has many shortcomings - for instance: 1) the amount of runoff generation depends not only on topographic characteristics, but also on the initial soil moisture and the soil type (Moore et al. 1991), and 2) the speed of the surface runoff would depend on the surface's roughness determined largely by the land cover - it would be interesting to investigate whether a relationship between the basin's discharge and the fraction of the basin's area prone to become saturated exists. Moreover, testing whether the land cover changes occurred on those areas with higher values of the topographic index would have influenced the discharge characteristics of the basin.

In order to compute the fraction of potential saturated areas (x_{i14}) within a given basin i only those cells having a topographic index greater than or equal to the upper quartile ($\mathrm{Q}_3 = \mathrm{P}_{75}$) of the empirical distribution function of the topographic index of a given spatial unit i would be taken into account. Hence, it is calculated by

$$x_{i14} = \frac{\sum_{k=\varsigma+1}^{N_i} I_{(k)}}{A_i} \qquad k \in \Omega_i, \tag{2.19}$$

where ς is equal to the rounding of $0.75 N_i$.

2.5.12 Mean Field Capacity [mm]

As mentioned in Section 1.2, a very important part of the water cycle takes place in the lithosphere. Hence, it would be reasonable to find out an observable that should be able to represent, at least partially, the important role of the soil matrix as a reservoir, and, at the same time, as a porous media where the subsurface flow would take place under the interaction of capillary and gravitational forces. Among many soil characteristics, the most commonly used are: field capacity, wilting point, and porosity.

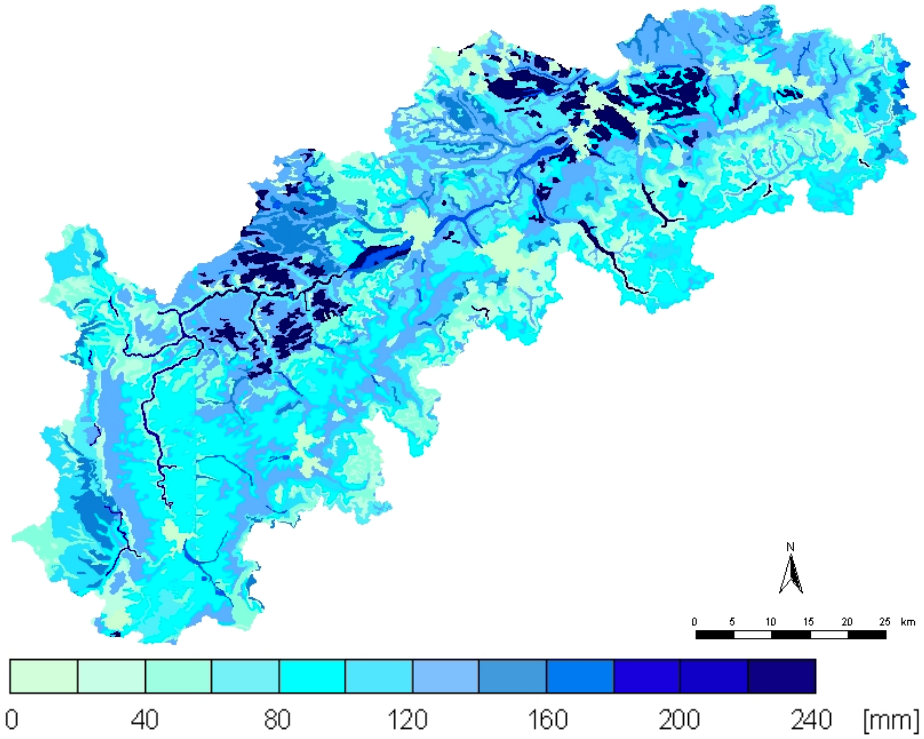

Figure 2.13 Main soil types and their associated field capacity in [mm] in the Study Area.

By definition, field capacity "is the amount of water held in a draining soil after gravity movement of water has largely ceased" (Ward and Robinson, 2000). Besides, it is intrinsically a soil type dependent characteristic. As a result of this soil water "constant", it can be stated, for instance, that catchments having mainly sandy soils would drain more rapidly than those having mostly clayish soils. Hence, the behaviours of such basins as to runoff generation would be different. Due to this reason, the average field capacity of the basin is considered as a potential explanatory variable, which is calculated as follows

$$x_{i15} = \frac{1}{N_i} \sum_{k \in \Omega_i} C_k \,, \tag{2.20}$$

where C_k is the observed field capacity in [mm] for a given cell k. The data used to estimate this indicator is shown in Figure 2.13 (LfU).

2.5.13 Fraction of Karstic Formations [-]

The kind of geological formations –along with their faults and interstices- underneath a given basin have a special relevance with regard to its water balance because they act as groundwater reservoirs

(i.e. aquifers), as well as pipelines for groundwater flow. The physical characteristics of a geological formation such as specific retention, specific yield, porosity and permeability would depend upon a number of factors, but in general, the materials that constitute them may be a determinant one (Ward and Robinson, 2000). This is the case when the underground is composed of limestone, a sedimentary rock full of fissures, sinkholes and caverns (i.e. karts) originated from groundwater flow erosion. Figure 2.14 shows the main geological formations of the Study Area (LfU).

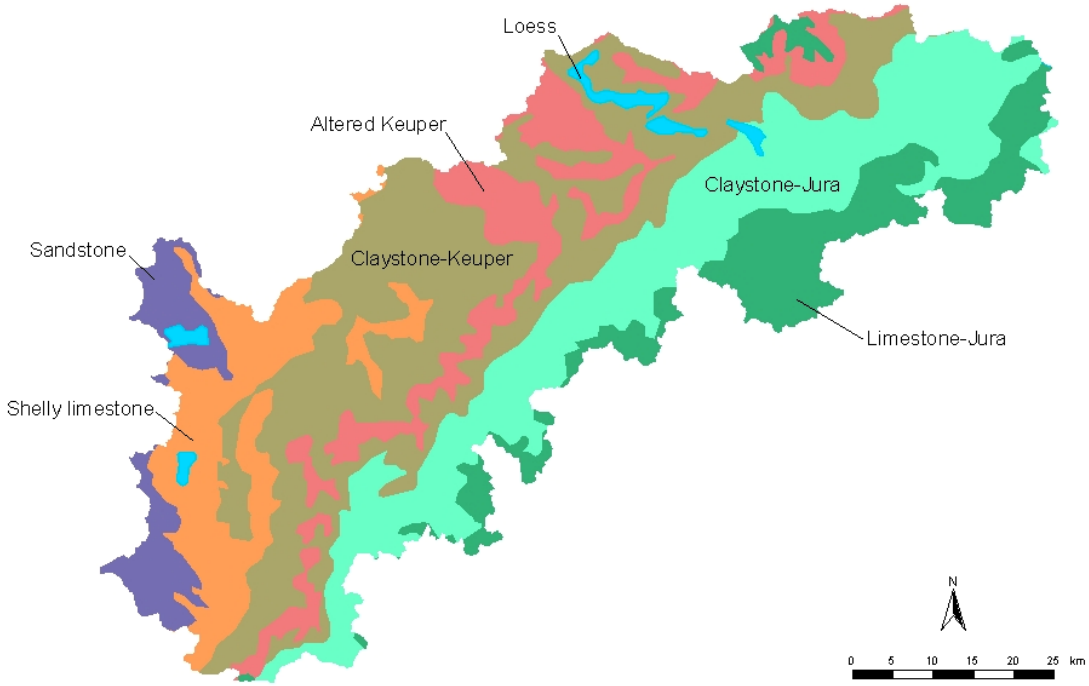

Figure 2.14 Main geological formations of the Study Area. The karstic formation corresponds to Limestone-Jura (LfU).

In general, a basin whose underground has large proportions of karstic formations would present huge abnormalities in its water budget, and thus in its discharge regime. Since such cases occur within the Study Area, the following indicator was developed to consider this fact, namely

$$x_{i16} = \frac{1}{N_i} \sum_{k \in \Omega_i} \mu_k \,, \tag{2.21}$$

where

$$\mu_k = \begin{cases} 1 & \text{if } k \in \text{karstic formation} \\ 0 & \text{otherwise} \end{cases} . \tag{2.22}$$

2.6 Land Use and Land Cover

From a hydrological point of view, land cover would be much more adequate than land use in the subsequent analyses since it is related with processes such as evapotranspiration, interception (canopy), and albedo; and with hydrologic parameters such as root zone depth and surface roughness that are governing processes such as the surface runoff and infiltration.

Due to these reasons, the land cover of the Study Area is to be estimated for successive points in time in the Study Area. Nevertheless, relationships between land use and land cover should be established in order to understand the system's behaviour under anthropogenic impacts.

In the present study, eight different land use categories disaggregated at a Municipality (*Gemeinde*) level have been obtained from the Statistical Office of Baden Württemberg (SLA) for the Study Area. They are called: forest, built-up and open areas, commercial use, industrial use, transportation, recreation areas, agricultural areas, water bodies and wetlands and 'other uses' (Flächenerhebung, SLA for the period 1981 to 1997). As a result of aggregating this information for the 216 municipalities comprised within the Upper Neckar Basin (i.e. the drainage area of the Plochingen gauging station; depicted with No. 3 in Figure 2.5) time series for each land use category have been obtained and depicted in Figure 2.15. These graphs clearly show the main land use changes that occurred within the Study Area in the last two decades, namely: agriculture has a steady negative average growth rate of about 0.48% per year whereas built-up, commerce, recreation, transportation, and water bodies and wetlands showed growth at average rates of 0.90%, 1.67%, 3.73%, 0.40% and 1.01% per year respectively. The category 'other-uses', on the contrary, abruptly declined with an average growth rate of about -2.32% per year. Moreover, forest, which had a period of fast growth from 1985 to 1993 (about 0.67% per year), reduced its pace to an insignificant 0.15% per year during the period 1993-1997.

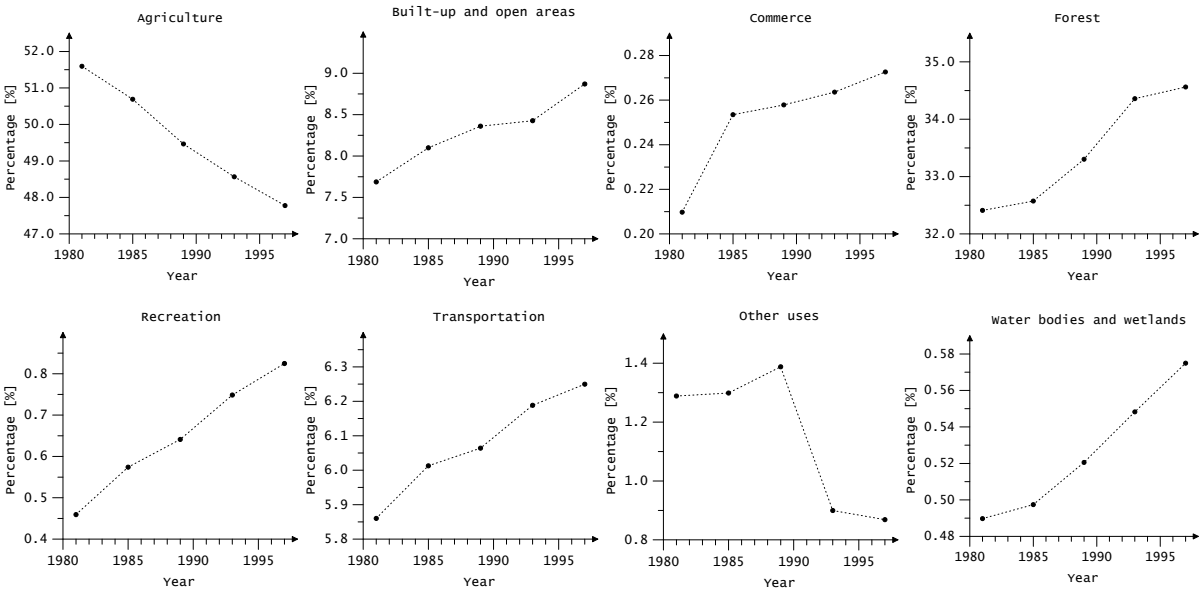

Figure 2.15 Land use time series in percentage for the Upper Neckar Basin from 1981 to 1997. These results were obtained by aggregating land use data for 213 Municipalities located within the catchment.

With regard to land cover categories, they were obtained from a classified LANDSAT TM scene for the State of Baden-Württemberg for the year of 1993 (IPF, 1995). This classification contains originally 64 sub-categories that were aggregated into 10 classes as is shown in Table 2.1 to ease the comparison between land cover and land use classes obtained from the mentioned data sources.

The land use and cover categories employed do not reveal a simple one to one relationship among them. This is due not only to the completely different gathering and surveying procedures, and spatial

resolutions, but also due to the different conventions of what a land use class represents. Therefore, to make these categories comparable, they had to be aggregated according to certain criterion. In the present case, according to the purpose of the study the following criterion was chosen: the aggregation procedure has to provide three land cover classes with remarkably different hydrologic responses, namely: forest, impervious areas and permeable areas (see Table 2.1).

Table 2.1 Correspondence of land use and land cover categories at the Municipal level.

Hydrologic Land Cover Category	**Land Use Survey (*Flächenerhebung*)**		**Classified LANDSAT TM 1993**	
Forest	F	Forest	DF CF MF	Deciduous forest Conifer forest Mixed forest
Impervious cover	BU C I T	Built-up area Commercial use Industrial use Transportation	DS SS I	Dense settlement Scattered settlement Industrial use
Permeable cover	R A O	Recreation areas Agricultural areas Others	G C V O	Grassland Cropland Vineyards Orchards

It was found that such aggregation fits very well at the municipal level as corroborated by Figure 2.16, especially with regard to forest and permeable cover. Quite the opposite, the area of impervious cover estimated by the land use survey often exceeds those values estimated by the LANDSAT. A plausible explanation of such a discrepancy comes from the fact that the land use survey data is based on the cadastral information, which has a very high spatial resolution whereas the estimates from the LANDSAT have a ground resolution of 30 m (only).

The definition of each land cover class adopted in this study is as follows:

Forest consists of areas covered by coniferous, deciduous, and mixed forest.

Impervious cover consists of areas covered by high and low density settlements, as well as industrial areas, airport runways, highways, and railway tracks. All of these categories have artificial drainage systems and their surface is totally or partially covered by asphalt, concrete, or any other sealing material.

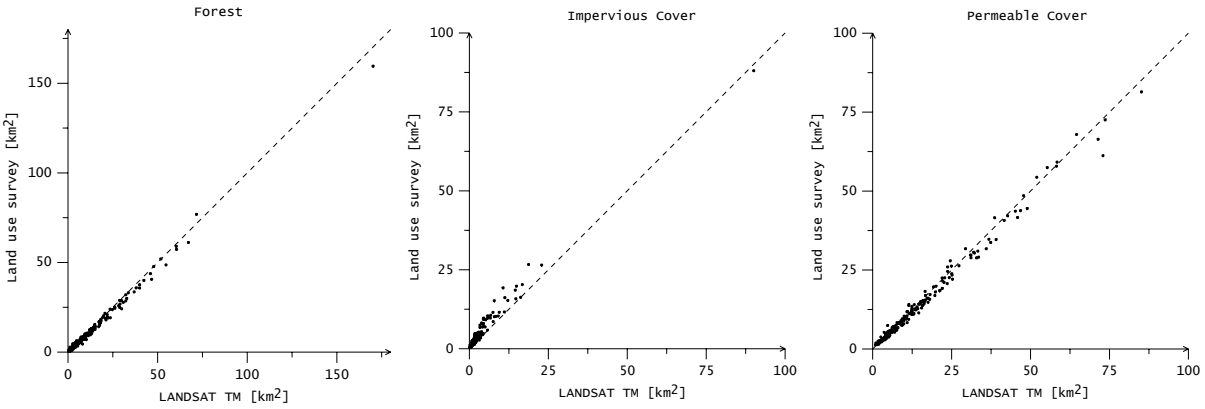

Figure 2.16 Comparison between the area of all municipalities within the Study Area for three different land cover types estimated from a classified LANDSAT TM image acquired in 1993 and data of the Land Use Survey in the same year (Flächenerhebung, SLA Baden-Württemberg 1993).

Permeable cover consists of areas covered by crops, grass, orchards, or a mixture of them, as well as wetlands and fallow lands. This category also includes the category water bodies (areas covered by rivers, lakes and reservoirs) which are negligible in the Study Area.

The land cover changes endured by the Study Area were estimated by means of a time series of land cover scenes consisting of one rasterised land cover map for 1960 and three LANDSAT scenes acquired in 1975, 1984 and 1993 respectively.

2.6.1 The Land Cover Time Series

The land cover in 1961

For the decade from 1961 to 1970 there is only one source of information that allows estimating the land cover in the Study Area, namely the topographic maps at scale 1 : 25 000 surveyed by the LVA during 1961 to 1963. These maps depict many kinds of vegetation and impervious covers that were aggregated and digitised in accordance with the definitions stated above. Forest corresponds in this case to three vegetation categories depicted in the topographic maps as deciduous forest, coniferous and mixed forest. Permeable cover consists of orchards, parks, vineyards, tree nursery, meadows, pasture, wetlands, moorland, quarries, and swampy areas. The rest, impervious cover, corresponds to what is categorised as settlements and transportation corridors. The resulted rasterised map is shown in Figure 2.17 (upper left). A subdivision in sub-categories is doubtful in this case since the reference maps do not allow such refinement.

The land cover in 1975

The state of the land cover in the Study Area during the decade from 1971 to 1980 was obtained from a LANDSAT TM5 scene acquired for 1975. This image was originally classified into 10 different land cover classes using a standard Maximum Likelihood Classifier with a spatial resolution of 50×50 m (LfU-IER-ILPÖ). In order to make compatible the land cover classes considered in this study with those of the original classification, the following reclassification and aggregation was conducted: a) forest comprises those areas originally classified as deciduous, conifer and mixed forest; b) impervious cover consists of scattered and dense settlements, industrial areas; and c) permeable cover contains grassland, arable land, vineyards-orchards and water bodies. The final land cover map obtained as a result of the reclassification is depicted in Figure 2.17 (upper right).

The land cover in 1984

The condition of the land cover in the Study Area during the decade between 1981 and 1990 is represented by a LANDSAT TM7 scene acquired for July 1984, with 7 spectral bands and a spatial resolution of 30×30 m (INS). In order to derive a land cover map from the raw data, it was first necessary to georeference it to the Gauss-Krueger coordinate system (UTM), and then to classify it into four land cover classes, namely: the three classes mentioned above plus water bodies. The reason for proceeding in this way is the diametric differences regarding the reflectance of the land cover categories defined before and water bodies. Had this not been done (i.e. performing the classification with three classes), the classifying rules would have been distorted, i.e. the land cover classes would have contained a number of misclassified pixels, thus affecting the overall classification accuracy.

After the classification was performed, the category -water bodies- was aggregated to permeable areas because of both its compatibility and insignificant overall share. In order to classify a satellite image, training and validation sites, as well as a classification algorithm are required. In this case, the unique sources for the former were the topographic maps and orthophotos available for the region (scale 1 : 25 000, LVA). Regarding the latter, a fuzzy rule-based classifier proposed by Bárdossy and Samaniego (2001) was used because its result, the land cover map for 1984 shown in Figure 2.17 (lower left), got the highest index of agreement (i.e. the lowest number of misclassified pixels) during the validation phase of the classification as compared with results obtained by standard methods such as maximum likelihood or unsupervised cluster-type classifiers.

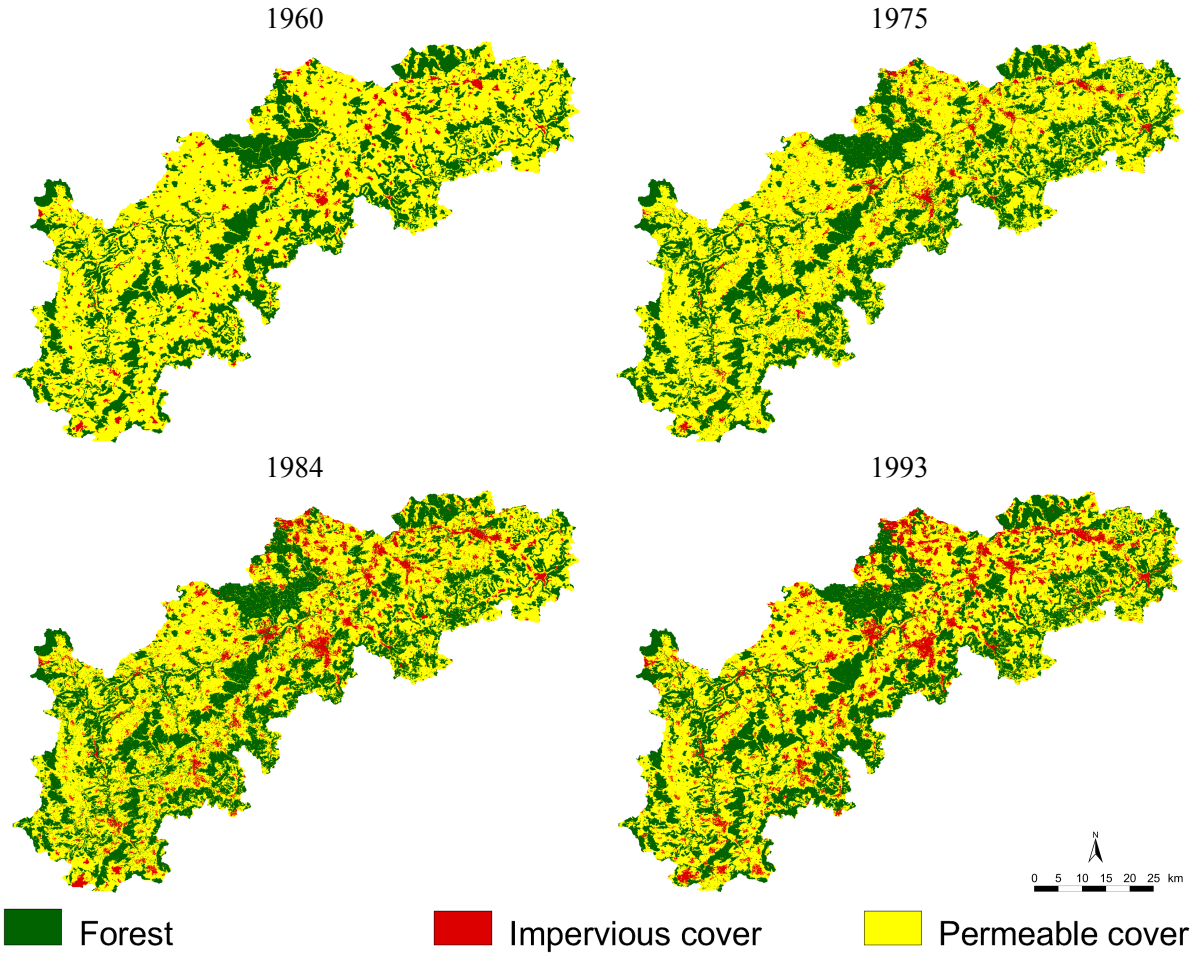

Figure 2.17 Time series of the land cover of the Study Area from 1960 to 1993. (LVA, LANDSAT).

The land cover in 1993

The last land cover map available for this study was a LANDSAT TM scene (IPK, 1995) with a spatial resolution of 30×30 m which originally classified its information into 16 classes containing 64 sub-categories. In order to fulfil the needs of the present study, the 16 original classes were aggregated as follows: a) forest, composed of conifer, deciduous, and mixed forest; b) impervious cover, composed of dense and scattered settlement, as well as of sealed industrial areas; and c) permeable cover, composed of the rest, namely: arable land, vineyards, intensive fruit production, fallow land, open areas (i.e. not sealed with no vegetation), intensive grassland, wetlands, extensive grassland

(dry), traditional orchards, and water bodies. The final result of this aggregation is shown in Figure 2.17 (lower right).

2.6.2 Fraction of a Given Land Cover [%]

In the present study, the proportion of a land cover category l in percent, in a given spatial unit i, and for the time t will be used as an indicator of the intensity of the land-atmosphere interactions (Section 2.6). Hence, the proportion of the spatial unit covered by forest ($l = 1$) can be computed by

$$x_{i17}^{t} = \frac{100}{N_i} \sum_{k \in \mathcal{L}_i} \mu_V^t(k), \tag{2.23}$$

where

$$\mu_V^t(k) = \begin{cases} 1 & \text{if} \quad V_k^t = l = 1 \equiv \text{forest} \\ 0 & \text{otherwise} \end{cases} \tag{2.24}$$

$\mathbf{V}^t$ Land cover image at point in time $t = 1961, 1975, 1984, 1993$.

$\mathcal{L}_i \subseteq \Omega_i$ A subset of the spatial unit Ω_i considered appropriate for the analysis.

In the same way, the fraction of impervious cover ($l = 2$) is estimated by

$$x_{i18}^{t} = \frac{100}{N_i} \sum_{k \in \mathcal{L}_i} \mu_V^t(k), \tag{2.25}$$

with

$$\mu_V^t(k) = \begin{cases} 1 & \text{if} \quad V_k^t = l = 2 \equiv \text{impervious} \\ 0 & \text{otherwise} \end{cases} \tag{2.26}$$

Finally, the fraction of permeable cover ($l = 3$) can be easily estimated by

$$x_{i19}^{t} = 100 - x_{i17}^{t} - x_{i18}^{t}, \tag{2.27}$$

since -by definition- the sum of the areas of the three land cover categories within a spatial unit i at any time t is always equal to A_i.

For the remaining points in time, i.e. for all t different from $1961, 1975, 1984,$ and 1993, a reasonable estimate for the proportion of land cover of a spatial unit i can be calculated by a linear interpolation of the closer upper and lower land cover observations since these variables are changing slowly over time.

The domain $\mathcal{L}_i$, where the previous functions are to be evaluated, will be chosen according to the necessities of the subsequent analyses. For instance, if $\mathcal{L}_i \equiv \Omega_i$, then previous variables will estimate the fraction of a given land cover type at basin level; whereas if $\mathcal{L}_i \equiv \mathcal{B}_i \subset \Omega_i$, these variables will estimate the same categories of land cover on the riparian zones of the stream network $\mathcal{N}_i$.

2.7 Climatic or Meteorological Factors

Climatic and meteorological factors are the most dynamic components of the basin's water cycle because of the intrinsic complexity and chaotic behaviour of the atmospheric processes governing the weather at the macroscale. In general, a time series of a climatic factor (i.e. an observable such as precipitation or temperature) is characterized by a combination of: 1) periodic variations (e.g. seasonal or cyclic oscillations); 2) gradual changes of the average (i.e. a trend); 3) sudden changes (e.g. a change in the climatic regime); 4) serial dependence (i.e. persistence or serial correlation); and 5) pure random component or noise (Chow 1964, Chatfield 1989). All these characteristics are to be considered during the estimation of the climatic factors as will be explained afterwards.

Since the water cycle exhibits an intrinsic seasonality -i.e. it behaves differently during summer and winter- and considering that the aim of the study is to filter out the likely effects of the land cover change from the climatic variations, the estimation of the climatic factors will be carried out for both "water seasons", namely: summer and winter. In the Study Area, summer, from a hydrological point of view, starts on the 1st of May and ends on the 31st of October, whereas winter spans from the 1st of November to the 30th of April.

Another reason why the climatic factors should be computed at annual or semi-annual intervals is related with the serial dependence among the observations of the climatic time series during the analysis. Serial dependence can be avoided if the autocorrelation $r(k)$ lies between the 95% confidence intervals given approximately by $\pm 2/\sqrt{T}$. Within such limits a time series can be considered as a random one (Chatfield 1989). Figure 2.18 shows the correlograms for the annual and daily precipitation time series for two catchments with different sizes in the Study Area. In the present study, the autocorrelation between observations a k apart from each other, of a time series $\{x_{ij}^1,\ldots,x_{ij}^t,\ldots,x_{ij}^T\}$ of an observable j in a given spatial unit i, during the period $t = 1,\ldots,T$, is given by

$$r_{ij}(k) \cong \frac{\sum_{t=1}^{T-k}\left(x_{ij}^t - \overline{x}_{ij}\right)\left(x_{ij}^{t+k} - \overline{x}_{ij}\right)}{\sum_{t=1}^{T}\left(x_{ij}^t - \overline{x}_{ij}\right)^2}, \tag{2.28}$$

where

$\overline{x}_{ij} = \frac{1}{T}\sum_{t=1}^{T} x_{ij}^t$ is the overall mean, and T is the number of observations.

2.7.1 Precipitation

Precipitation is a major factor governing the water balance of a region (Ward and Robinson 2000), hence its occurrence and spatial distribution are key elements to understand the water cycle at the catchment level. Since the complex mechanisms governing this phenomenon are a science of their own, they can not be covered in this study; instead of that, a statistical analysis will be used to predict the precipitation $p_k^t\ [mm]$ on each cell $k \in \Omega_i$ for every day during the interval $t \in [01.11.1960,\ldots,31.10.1993]$. For this analysis the spatial resolution of every cell is 300×300 m.

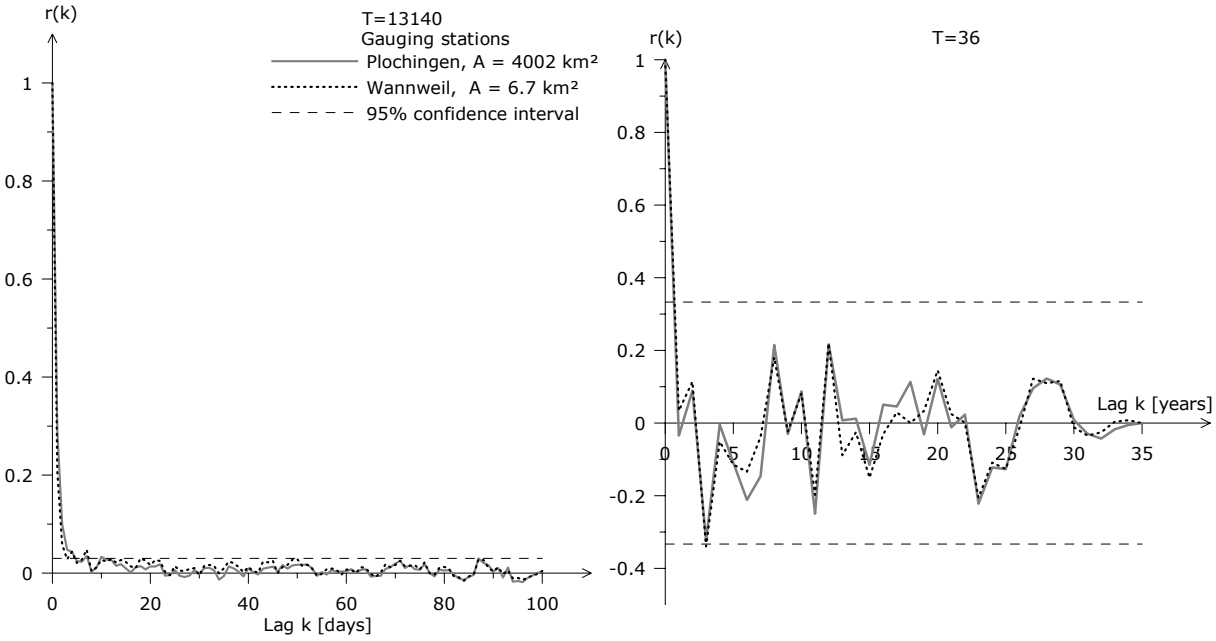

Figure 2.18 Correlograms of daily (left panel) and annual (right panel) precipitation for two basins with different sizes in the Study Area.

Thus, the goal is to estimate the spatial distribution of p_k^t based on daily raingauge records available for the 288 meteorological stations located both inside and in the surroundings of the Study Area (see Figure 2.19). Traditional interpolation methods such as the arithmetic mean, Thiessen-polygons, isohyetal, and inverse distance among others can be used, but they have the following shortcomings: either a) the spatial continuity is ignored or lost at longer distances, or b) their estimation error is not unbiased. Furthermore, additional information, for instance the variation of either the precipitation or the surface temperature according to the elevation (i.e. the orographic effect) can not be thoroughly considered.

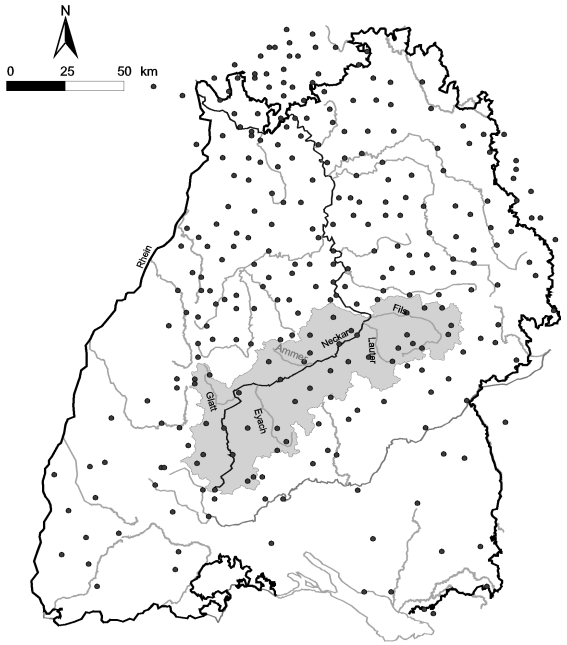

Figure 2.19 Meteorological stations located in the State of Baden-Württemberg and its neighbouring States used in this study (Source LfU and DWD).

Because of that, a geostatistical technique called External Drift Kriging[5] (EDK) (Ahmed and de Marsily 1987) using a DEM as additional information is to be used. This method estimates the value of a variable at an unsampled point, say p_k^t, from the neighbouring ones within the field of values. The variability within the field is assumed to be function of the distance and direction (Wilby, 1997), which is represented by a variable's variogram.

In practice, the variogram for a given variable has to be estimated from the available data (i.e. a sample), hence it is called experimental or sample variogram. In order to calculate it, the following definitions have to be introduced.

Let the regionalized variable precipitation $\{p_k^t : k \in \Omega_i \; t = 1,\ldots,\mathcal{T}\}$ be a realization of a random function $\{P_k : k \in \Omega_i \subset \mathbb{R}^3\}$. Based on this definition, and assuming that the "*intrinsic hypothesis"* holds, i.e. the expectation of this random function is constant all over the domain Ω_i and the variance of the increment of the random function P_k at two different locations, say $\vec{k}_l$ and $\vec{k}_{l'}$, depends only on the vector separating them, i.e. $\vec{h}$ (Bárdossy 1997, Chilès and Delfiner 1999), the variogram function can be defined as follows

$$\hat{\gamma}^t(h) = \frac{1}{2N_h} \sum_{\vec{k}_l - \vec{k}_{l'} \approx \vec{h}} \left(p_{k_l}^t - p_{k_{l'}}^t\right)^2, \tag{2.29}$$

where

$\vec{k}_l, \vec{k}_{l'}$ is the position vectors of raingauge stations l and l' [m],

$p_{k_l}^t$ is the observed precipitation in the raingauge station l in time t expressed in [mm],

N_h the number of raingauge stations separated by a distance $h \pm \varepsilon\,[\mathrm{m}]$,

ε a tolerance value in [m],

$\hat{\gamma}^t(h)$ the sample variogram for daily (or annual) precipitation in time t in [mm^2]

l $= 1,\ldots,\mathcal{L}$, an index denoting those points of the domain with known values of the random function (i.e. the raingauge stations in Baden-Württemberg and its surroundings, $\mathcal{L} = 288$),

t a time index. Only for the sake of simplicity, it may represent in this case either daily or annual precipitation.

As an example, Figure 2.20 shows the sample variogram for the annual average precipitation in the State of Baden-Württemberg obtained from the 288 raingauge stations depicted in Figure 2.19 during the period 1961-1995.

---

[5] Word coined in recognition of D.G. Krige, a South African mining engineer, who used for first time statistical methods to assess ore reserves in the early 1950s. Kriging, as a Geostatistical procedure was later formalized by G. Matheron in 1970.

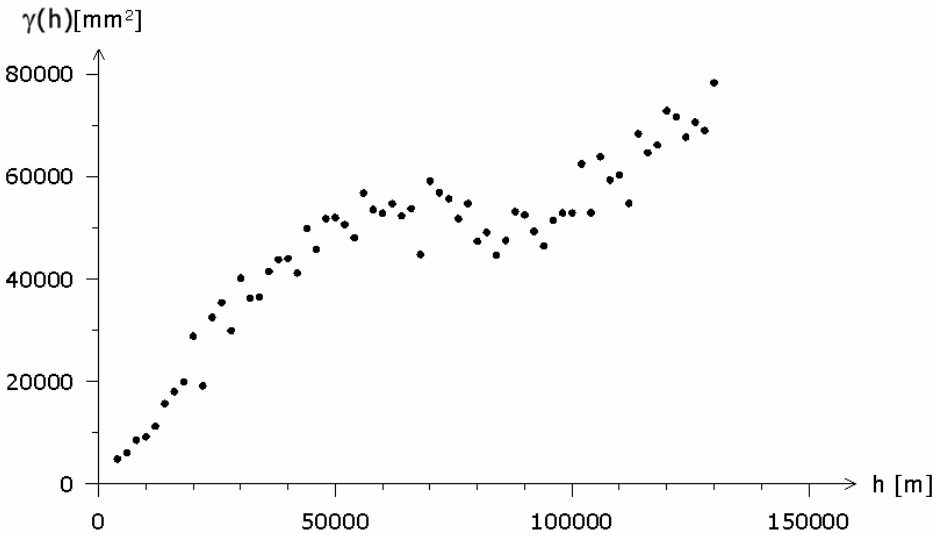

Figure 2.20 Experimental variogram for the annual average precipitation for the State of Baden-Württemberg.

Based on the sample variogram, a theoretical one $\gamma(h)$ suitable for the further analysis can be fitted using a robust method, e.g. L1 norm (Chilès and Delfiner 1999). In the present study, an isotropic theoretical variogram composed of a pure nugget effect and a spherical variogram was adopted for the daily precipitation based on a previous work carried out by Bárdossy et al. (CC-HYDRO, 1999). Its equation is:

$$\gamma(h) = \begin{cases} 0 & \text{if} \quad h = 0[m] \\ 0.02 & \text{if} \quad 0 < h \le 1[m] \\ 0.98\left(\frac{3}{2}\frac{h}{r_p} - \frac{1}{2}\frac{h^3}{r_p^{\,3}}\right) & \text{if} \quad 1 < h \le r_p = 40\,000[\mathrm{m}] \\ 0.98 & \text{if} \quad h > r_p \end{cases}, \tag{2.30}$$

where r_p is a constant denoting the range of the theoretical variogram for daily precipitation in [m].

A linear estimator for the precipitation $\hat{p}_k^t$ at an unsampled location k in time t can be obtained as a linear combination of all sampled locations by

$$\hat{p}_k^t = \sum_{l=1}^{L} \lambda_l^t p_{k_l}^t \,. \tag{2.31}$$

In order to determine the weights λ_l^t, the fitted variogram (2.30) as well as the supplementary knowledge available, i.e. that precipitation is related to the terrain's elevation (Gilman in Chow 1964), are to be used. The inclusion of this additional information implies a modification of the first assumption of the intrinsic hypothesis, namely: the expectation of p_k^t is in a linear relationship with the elevation Z_k, in other words

$$E\left[p_k^t \middle| Z_k\right] = c_1 + c_2 Z_k \quad \forall\, k \in \Omega_i \,, \tag{2.32}$$

where c_1 and c_2 are unknown constants.

Hence, the expectation of the linear estimator is

$$E\left[\hat{p}_k^t\right] = E\left[\sum_{l=1}^{\mathcal{L}} \lambda_l^t p_{k_l}^t\right] = \sum_{l=1}^{\mathcal{L}} \lambda_l^t E\left[p_{k_l}^t\right] = \sum_{l=1}^{\mathcal{L}} \lambda_l^t \left[c_1 + c_2 Z_{k_l}\right] = c_1 + c_2 Z_k\,, \tag{2.33}$$

which implies the following constraints for the weights, namely

$$\sum_{l=1}^{\mathcal{L}} \lambda_l^t = 1\,, \tag{2.34}$$

and

$$\sum_{l=1}^{\mathcal{L}} \lambda_l^t Z_{k_l} = Z_k\,. \tag{2.35}$$

There are an infinite number of combinations for the weights λ_l^t that fulfil the previous constraints, but only one of them (i.e. "*the best linear unbiased estimator*") will minimize the error $\hat{p}_k^t - p_k^t$ characterized by its expected mean square $E\left[\left(\hat{p}_k^t - p_k^t\right)^2\right]$ (Chilès and Delfiner 1999).

Therefore, the minimisation problem can be stated as follows

$$\begin{cases} \min E\left[\left(\hat{p}_k^t - p_k^t\right)^2\right] \\ \text{subject to} \quad \sum_{l=1}^{\mathcal{L}} \lambda_l^t = 1 \quad \text{and} \quad \sum_{l=1}^{\mathcal{L}} \lambda_l^t Z_{k_l} = Z_k \end{cases}. \tag{2.36}$$

Lagrange multipliers μ_1 and μ_2 can be used to solve (2.36) since it is a constrained optimisation, which will lead to the following system of equations (Ahmed and De Marsily 1987)

$$\begin{cases} \sum_{l'=1}^{\mathcal{L}} \lambda_{l'}^t \gamma(k_l - k_{l'}) + \mu_1 + \mu_2 Z_{k_l} = \gamma(k_l - k) \qquad l', l = 1, \ldots, \mathcal{L} \\ \sum_{l'=1}^{\mathcal{L}} \lambda_{l'}^t = 1 \\ \sum_{l'=1}^{\mathcal{L}} \lambda_{l'}^t Z_{k_l} = Z_k \end{cases}. \tag{2.37}$$

This system, which is a function of the theoretical variogram, has to be solved for each cell k and each point in time t within the domain Ω_i. As an example, Figure 2.21 shows the results obtained with this method for the spatial distribution of the annual cumulated precipitation in 1963, 1973, 1983 and 1993.

Cumulative precipitation [mm]

Based on the daily interpolated precipitation $\hat{p}_k^{t(d)}$ for a day d of the water year t and considering that the area of each cell $k \in \Omega_i$ is constant; the annual precipitation in a given catchment Ω_i at the end of a "water year" t can be obtained by

$$x_{i20}^t = P_i^t = \left\langle \hat{p}_k^{t(d)} \right\rangle_i = \iint_{\Omega_i} \int_t \hat{p}_k^{t(d)} d\Omega dt \cong \frac{1}{N_i} \sum_{k \in \Omega_i} \sum_{d=1}^{365} \hat{p}_k^{t(d)}\,. \tag{2.38}$$

The beginning of the water year t is the 1st of Nov. of the Julian year $t-1$ (i.e. $d = 1$), whereas its ending is on the 31st Oct. of the Julian year t (i.e. $d = 365$). For instance, the "water year" 1966 begins on 1st of Nov. of the Julian year 1965 and ends on the 31st of October of the Julian year 1966.

Similarly, the cumulative winter precipitation (from the 1st of Nov. to the 30th of Apr.) occurred in a basin i during a water year t is

$$x_{i21}^{t} = \frac{1}{N_i} \sum_{k \in \Omega_i} \sum_{d=1}^{181} \hat{p}_k^{t(d)} , \tag{2.39}$$

and hence, the cumulative summer precipitation (from the 1st of May. to the 31st of Oct.) can be obtained as

$$x_{i22}^{t} = P_i^t - x_{i21}^{t} . \tag{2.40}$$

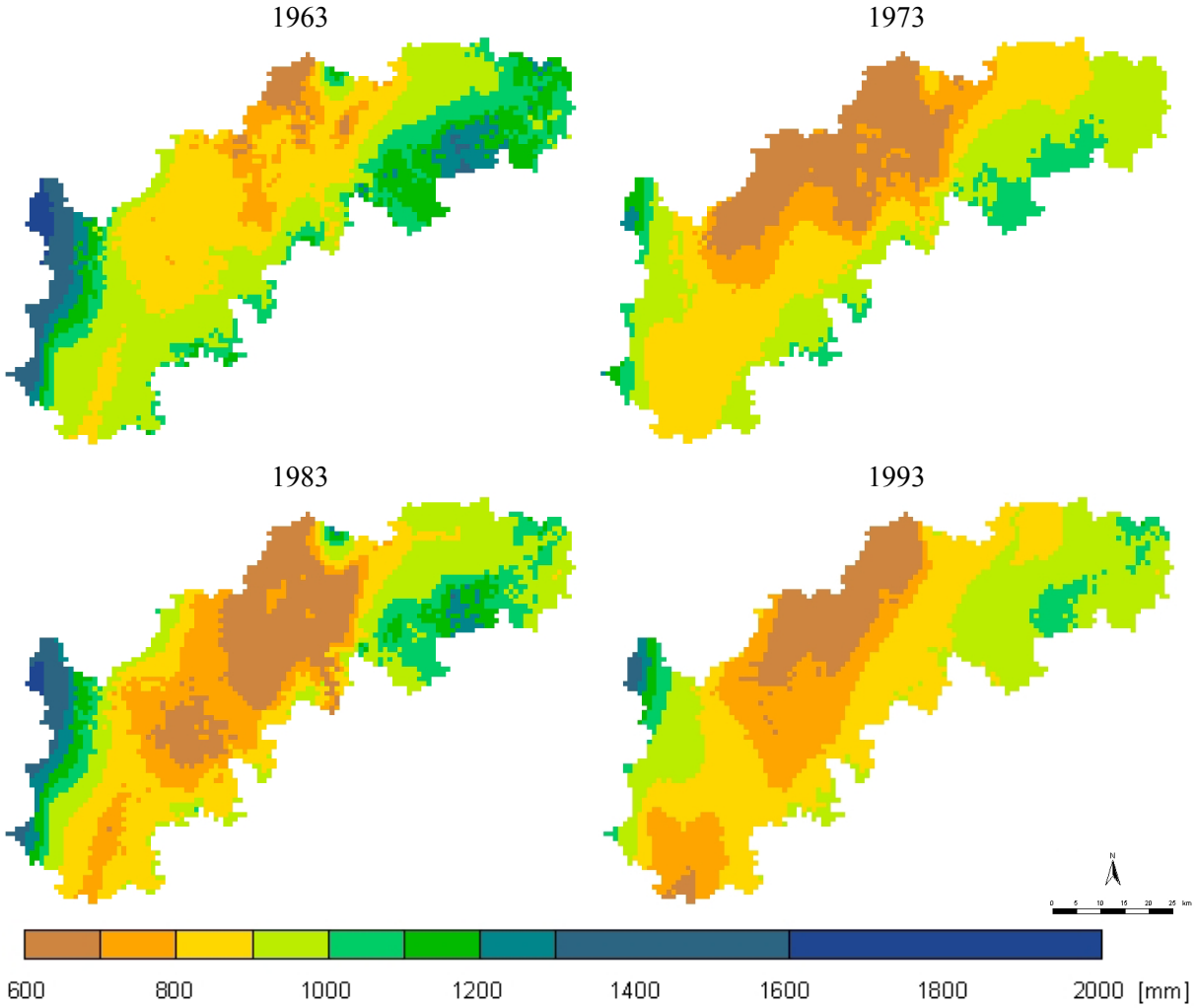

Figure 2.21 Spatial distribution of annual precipitation with in the Study Area for the years 1963, 1973, 1983 and 1993.

Mean precipitation [mm]

In order to estimate the mean precipitation at the spatial unit Ω_i in the "water year" t the following procedure is to be applied. Firstly, a daily expected value at this spatial level can be obtained by averaging daily precipitation values obtained before [see (2.31)] at the cell level for all those cells contained within a given basin i. This procedure will generate a time series of expected daily precipitation at the basin level, say $\overline{p}_i^{t(d)}$, which can be estimated by

$$\overline{p}_i^{t(d)} = \frac{1}{N_i} \sum_{k \in \Omega_i} \hat{p}_k^{t(d)} \,. \tag{2.41}$$

Once this time series has been estimated, the mean or expected precipitation [mm] in basin i in the "water year" t is

$$x_{i23}^t = \frac{1}{365} \sum_{d=1}^{365} \overline{p}_i^{t(d)} \,. \tag{2.42}$$

Using the same reasoning, the mean precipitation during winter and summer in the "water year" t can be calculated by

$$x_{i24}^t = \frac{1}{181} \sum_{d=1}^{181} \overline{p}_i^{t(d)} \,, \tag{2.43}$$

and

$$x_{i25}^t = \frac{1}{184} \sum_{d=182}^{365} \overline{p}_i^{t(d)} \,, \tag{2.44}$$

respectively. Precipitation time series have been provided by the DWD, which consider the length of the "water year" equal to 365 days.

Antecedent precipitation index (API)

After a rainfall, an affected basin's topsoil layer will dry up due to combined effects of evapotranspiration and infiltration. A simple approximation to this complex problem is to assume that a percentage of the precipitation $(1-\kappa)\%$ is lost every day. Then a gross indicator for the residual soil moisture or antecedent precipitation index can be estimated as follows (Linsley, Kohler and Paulhus 1982)

$$x_{i26}^{t(d)} = \sum_{c=0}^{C} \kappa^c \overline{p}_i^{t(d-c)} \,, \tag{2.45}$$

where

κ recession constant, commonly ranging within the interval $0.85 < \kappa < 0.98$ (Chow, 1964).

c $0,\ldots,C$, time index denoting the precipitation occurred c days before the event $t(d)$. t represents in this case a water year and d a given day of that year. C could be 15, 30, 60, 90 or 120 days.

Based on (2.45), the maximum antecedent precipitation of a given spatial unit i in the "water year" t is

$$x_{i27}^t = \max\left(x_{i26}^{t(d)}\right) \quad \forall d = 1,\ldots,365 \,. \tag{2.46}$$

Maximum values of API at seasonal basis can also be estimated using (2.45). Important values for further analysis may be the maximum API during winter and summer, such indicators are given by

$$x_{i28}^t = \max\left(x_{i26}^{t(d)}\right) \quad \forall d = 1,\ldots,181 \,, \tag{2.47}$$

and

$$x_{i29}^{t} = \max\left(x_{i26}^{t(d)}\right) \quad \forall d = 182,\ldots,365\,, \tag{2.48}$$

respectively. An example of the yearly development of variable x_{i26}^{t} can be seen in Figure 2.23.

2.7.2 Temperature

Air temperature at surface level constitutes another basic indicator of the system because of its tight relationships with the potential evapotranspiration and snowmelt, which, in turn, will determine the amount of discharge produced within a basin during a period of time.

The spatial distribution of temperature υ_k^t [°C] for all cells $k \in \Omega_i$ in a given time t is also strongly related with the terrain's elevation (Petterssen in Chow, 1964). Hence, EDK (see Section 2.7.1) can also be used to determine the temperature for all unsampled cells within the domain based on the information available, namely daily average temperatures measured in every station shown in Figure 2.19 during the period $\{01.11.1960,\ldots,31.10.1993\}$. For this analysis the spatial resolution of every cell is 300×300 m, too.

In this case also, a theoretical variogram fitted by Bárdossy et al. (CC-HYDRO, 1999) for the State of Baden-Württemberg will be used, namely

$$\gamma(h) = \begin{cases} 0 & \text{if} \quad h = 0[\mathrm{m}] \\ 0.201231 & \text{if} \quad 0 < h \le 1[\mathrm{m}] \\ 1.185569\left(\dfrac{3}{2}\dfrac{h}{r_\upsilon} - \dfrac{1}{2}\dfrac{h^3}{r_\upsilon^{\,3}}\right) & \text{if} \quad 1 < h \le r_\upsilon = 39\,000[\mathrm{m}] \\ 1.185569 & \text{if} \quad h > r_\upsilon \end{cases}, \tag{2.49}$$

where r_υ is a constant denoting the range of the theoretical variogram for daily temperature in [m].

Figure 2.22 depicts a sample of the time series of mean temperature in January in the Study Area obtained by EDK.

Higher temperatures during certain months of the year may be important indicators of the behaviour of the system. For instance, during January they could be related to snowmelt and lower snow accumulation, which in turn would contribute to winter flooding. Conversely, higher temperatures would imply long drought periods (i.e. low flows in streams) during the summer season, and eventually, large amounts of water will be evaporated since the ground surface has been heated up. This warm-moist air would rise until it cools down, condensates, and finally triggers a local intensive precipitation (Ward and Robinson 2000). This phenomenon is called convective precipitation. Such intensive rainfall would, in turn, generate high peak flows and possibly flooding events in small catchments. Due to these reasons, the following indicators will be calculated based on the daily interpolated temperature $\hat{\upsilon}_k^{t(d)}$ for each cell k and in time $t(d)$.

Mean temperature [°C]

The mean temperature for the spatial unit Ω_i in time $t(d)$ is estimated by

$$\overline{v}_i^{t(d)} = \frac{1}{N_i} \sum_{k \in \Omega_i} \hat{v}_k^{t(d)} , \tag{2.50}$$

then, the mean temperature of January and July in the "water year" t for the spatial unit Ω_i are

$$x_{i30}^t = \frac{1}{31} \sum_{d=62}^{92} \overline{v}_i^{t(d)} , \tag{2.51}$$

and

$$x_{i31}^t = \frac{1}{31} \sum_{d=243}^{273} \overline{v}_i^{t(d)} , \tag{2.52}$$

respectively. Temperature time series provided by the DWD consider the length of the "water year" equal to 365 days.

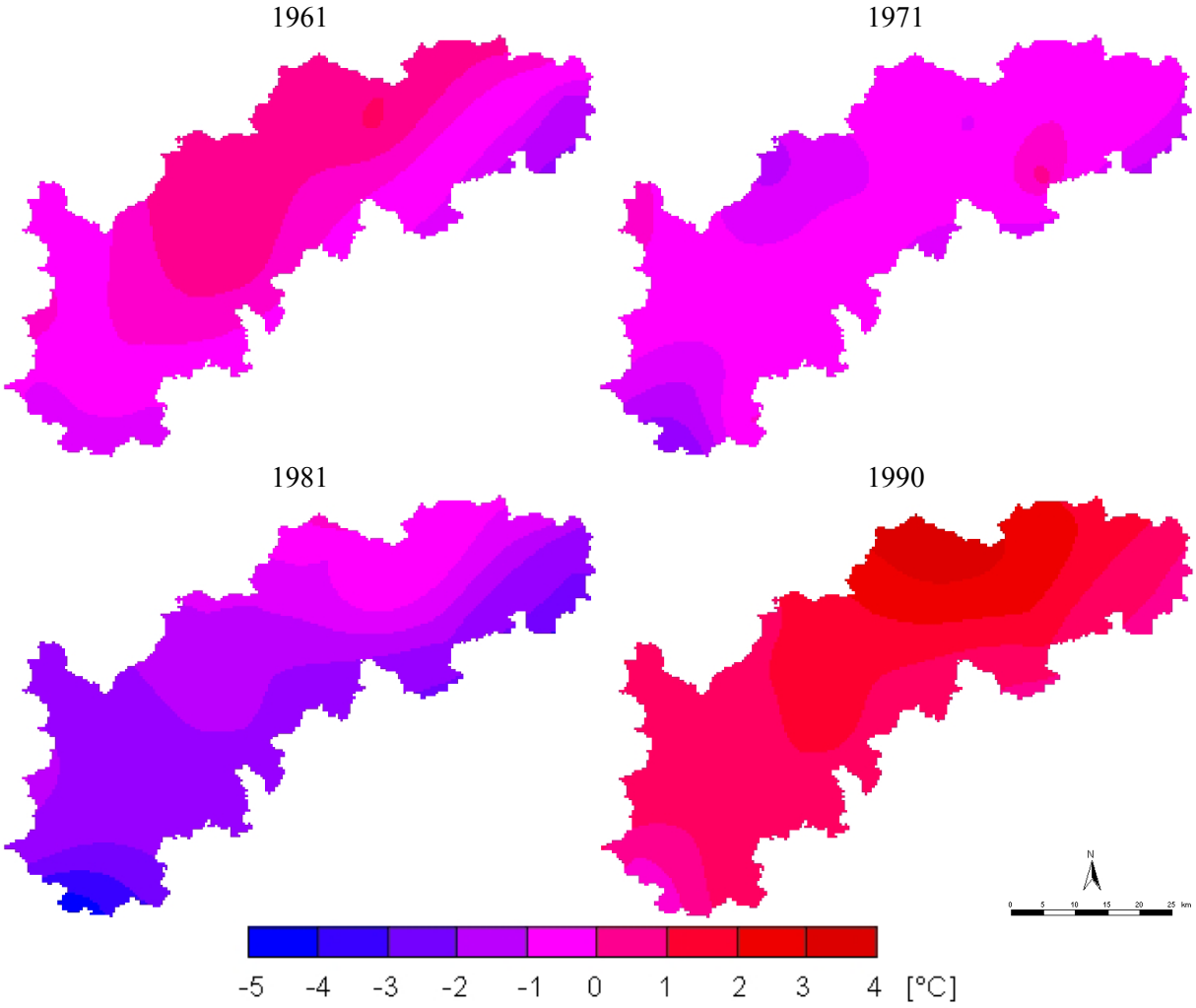

Figure 2.22 Sample of the spatial distribution of the mean temperature in January in the Study Area for the years 1961, 1971, 1981 and 1990 (Source data DWD).

Maximum temperature [°C]

The maximum temperature occurring in January and July in the "water year" t for the spatial unit Ω_i are

$$x_{i32}^{t} = \max\left(\overline{v}_i^{t(d)}\right) \quad d = 62,\ldots,92\,, \tag{2.53}$$

and

$$x_{i33}^{t} = \max\left(\overline{v}_i^{t(d)}\right) \quad d = 243,\ldots,273\,, \tag{2.54}$$

respectively.

Antecedent temperature index (ATI) [K]

As explained before the amount of heat cumulated on the ground surface would originate many meteorological phenomena closely related with the runoff of a catchment. Hence, Hopkins and Hackett (1961) devised an indicator proportional to the cumulated seasonal gain or loss of heat in the system in a given point in time. An example of the yearly development of this index can be seen in Figure 2.23. This indicator is proportional to the difference between the current air temperature and antecedent temperature index (Melloh 1999). It can be estimated recursively as follows

$$x_{i34}^{t(d)} = x_{i34}^{t(d-1)} + \zeta\left(\overline{v}_i^{t(d)} - x_{i34}^{t(d-1)}\right), \tag{2.55}$$

where

ζ temperature weighting multiplier for the previous day period. Commonly ranging within the interval $0.1 < \zeta \leq 1$ (Melloh, 1999).

$x_{i34}^{t(d)}$ antecedent temperature index for the day d of year t. $x_{i34}^{t(d)} = 0$ if $d = 1 \wedge t = 1961$, which corresponds to the beginning of the winter in year 1961.

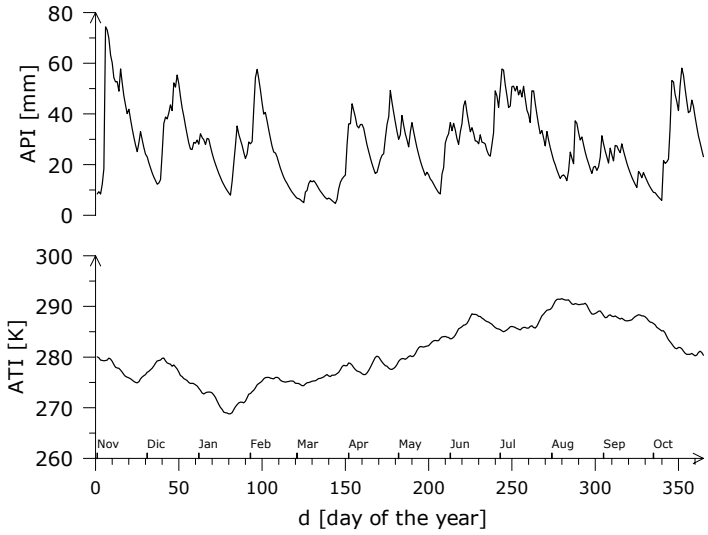

Figure 2.23 Comparison of the daily development of the API and ATI for catchment No. 3 during the water year 1980.

The maximum ATI occurring either during the "water year" or during its winter or its summer t for the spatial unit Ω_i can be calculated by

$$x_{i35}^{t} = \max\left(x_{i34}^{t}\right) \quad d = 1,\ldots,365\,, \tag{2.56}$$

$$x_{i36}^{t} = \max\left(x_{i34}^{t}\right) \quad d = 1,\ldots,181\,, \tag{2.57}$$

and

$$x_{i37}^{t} = \max\left(x_{i34}^{t}\right) \quad d = 181,\ldots,365\,, \tag{2.58}$$

respectively.

2.7.3 Circulation Patterns [-]

Many anomalies of the water cycle (e.g. low flows or extraordinary floods) that occur at a mesoscale depend on the occurrence of particular macroscale (or continental) atmospheric circulation patterns. In recent studies, for instance, Redmont and Koch (1991) have linked the Pacific North America Index (PNA) to precipitation, temperature, and annual stream flow. Bárdossy and Plate (1992) have modelled the spatial distribution of precipitation related to the occurrence of atmospheric circulation patterns (CPs). Duckstein et al. (1993) have linked daily CP occurrences and partial duration of floods. Dracup and Kahya (1994) and then Piechota and Dracup (1996) have related streamflow anomalies and the occurrence of indices based on sea level pressure such as El Niño Southern Oscillation (ENSO). Shorthouse and Arnell (1997) have correlated the North Atlantic Oscillation Index (NAOI) and the average monthly runoff. Stahl and Demuth (1999) have successfully linked streamflow drought and CPs for mesoscale basins in southern Germany.

In the present case, the European atmospheric circulation patterns (CPs) or "*Großwetterlagen*" according to Hess and Brezowsky (1969) will be used to downscale their effects to mesoscale catchments, especially with regard to total drought duration and total duration of peak flows. The CP is a synoptic meteorological classification used by the German Weather Service [*Deutscher Wetterdienst* (DWD)], which is based on mean air pressure distribution over Europe and the northern Atlantic Ocean. This index is defined for a big spatial domain comprised between the coordinates 40°W, 30°N and 60°E, 80°N (Bárdossy, 1993).

The CPs proposed by Hess and Brezowsky distinguish between three major circulation types, namely: zonal, mixed, and meridional circulation types. These types are further subdivided according to the direction of movement of frontal zones, location of high and low pressure areas, and cyclonic and anti-cyclonic rotation. As a result 29 CPs plus one unclassified CP are obtained (Hess and Brezowsky, 1969), (see Appendix 7).

For the present study daily CPs occurrences for the period 1.1.1960 to 31.10.1993 were obtained from DWD. It has been observed and reported by many authors (e.g. Bárdossy, 1993, Stahl and Demuth, 1999) that the occurrence of certain types of CPs can be linked with the amount of precipitation in a given basin, and this, in turn, with the occurrence of wet and dry spells.

In order to cluster the CPs onto three groups, e.g. wet, normal and dry periods, a seasonal wetness index W_j can be estimated. This index estimates the ratio between the relative amount of precipitation occurring when a given CP-type j takes place, and the relative frequency of such CP. This index can be explicitly written as

$$W_j = \frac{\frac{1}{P}\sum_{d=1}^{\mathrm{T}} p_{\Omega j}^{d}}{\frac{1}{\mathrm{T}}\sum_{d=1}^{\mathrm{T}} \mu_j^{d}}, \tag{2.59}$$

where,

$$\mu_j^d = \begin{cases} 1 & \text{if } \mathrm{CP}(d) = j \\ 0 & \text{otherwise} \end{cases} \tag{2.60}$$

$$p_{\Omega j}^d = \begin{cases} \overline{p}_\Omega^d & \text{if } \mathrm{CP}(d) = j \\ 0 & \text{otherwise} \end{cases} \tag{2.61}$$

$$P = \sum_{d=1}^{\mathrm{T}} \overline{p}_\Omega^d \tag{2.62}$$

d Daily time index $\in \{1.11.1960, \ldots 31.10.1993\}$.

j CP-type index, $j = 1, \ldots, 30$; The equivalence of the CP indexes and the CP description can be found in Appendix 7.

T Total number of days either in summer or in winter season during the period $\{1.11.1960, \ldots 31.10.1993\}$.

P Total summer or winter precipitation in [mm] occurred at the Study Area (Ω) during the period $\{1.11.1960, \ldots 31.10.1993\}$.

$\mathrm{CP}(d)$ Atmospheric circulation pattern index according to Hess and Brezowsky for a given day d.

Using the index W_j the CPs were grouped into three categories by applying the following rules:

$$\text{if } \begin{cases} W_j \leq 0.6 & \Rightarrow \text{Dry period} \\ 0.6 < W_j \leq 1.0 & \Rightarrow \text{Normal period} \\ W_j > 1.0 & \Rightarrow \text{Wet period} \end{cases}. \tag{2.63}$$

The results of the above classification are shown in Table 2.2.

Table 2.2 Classification of circulation patterns (CPs) for winter and summer seasons according to the wetness index W for the Study Area.

Category	Circulation patterns winter	Circulation patterns summer
Dry	BM, HB, HFa, HM, HNa, HNFa, NEa, NWa, Sa, SEa, SEz, SWa, Wa	BM, HB, HFa, HM, HNa, NEa, NWa, Sa, SEa, SWa, Wa
Normal	HNFz, NEz, Sz, TB	HNFa, Na, Sz, U
Wet	HFz, HNz, Na, NWz, Nz, SWz, TM, TRM, TRW, U, Ws, WW, Wz	HFz, HNFz, HNz, NEz, NWz, Nz, SEz, SWz, TB, TM, TRM, TRW, WS, WW,Wz

In order to study possible relationships between the occurrence of "dry" circulation patterns and low flows occurring mainly during summer (based on the water budget of the Study Area it is clear that the main impact of low flows will occur during this season), two indicators were considered: 1) one that tallies the total number of occurrences of CPs clustered as "dry periods" for a given spatial unit i during the summer season of a year $t \in [1961, \ldots, 1993]$, that have a decreasing antecedent

precipitation index (x_{26}) for this spatial unit; and 2) one that reckons the total number of occurrences of CPs categorized as "dry periods" for each summer for the period 1961 to 1993. This second indicator is not spatial-unit specific because of the nature of the input data employed. Formally, these indicators can be written as

$$x_{i38}^{t} = \sum_{d=d_w+1}^{d_e} \mu_i^{t(d)} \quad , \tag{2.64}$$

$$x_{39}^{t} = \sum_{d=d_w+1}^{d_e} \mu^{t(d)} \quad , \tag{2.65}$$

where

$$d_e = \begin{cases} 365 & \text{if } t \text{ is a normal year} \\ 366 & \text{if } t \text{ is a leap year} \end{cases} \tag{2.66}$$

$$d_w = \begin{cases} 181 & \text{if } t \text{ is a normal year} \\ 182 & \text{if } t \text{ is a leap year} \end{cases} \tag{2.67}$$

$$\mu_i^{t(d)} = \begin{cases} 1 & \text{if } \begin{cases} \mathrm{CP}(t(d)) \in \{1\ 5\ 7\ 9\ 10\ 14\ 16\ 18\ 20\ 24\ 26\} \\ \wedge \\ x_{i26}^{t(d)} - x_{i26}^{t(d-1)} < 0 \end{cases} \\ 0 & \text{otherwise} \end{cases} \tag{2.68}$$

$$\mu^{t(d)} = \begin{cases} 1 & \text{if } \mathrm{CP}(t(d)) \in \{1\ 5\ 7\ 9\ 10\ 14\ 16\ 18\ 20\ 24\ 26\} \\ 0 & \text{otherwise} \end{cases} . \tag{2.69}$$

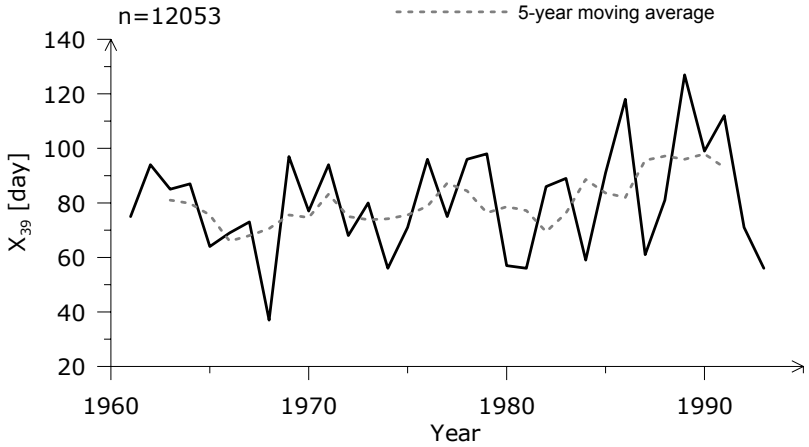

Figure 2.24 Time series showing the absolute frequency of occurrence of CPs classified as "dry periods" within the Study Area during summer.

By plotting the indicator x_{39} vs. time in Figure 2.24 it can be concluded that there exists a marked trend within the Study Area to have circulation patterns prone to cause droughts. It is also interesting to note that the relative increment of this indicator for a given year with its immediate subsequent

($x_{39}^{t+1} - x_{39}^{t}$) tends to grow along the time axis. Such developments are clear indications of macroclimatic changes, which in the present study can be considered as exogenous climatic variables.

For the analysis of peak flows two variables have been devised. Firstly, a variable that reckons the number of days in summer on which both the occurrence of "wet" circulation periods and an antecedent precipitation index greater than a given threshold occur simultaneously. In other words, a flood may be expected if a certain climatic condition and a given amount of precipitation during a continuous period have happened. Secondly, a variable that counts the number of occurrences of wet circulation periods during winter.

The former of the two variables mentioned above can be explicitly written as

$$x_{i40}^{t} = \sum_{d=d_w+1}^{d_e} \mu_i^{t(d)} \quad , \tag{2.70}$$

with

$$\mu_i^{t(d)} = \begin{cases} 1 & \text{if} \quad \begin{cases} \mathrm{CP}(t(d)) \in \{2\ 3\ 4\ 6\ 8\ 11\ 13\ 15\ 17\ 19\ 21\ 23\ 25\ 28\ 29\} \\ \wedge \\ x_{i26}^{t(d)} \geq \mathrm{F}_i\,(0.80) \end{cases} \\ 0 & \text{otherwise} \end{cases} \tag{2.71}$$

where

$\mathrm{F}_i\,(0.80)$ is a threshold value representing an antecedent precipitation index (API) in $[\mathrm{mm}]$ equal to the 80th percentile of variable x_{26}, or in other words, the API to be equalled or exceeded 20% of the time in basin i. Values above this threshold can be regarded as days on which heavy rainfall occurred just before the day d, and thus, saturation of the upper soil horizons had been reached,

and the latter variable as

$$x_{i41}^{t} = \sum_{d=1}^{d_w} \mu_i^{t(d)} \ , \tag{2.72}$$

with

$$\mu_i^{t(d)} = \begin{cases} 1 & \text{if} \quad \{\mathrm{CP}(t(d)) \in \{2\ 3\ 4\ 6\ 8\ 11\ 12\ 13\ 15\ 17\ 21\ 29\ 30\} \\ 0 & \text{otherwise} \end{cases} . \tag{2.73}$$

2.8 The System's Output: Runoff

Runoff is the *throughput* of the water cycle that appears at the outlet of a catchment during a given period (see Figure 2.4). In other words, it "is that part of the precipitation, as well as any other flow contributions, which appears in surface streams of either perennial or intermittent flow" (Chow, 1964). In accordance with these definitions, runoff can be measured as the volume of water per unit of

time $[\mathrm{m^3 s^{-1}}]$, but in order to ease comparison among catchments with different sizes, runoff can be expressed also in $[\mathrm{m^3 s^{-1} km^{-2}}]$, or simply in $[\mathrm{mm}]$, i.e. *specific runoff*.

Consequently, the runoff cycle is inherently dependent on the nature of two main cyclic processes: precipitation and air surface temperature. The latter, as opposed to the former, has a marked annual seasonality. As a result, runoff will exhibit some annual fluctuations and persistence along the time axis. As shown in Figure 2.25 (left panel), the bigger the size of the catchment, the higher the serial correlation coefficients $r(k)$ turn out to be. But in any case, when the lag is greater than 100 days the serial correlation is not significant anymore (at a p-value of 5%). This means that those values to be obtained for the subsequent analyses should be separated at least by 100 days to avoid autocorrelation. In the present study specific runoff, or any of its characteristics, will be evaluated annually or semi-annually.

Besides that, as it is depicted in Figure 2.25 (right panel), cumulated specific runoff exhibits a clear seasonality almost independent of catchment size. This means that cyclic fluctuations have a macroclimatic origin. Additionally, the correlogram also shows that cumulated annual runoff has a non-significant serial correlation.

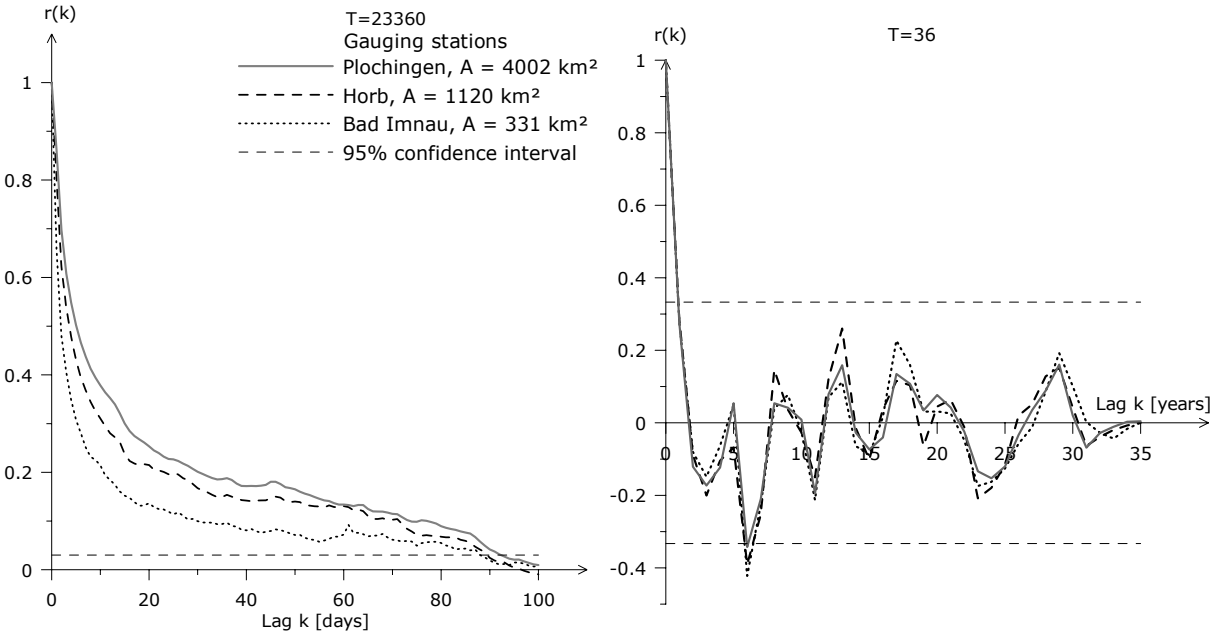

Figure 2.25 Autocorrelation functions of daily (left panel) and annual (right panel) discharge for three basins within the Study Area.

The basic information employed in this study regarding runoff has been obtained from LfU and DWD as time series of mean daily flows from midnight to midnight $q_i^{t(d)}\,[\mathrm{m^3 s^{-1}}]$ for each station i (see Figure 2.5) during the period $t \in [01.11.1960, \ldots, 31.10.1993]$. This data considers leap years.

2.8.1 Specific Runoff [mm]

The annual specific discharge [mm] for the spatial unit Ω_i cumulated at the end of the water year t is computed as follows

$$Q_{i1}^{t} = \frac{1}{A_i} \int_{d=1}^{d_e} q_i^{t(d)} dt = 86.4 \frac{1}{A_i} \sum_{d=1}^{d_e} q_i^{t(d)}, \tag{2.74}$$

where

$$d_e = \begin{cases} 365 & \text{if } t \text{ is a normal year} \\ 366 & \text{if } t \text{ is a leap year} \end{cases}. \tag{2.75}$$

The cumulated specific runoff in the winter season is then

$$Q_{i2}^{t} = 86.4 \frac{1}{A_i} \sum_{d=1}^{d_w} q_i^{t(d)}, \tag{2.76}$$

where

$$d_w = \begin{cases} 181 & \text{if } t \text{ is a normal year} \\ 182 & \text{if } t \text{ is a leap year} \end{cases}. \tag{2.77}$$

Finally, the cumulated specific runoff during the summer season is

$$Q_{i3}^{t} = Q_{i1}^{t} - Q_{i2}^{t}. \tag{2.78}$$

2.8.2 Characteristics of High Flows

In water management and planning it is always a very pertinent task to estimate the magnitude and the period of return (i.e. the inverse of the frequency of recurrence) of peak flows for a given location. Such characteristics of the runoff will govern the design of physical infrastructure along or across a stream (e.g. bridges, dams, river ports, flood walls, culverts) (Chow, 1964) on the one hand, and will guide planners to delimit either floodplains for protection or flooding prone areas where certain land uses must be avoided, on the other hand. Additionally, for other design purposes (e.g. embankments) it will be necessary to know the total duration that a stream's flow persists at flood stage.

For the reasons mentioned above, it is very important to determine whether these characteristics of the runoff would endure alteration in the future due to continuous changes of the land cover upstream of a place of interest. Because of that in this study the following characteristics of the high flows will be analysed.

Specific peak discharge [mm]

The specific peak discharges for a spatial unit Ω_i occurring during both the winter and summer seasons of a water year t expressed in [mm] are

$$Q_{i4}^{t} = 86.4 \frac{1}{A_i} \max\left(q_i^{t(d)}\right) \quad d = 1, \ldots, d_w, \tag{2.79}$$

and

$$Q_{i5}^{t} = 86.4 \frac{1}{A_i} \max\left(q_i^{t(d)}\right) \quad d = d_w + 1, \ldots, d_e, \tag{2.80}$$

respectively. A graphical representation of a peak flow can be seen in Figure 2.26.

Specific volume of the annual peak event [mm]

Runoff is composed of surface runoff and baseflow. The latter comprises all those long term sources entering the streams such as groundwater, whereas the former is the proportion contributed by precipitation. The estimation of the baseflow for each basin is not attempted here because it accounts for less that 10% of total flow in peaks (Laenen 1980). Moreover, if the basin is largely covered by impervious surfaces, this percentage is even lower, and it is often neglected (Bedient and Huber, 1992). Hence, the specific volume of the annual peak event occurring a day d_P can be approximated by

$$Q_{i6}^{t} = 86.4\frac{1}{A_i}\sum_{d=d_P-\Delta_0}^{d_P+\Delta_1} q_i^{t(d)} \quad \wedge \quad q_i^{t(d_P)} = \max\left(q_i^{t(d)}\right) \quad d \in [1, d_e]. \tag{2.81}$$

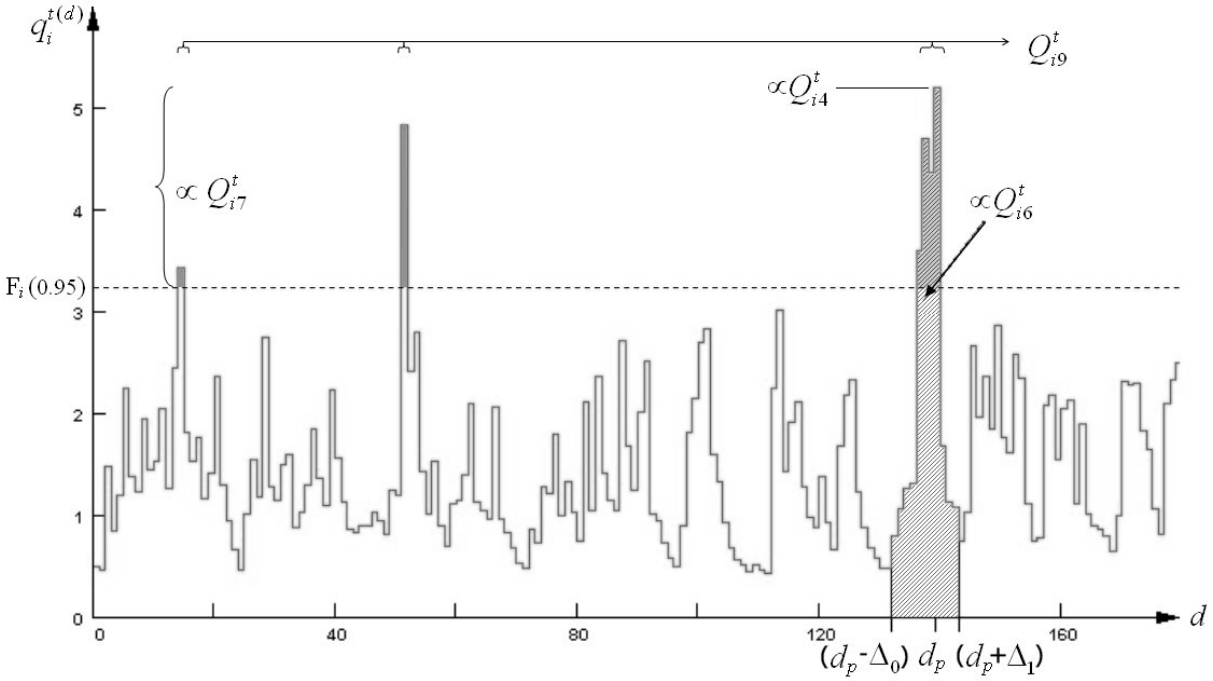

Figure 2.26 Schematic representation of a hydrograph depicting a peak flow occurring in winter, the specific volume of this event, the seasonal specific volume of all high flows, and their total duration in winter for a basin *i* during the water year *t*.

As it is written in (2.81), the volume of a peak event is defined by taking into account its duration. Hence, in order to have a reliable estimate of this volume, it would be very important to define the duration of the peak event (i.e. $\Delta_0 + \Delta_1$), or in other words, its beginning and its end. There are a number of possibilities with varying degrees of complexity to estimate them. The simplest one has been used by Potter (1991). It consists in defining $\Delta_0 = \Delta_1 = 1$. The main drawback of this method is that the catchment's size is not considered and, thus, the flow concentration time is underestimated. More sophisticated techniques would involve the estimation of the baseflow using the instant hydrograph (Dawdy et al. 1972, Dingman 1994, McCuen, 1998). Since the available data is the mean daily discharge this method can not be applied. A compromise between these possibilities would be to take the beginning of the peak event as the first rise of stream flow calculated as follows

$$\Delta_0 = \max\big(t(d_P) - t(d)\big) \quad \forall d \in \left\{ \frac{d^2}{dt^2} q_i^{t(d)} > 0 \ \wedge \ t(d) < t(d_P) \right\}, \tag{2.82}$$

where the second derivative can be estimated by finite differences as

$$\frac{d^2}{dx^2} q_i^{t(d)} \cong \frac{q_i^{t(d-1)} - 2q_i^{t(d)} + q_i^{t(d+1)}}{\Delta d^2} = q_i^{t(d-1)} - 2q_i^{t(d)} + q_i^{t(d+1)}. \tag{2.83}$$

According to Chow (1964), the end of the event can be estimated approximately by

$$\Delta_1 = 0.8267\, A_i^{0.2}, \tag{2.84}$$

where the A_i is the area of the basin in [km²].

Seasonal specific volume of high flows [mm]

Given the original set $\{q_i^{1960(1)}, q_i^{1960(2)}, \ldots, q_i^{1993(364)}, q_i^{1993(365)}\}$ of mean daily discharge for the spatial unit i, the order statistic of this sample would be the same figures but sorted in ascending order, i.e. $\{q_i^{(1)}, q_i^{(2)}, \ldots, q_i^{(\mathrm{O}_i)}\}$, where O_i is the number of valid observations available for basin i different from zero. Here, the j^{th} smallest of the O_i data values is denoted by $q_i^{(j)}$.

In this study, high flows are by definition those values equal to or higher than the 95th percentile. Based on the ordered sample, this statistic is estimated as follows

$$\mathrm{F}_i(0.95) = q_i^{(\iota)}, \tag{2.85}$$

where ι is an integer rounding of the product $\frac{95}{100}\mathrm{O}_i$, and $\mathrm{F}_i(\bullet)$ is the distribution function of daily mean discharge for catchment i.

Then, the winter and summer specific volumes of high flows can be calculated by

$$Q_{i7}^t = 86.4 \frac{1}{A_i} \sum_{d=1}^{d_w} \mu_{95_i}^{t(d)} q_i^{t(d)}, \tag{2.86}$$

and

$$Q_{i8}^t = 86.4 \frac{1}{A_i} \sum_{d=d_w+1}^{d_e} \mu_{95_i}^{t(d)} q_i^{t(d)}, \tag{2.87}$$

respectively. Where

$$\mu_{95_i}^{t(d)} = \begin{cases} 1 & \text{if} \quad q_i^{t(d)} \geq \mathrm{F}_i(0.95) \\ 0 & \text{otherwise} \end{cases}. \tag{2.88}$$

The graphical representation of these indicators is depicted in Figure 2.26.

Total duration of high flows [day]

This indicator, as shown in Figure 2.26, accounts for the total number of days in a given season, either summer or winter, that have a daily mean discharge greater than or equal to a given threshold, for instance the 95th percentile. Using the membership function shown in (2.88), this indicator can be calculated for winter and summer as

$$Q_{i9}^{t} = \sum_{d=1}^{d_w} \mu 95_i^{t(d)} , \tag{2.89}$$

and

$$Q_{i10}^{t} = \sum_{d=d_w+1}^{d_e} \mu 95_i^{t(d)} , \tag{2.90}$$

respectively.

Frequency of recurrence of high flows [year^{-1}]

This indicator quantifies the total number of high flow events $\mathcal{H}_i^t$ that occur in the basin Ω_i during the period from $t(d_0)$ to $t(d_1)$, where d_0 and d_1 represent the beginning and the end of a season in the water year t. The k high flow event $\mathcal{H}_i^{t(k)}$ can be defined as a set given by

$$\mathcal{H}_i^{t(k)} = \left\{ q_i^{t(d)} \middle| \ \forall\, q_i^{t(d)} \geq \mathrm{F}_i(0.95) \ \wedge \ t(d_0) \leq d = t(d_0^k), \ldots, t(d_1^k) \leq t(d_1) \right\}, \tag{2.91}$$

where $t(d_0^k)$, and, $t(d_1^k)$ are the beginning and the end of the high flow event k during the year t respectively. Based on this definition, the frequency of high flows occurring during winter and summer can be estimated as the cardinality of the following sets

$$Q_{i11}^{t} = \left| \left\{ \mathcal{H}_i^{t(k)} \middle| \ \ d_0 = 1 \ \wedge \ d_1 = d_w \right\} \right|, \tag{2.92}$$

and

$$Q_{i12}^{t} = \left| \left\{ \mathcal{H}_i^{t(k)} \middle| \ \ d_0 = d_{w+1} \ \wedge \ d_1 = d_e \right\} \right|. \tag{2.93}$$

In the previous equations d_w and d_e are determined according to (2.77) and (2.75) respectively.

2.8.3 Characteristics of Low Flows

The *minimum* low flow that may occur in most small basins and some larger ones is obviously zero. Hence, in these cases the frequency of occurrence of zero flow would be a suitable drought indicator. This is, however, not the case in the present study. Often, the disastrous effects associated with low flows (e.g. degradation of water quality, reduction of the amount of water available for supply) are experienced long before a flow of zero is reached, hence a more useful index should be defined. Such an index should consider the frequency and duration of spells of low flows or droughts as represented in Figure 2.27. Many low flow definitions can be found in the literature, for instance in Pirt (1983), Correira et al. (1987), Demuth and Külls (1997), and Moore (1997). In this study, however, low flows are those discharge observations corresponding to a basin i that are smaller than or equal to a threshold value, for example, the 10$^{\text{th}}$ percentile of the daily mean discharge $\mathrm{F}_i(0.10)$ [see (2.85)].

Based on this definition, the water *deficit* $D_i^{t(d)} \left[\mathrm{m^3 s^{-1}}\right]$ occurring a day d in the water year t is defined by (Correira et al. in Duckstein and Plate 1987) as

$$D_i^{t(d)} = \begin{cases} \mathrm{F}_i(0.10) - q_i^{t(d)} & \text{if} \quad q_i^{t(d)} \leq \mathrm{F}_i(0.10) \\ 0 & \text{otherwise} \end{cases}. \tag{2.94}$$

Then, let a low flow spell k occurring during the year t within the basin i, say $\xi_i^{t(k)}$ be represented by the set

$$\xi_i^{t(k)} = \left\{ D_i^{t(d)} \middle| \ \forall \ D_i^{t(d)} \neq 0 \ \wedge \ d = t(d_0^k),\ldots,t(d_1^k) \right\}, \tag{2.95}$$

where $t(d_0^k)$, and, $t(d_1^k)$ are the beginning and the end of the low flow spell k during the year t respectively. Based on this definition, the *duration* [day] of such low flow event is

$$\Lambda_i^{t(k)} = t(d_1^k) - t(d_0^k) + 1 \qquad \forall k = 1,\ldots,\mathrm{K}_i^t, \tag{2.96}$$

where K_i^t is the number of low flow spells or droughts occurring in basin i during the water year t.

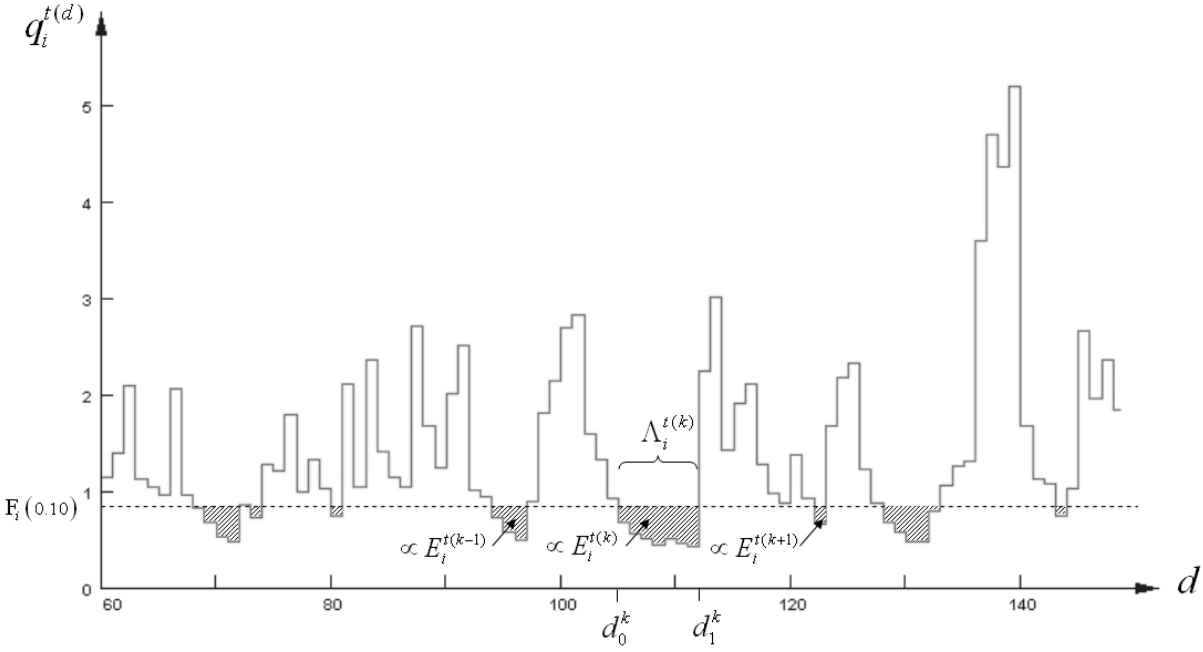

Figure 2.27 Schematic hydrograph depicting the occurrence of low flow spells, their respective deficit, and the duration of the k^{th} low flow spell of a given basin *i* during the water year *t*.

Furthermore, *total specific deficit of a drought* k [mm] can be defined as

$$E_i^{t(k)} = 86.4 \frac{1}{A_i} \sum_{d=d_o^k}^{d_1^k} D_i^{t(d)} \,. \tag{2.97}$$

Finally, the *intensity* of a drought k expressed in [mm/day] can be calculated as the ratio of its total deficit to its duration, namely

$$\Xi_i^{t(k)} = \frac{E_i^{t(k)}}{\Lambda_i^{t(k)}} \,. \tag{2.98}$$

Maximum drought duration [day]

The maximum drought duration occurring at the basin i during the year t is estimated using (2.96) as follows

$$Q_{i13}^t = \max\left(\Lambda_i^{t(k)}\right) \quad \forall k = 1,\ldots,\mathrm{K}_i^t \,. \tag{2.99}$$

Total drought duration [day]

The total number of days that a given basin i in a given water year t has endured a low flow regime can be calculated by

$$Q_{i14}^{t} = \sum_{k=1}^{\mathrm{K}_i^t} \Lambda_i^{t(k)} . \tag{2.100}$$

Maximum drought intensity [mm/year]

The maximum drought intensity referred to yearly basis based on (2.98) is given by

$$Q_{i15}^{t} = 31536 \left(\max \left(\Xi_i^{t(k)} \right) \right) \quad \forall k = 1, \ldots, \mathrm{K}_i^t . \tag{2.101}$$

Cumulative specific deficit [mm]

The total water deficit endured by the basin i during a water year t is

$$Q_{i16}^{t} = \sum_{k=1}^{\mathrm{K}_i^t} E_i^{t(k)} . \tag{2.102}$$